Effect of Temperature on the Fatigue Behavior of Plain Weave Woven Carbon Fabric-Reinforced Composite Plastic

by

Rehan Ikram Khan

A Thesis Presented to the

FACULTY OF THE COLLEGE OF GRADUATE STUDIES

KING FAHD UNIVERSITY OF PETROLEUM & MINERALS

DHAHRAN, SAUDI ARABIA

In Partial Fulfillment of the
Requirements for the Degree of

MASTER OF SCIENCE

In

MECHANICAL ENGINEERING

December, 2000

INFORMATION TO USERS

This manuscript has been reproduced from the microfilm master. UMI films the text directly from the original or copy submitted. Thus, some thesis and dissertation copies are in typewriter face, while others may be from any type of computer printer.

The quality of this reproduction is dependent upon the quality of the copy submitted. Broken or indistinct print, colored or poor quality illustrations and photographs, print bleedthrough, substandard margins, and improper alignment can adversely affect reproduction.

In the unlikely event that the author did not send UMI a complete manuscript and there are missing pages, these will be noted. Also, if unauthorized copyright material had to be removed, a note will indicate the deletion.

Oversize materials (e.g., maps, drawings, charts) are reproduced by sectioning the original, beginning at the upper left-hand corner and continuing from left to right in equal sections with small overlaps.

Photographs included in the original manuscript have been reproduced xerographically in this copy. Higher quality 6" x 9" black and white photographic prints are available for any photographs or illustrations appearing in this copy for an additional charge. Contact UMI directly to order.

ProQuest Information and Learning
300 North Zeeb Road, Ann Arbor, MI 48106-1346 USA
800-521-0600

EFFECT OF TEMPERATURE ON THE FATIGUE BEHAVIOR OF PLAIN WEAVE WOVEN CARBON FABRIC-REINFORCED COMPOSITE PLASTIC

BY

REHAN IKRAM KHAN

A Thesis Presented to the

DEANSHIP OF GRADUATE STUDIES

KING FAHD UNIVERSITY OF PETROLEUM & MINERALS

DHAHRAN, SAUDI ARABIA

In Partial Fulfillment of the
Requirements for the Degree of

MASTER OF SCIENCE

In

MECHANICAL ENGINEERING

DECEMBER 2000

KING FAHD UNIVERSITY OF PETROLEUM & MINERALS
DHAHRAN, SAUDI ARABIA
DEANSHIP OF GRADUATE STUDIES

This thesis, written by

REHAN IKRAM KHAN

under the direction of his thesis advisor and approved by his thesis committee, has been presented to and accepted by the Dean of Graduate Studies, in partial fulfillment of the requirement for the degree of

MASTER OF SCIENCE IN MECHANICAL ENGINEERING

Thesis Committee

Dr. Zafarullah Khan (Chairman)

Dr. Anwar K. Sheikh (Member)

Dr. F. A. Al-Sulaiman (Member)

Dr. Nesar Merah (Member)

15/9/1421

Department Chairman (Mech. Engg)
(Dr. Al-Farayedhi, Abdulghani)

Dean of Graduate Studies
(Dr. Osama Ahmad Jannadi)

Date: 16/9/1421

To my dearest
Ammie, Abbu, loving
brother and sisters

Acknowledgements

In the name of Allah, Most Gracious, Most Merciful. Read in the name of thy Lord and Cherisher, Who Created man from a {leech like} clot. Read and thy Lord is most Bountiful. He Who taught {the use of} the pen. Taught man that which he knew not. Nay, but man doth transgress all bounds. In that he looketh upon himself as self sufficient. Verily, to thy Lord is the return {of all}.

(The Holy Quran, Surrah Al-A'alaq, No. 96)

Praise and Glory be to Almighty Allah, subhanahu-wa-tala, for bestowing me with the health, spirit, strength and patience to complete this work. I feel honored as well as privileged to Glorify His name and give due reverence to Allah and only Allah Almighty that this small objective is accomplished.

Acknowledgement is due to KFUPM for the support given to this research work through its tremendous facilities.

I acknowledge, with deep gratitude, appreciation, and inspiration for the careful guidance and encouragement given to me by thesis advisor, Dr. Zafarullah Khan. He has taken care and showed great interest in the work by assisting and giving constructive comments with patience, inspite of his busy schedule. I am especially thankful to Dr. Faleh A. Al-Sulieman, for practical interest and due contribution in the experimental work. I am also thankful to my thesis committee member, Dr. Necar Merah, for his expert opinion,

constructive criticism, and help. Thanks are also in order to my thesis committee member, Dr. Anwar K. Sheikh, for his useful comments on the research work conducted and review of the thesis. I am also thankful to the ME Department Chairman, Dr. A. Al-Farayedhi, for his spirited research support and also other faculty members of ME department.

I would like to thank Dr. Qutab Ali Khan and his staff for conducting X-ray Radiography at the university medical center. Special thanks for Mr. Yonus Selander in Central Research Workshop for his help in preparation of specimens, without his special help this work would not have finished on time. Thanks are also due to Mr. Riyaz for his expert guidance and support in SEM fractography.

I owe special thanks to Mr. Zainulabideen and my friend Mohammad Irfan-ul-haq for their laboratory collaboration and great companionship. It was a great experience working in such a cordial and friendly environment. Both of them made my time during this study an unforgettable experience.

Notable mentions go to all my friends and colleagues in and outside the department like Irfan (BG), Atique, Mehmood, Owais Iqbal, Asif (CG), Science-dan, Tariq (CH), Mofi, Arshad, Masroor, Hafiz Saeed, Abdul Hamid, Shafique Awan, Rashid, Imran and many others. These are the ones that made my stay here memorable and it is their comradeship that I will always cherish in my professional career ahead.

Last but not least, I express my profound gratitude to my beloved parents, brother, sisters, brothers-in-law, and all other family members for their love, constant prayers, continuing support, encouragement, understanding, and for enduring the geographical distance from me during my graduate studies. Their sacrifices, prayers and prescience made this work possible.

Table of Contents

List of Tables

List of Figures

Nomenclature

A	Material Constant
B	Material Constant
C	Material Constant
D	Damage Parameter
D_o	Damage at zero cycles
D_i	Initial damage state
V_f	Fiber Volume Fraction
T_g	Glass Transition Temperature
N	Number of fatigue cycles
N_f	Cycles to failure
ϵ	Strain
ϵ_f	Failure Strain
P_{max}	Maximum applied load
P_{min}	Minimum applied load
R	Stress Ratio
σ_{max}	Maximum Applied Stress
σ_{UTS}	Ultimate Tensile Strength
E	Elastic Modulus

E_o	Elastic Modulus at zero cycles
ϕ	Stress State Function
dD/dN	Damage rate
dE/dN	Modulus Reduction Rate
F	Defining monotonic failure surface from Hill's theory
σ_L	Applied stress in longitudinal direction
σ_{LU}	Ultimate Applied stress in longitudinal direction
$D_{critical}$	Critical Damage showing lowest stiffness value on the stage II portion of the modulus degradation curves
P	Material Constant to Calculate $D_{critical}$ as function of Temperature
Q	Material Constant to Calculate $D_{critical}$ as function of Stress State Function ϕ
f	Frequency of loading
$\Delta\sigma$	Stress Amplitude

Abstract

Name:	Rehan Ikram Khan
Title:	Effect of temperature on the fatigue behavior of Plain Weave Woven Carbon Fabric-reinforced Composite Plastic.
Major Field:	Mechanical Engineering
Date of Degree:	December, 2000 (Ramadan 1421)

During service, engineering structures and components made from Carbon Fiber-reinforced Plastics (CFRPs) are often subjected to cyclic loading as well as varying environmental temperatures. Fatigue failure of CFRPs is complicated and quite different from those of isotropic materials. In this study, the influence of environmental temperature on fatigue response of Plain Weave Woven Carbon Fabric-reinforced Composite Plastic was examined. The 8-ply laminates were obtained from epoxy resin prepreg fabric layers, stacked in two different sequences producing unidirectional $[0]_8$ and angle plied $[0,0,45,-45]_s$ orientations. The fatigue tests were carried out at –20°C, 0°C, 24°C, 100°C, and 150°C. Enhanced-dye penetrant X-ray radiography and Scanning Electron Microscope Fractography was used to characterize the fatigue damag. The fiber/matrix interface strength, that is the most critical parameter in initiation of primary matrix cracks and interply delamination was found to vary with testing temperature. It was found that there was no change in sequence of damage events but duration of each event and hence cumulative damage rates were different with varying temperatures. The fatigue life at elevated temperature was found to decrease with increasing temperature but decreasing temperature below ambient conditions caused an increase in fatigue life for both classes of woven laminates. An analytical model used for CFRP life prediction based on Stiffness Degradation during cyclic loading has been successfully employed. A parameter $D_{critical}$ (critical damage) that was a function of testing temperature and indicated the least stiffness value in Modulus Degradation curves was introduced. A reasonably good correlation has been obtained between predicted and experimental lives.

Master of Science Degree
Department of Mechanical Engineering
King Fahd University of Petroleum and Minerals
Dhahran, Saudi Arabia
December 2000

ملخص البحث

الإسم : ريحان اكرام خان

الموضوع : :تأثير الحرارة على كلال الأنسجة الصافية المصنوعة من الألياف الكاربونية المعززة بمركبات البلاستيك :

تخصص : هندسة ميكانيكية

تاريخ الدرجة : ديسمبر ٢٠٠٠ م

تتعرض الأشكال الهندسية والمواد المصنوعة من الألياف الكربونية المعززة بمركبات البلاستيك الى التحميل الدوري وكذلك الى تغير الدرجات البيئية المحيطة . كلال هذه الأنسجة معقد ويختلف عن المواد الموحدة الخواص . في هذه الدراسة يتم فحص تأثير درجات الحرارة المحيطة على كلال الأنسجة الصافية المصنوعة من الألياف الكاربونية المعززة بمركبات البلاستيك . وتم عمل نسيج من ٨ رقائق من خلال استخدام رقائق الراتنج والتي توضع فوق بعضها بشكل متغاير لإنتاج نسيج لااتجاه له ورقائق ذات زوايا (٠ ، ٠ ، ٤٥ ، – ٤٥) . تم فحص الكلال عند درجات حرارة – ٢٠ و : و ٢٤ و ١٠٠ و١٥٠ وبذلك تغطي هذه التجارب كل درجات الحرارة البيئية الطبيعية . وكذلك تم استعمال طريقة تغلغل الصبغات المعززة وأشعة اكس والتصوير الجزئي باستخدام المسح بالمجهر الإلكتروني لتحديد صفات الكلال في حالات بيئية مختلفة . وجد أن قوة تماسك سطح النسيج (والذي تعد العامل الحاسم في بداية التشقق وانفصال الطبقات عن بعضها) تتغير بتغير درجة حرارة الإختبار . وقد لوحظ عدم وجود اختلاف في ترتيب مراحل التلف لكن كان الإختلاف في مدة كل مرحلة وعليه فإن نسبة التلف المتزايد تختلف تبعا لتغير الحرارة . كما أن فترة الكلال تتناقص بازياد الحرارة لكن تخفيض الحرارة وجعلها أقل من الظروف المحيطة يزيد من فترة الكلال لكلا النوعين من نسيج الرقائق . كما جرب بنجاح نموذج تحليلي يستخدم للتنبؤ بفترات هذه الأنسجة معتمدا على الإنحلال التيبي خلال التحميل الدوري . وكذلك تم الحصول على معامل التلف الحرج والذي يعد وظيفة من وظائف اختبارات الحرارة كما يحدد القيمة الصغرى للتيبي في معامل منحنيات الإنحلال . كما تم الحصول على العلاقة بين القيم المتوقعة وقيم التجارب متناسبة .

درجة الماجستير

قسم الهندسة الميكانيكية

جامعة الملك فهد للبترول والمعادن

الظهران – المملكة العربية السعودية

ديسمبر ٢٠٠٠ م

CHAPTER 1

INTRODUCTION

1.1 GENERAL BACKGROUND

The present day increasingly complex design of engineering components and structures, the demand of their superior performance, and the weight saving requirements have propelled the material scientists, engineers, and designers into a continued search for new materials, which can satisfy the above needs. Development of composite materials was a result of the impetus to provide a material that can optimize the above challenges. Since 1960s, when the first fiber reinforced plastics were developed, the extent and scope of their application has been continuously increasing and now it ranges from a simple sports gear industry to modern, automotive, marine, advanced aviation, and space technology.

A composite is formed when two or more materials are judiciously combined, usually with the intent of achieving better properties than those offered by individual materials by themselves. Fiber reinforced composites have gained an ever increasing

popularity among all other composites such as filled and particulate types. The main reason for this is due to the fact that the fibrous form of most materials is several times stronger than its bulk form. In the fibrous form, the surface area to volume ratio is significantly low, and hence less number of surface flaws exist in fibrous form as compared to bulk form. Another factor that makes fiber-reinforced composites attractive is their ability to be tailored in different ways. The most efficient method yet found to get maximum advantage of two different materials is to combine a fibrous material of high tensile strength and high elastic modulus with a light weight material of lower strength and lower elastic modulus, yet good ductility. A high strength fiber and a polymer matrix provide an ideal combination to produce such a material. Hundreds of polymer matrix composites (PMCs) have been developed and are being successfully employed in modern engineering applications as described in the next section.

1.2 APPLICATIONS OF COMPOSITES

Over the past few decades composite materials have found their way in a wide spectrum of applications in advanced engineering structures and components. Scientists and engineers are constantly engaged in an extensive amount of research directed toward performance enhancement, which is widening the usage of the composites in increasingly challenging engineering applications.

In the aerospace field, military aircraft, with their higher performance demands, have been the first to use fiber-reinforced plastics (FRPs) extensively. The F/A- 18 and AV-8B aircrafts, for example, use pre-formed load bearing wing. Civil aviation applications have been slower to develop, but there are numerous examples

of large passenger aircraft flying with FRP-skinned panels. Many military and civil aircrafts use substantial quantities of lightweight and high strength carbon, Kevlar, and glass fiber reinforced composites, as laminated panels, moldings, and honeycomb structures.

Naval applications include either monolithic or sandwich construction for vessels such as mine-hunters and superstructure materials, where lightweight and apparent fire resistance (for some fire retardant resin systems) offer clear benefits over aluminum alloys. FRP laminates have also been extensively used in the hulls and masts of racing yachts. An additional use for composite materials is in flywheels for energy storage in power system, where, lightweight and high stiffness of the hubs are important factors in enhancing the efficiency of the system.

1.3 CARBON FIBER REINFORCED COMPOSITES

Among the large variety of polymer matrix composites, carbon fiber reinforced plastics (CFRPs) are gaining an ever-increasing attention of designers as one of the most attractive composite material. Carbon fiber reinforced plastic composite posses attractive mechanical properties such as high specific stiffness and high strength in addition to a relatively high tolerance to environmental influence. Furthermore, components made of these composites achieve a weight saving of about 20% when compared with conventional structural materials made of light metals. The advanced CFRPs should primarily see wide spread applications as structural materials well in to the next century. However, materials incorporating long fibers and matrices whose mechanical properties are very different are typicaly anisotropic materials. The fracture mechanism, in particular, in laminate composites that are used for a structural

component is thus extremely complicated when compared with conventional metallic materials. Fracture processes in these composites include a complex, interdependent combination of matrix cracking, fiber breakage, fiber/matrix interfacial debonding, and delamination.

Continuous reinforcements in the form of axial filaments and continuous strand mats are used for pultruded materials. The fiber reinforcements have a strong influence on the mechanical properties of the material. However, due to their method of manufacture, the fiber properties are somewhat variable. The fibers are usually held in place in the composite material by resinous materials. The resin affects the chemical resistance of the composite material, and provides a channel for the distribution of load between the fibers.

1.4 WOVEN AND NON-WOVEN CFRP COMPOSITES:

Recently, composite structures reinforced with woven fabrics have found extensive use because of their advantages compared to tape lay-ups. Woven fabrics are easier to handle (ensuring economical and automated fabrication), conform to complex shapes, provide better resistance, and exhibit larger damage tolerance than non-woven unidirectional materials.

Some mechanical properties of woven materials, such as axial strength and stiffness, are smaller than laminated composites. Many types of weaves are available such as, satin, plain, and twill, etc. are available. It has been shown that weave with less fiber distortion such as satin weaves (in particular five or eight harness satin weaves for CFRPs) result in smaller reduction in mechanical properties. Moreover,

mechanical properties of woven laminates are also critically dependent on the perfection of the weave and amount of damaged fibers.

1.5 FATIGUE IN COMPOSITES

Engineering components and structures are frequently subjected to cyclic loading. Fatigue is therefore an important issue in the design of mechanical or structural components. In recent years, owing to the rapid development and wide range of applications in composite materials, traditional fatigue analysis thus far used for metallic materials has been employed and/or extended to the design and analysis of composite structures. However, the fatigue damage in composites is a much more complex phenomenon than that occurs in metals.

Fatigue damage in fiber reinforced composite materials can be defined as the development of irreversible changes such as matrix cracking, fiber debonding, fiber fracture, and ply delamination. Fatigue failure can occur if the residual strength of a material degrades to the level of applied load. Matrix cracking, delamination, fiber fracture, and interfacial debonding can cause this degradation. Any combination of these may be responsible for fatigue damage, which may result in reduced fatigue strength and stiffness. Material properties, specimen geometry, stacking sequence, load levels, loading rate, waveform types and frequency, time, and temperature are also critical variables in composite fatigue as they are in any fatigue study. Variation in any of these variables could result in different damage processes and damage evolution mechanisms.

Fatigue damage in composites can be evaluated by measuring the material properties such as stiffness and strength. The stiffness reduction of composite

laminates is a meaningful measure of fatigue damage and it can be measured non-destructively. However, in order to predict the fatigue life of a composite laminate based on stiffness reduction, the stiffness at fatigue failure, referred to as the failure stiffness, should be evaluated. Various failure criteria in terms of the failure stiffness have been investigated in literature.

During cyclic loading, different regions inside a composite material have different micro-responses. The weaker matrix can act temporarily as a homogenous material like the conventional metal but only until some other constituent of the composite takes over in the deformation process. The matrix exploits the inherent defects of manufacturing like voids and impurities and produces a crack. After sufficient matrix cracking the crack encounters the fiber/matrix interface. Here the circumferential stiffness of the fibers does not allow it to be broken by the crack, and hence the crack moves along the fiber-matrix interface. This type of process eventually leads to damage called delamination, where the laminae are separated from each other. Fiber/matrix debonding may also contribute to delamination. From here onward, the large alteration in the integrity of internal structure of the composite dictates reduction in strength and stiffness of the composite as a whole. The load bearing fibers are always the ones in the direction of the loading and at this stage the failure and fracture of the composite member is directly linked to the fiber fracture. When they break the composite fails completely.

Under cyclic loading all types of individual damages caused by fatigue are intricately amalgamated. With the onset of matrix cracking, somewhere, nearby a fiber breaks and that fiber pulls out of the matrix (conveniently termed as "fiber pull-out").

The neighboring fibers also start debonding and simultaneously other localities experience similar damage. Fiber pullouts force voids to grow larger but their growth process is slow. This damage process is over taken by the more dominant fiber fracture and delamination induced by matrix cracks. The delamination process is very much dependent on the stacking sequence of the plies. If there are angle-plies involved, the damage by delamination will start from the interface joining different direction laminates. For example, in a (0,0,+/- 45) fiber composite, the interface of the 0° and the 45° will be most prone to delamination as compared to other interfaces having uni-directional laminates. In addition, the fiber fracture in different angled-plies is different. For example, in a composite of the 0° and 90° plies, the 90° plies will not bear any load and will not hinder damage. They will straight away split in the transverse direction and the remaining load will be transferred to the 0° fibers. Again, the fracture will take place according to the load bearing capacity of the 0° fibers.

The cumulative fatigue damage is usually characterized using different destructive and non-destructive techniques. These techniques such as X-Ray Radiography, C-Scan, Acoustic Energy Discrimination method, Fractography, and Edge Replication de-plying technique, Optical Microscopy etc., have been used over the last three decades in order to examine the fatigue damage process in fiber reinforced composites. Different damage modes under fatigue loading are observed with different techniques. For example, the delamination has been examined by X-Ray radiograph and Edge Replication. These techniques eventually help in characterizing the damage and which in turn guide designers for predicting that

behavior, qualitatively and even quantitatively. This in the end can become the basis for the design of components; with fiber reinforced composites such as CFRP.

1.6 SCOPE AND OBJECTIVE OF THE PRESENT STUDY

The preceding discussion must certainly have highlighted that composites such as Woven CFRPs have emerged as one of the most promising and challenging classes of materials to meet the present and future material requirements to produce complex, light weight yet high performance engineering structures and components. The heterorganic property characteristic of this material has made it a popular candidate for use where such "dexterity and smartness" of the material is required.

In addition to simple structural applications of CFRPs where environment is not severe, these materials are now rapidly becoming candidates for applications where elevated or cryogenic temperatures are encountered. Polymer matrix composites (PMCs) are being recommended for selected components of newer engines, where elevated temperatures prevail. These materials will serve as both load bearing and non-load bearing components. Anticipated service environments may reach and maintain levels up to 300°C. Selection of CFRPs for this type of hostile environment primarily depends on the glass transition temperature of matrix. With increasing use of CFRPs in this type of applications, it is becoming increasingly essential that the effect of temperature on the fatigue resistance of CFRPs should be investigated.

Matrix and interface dominated properties of CFRPs are expected to vary significantly as a function of temperature. The fiber/matrix bonding is supposed to be

a temperature dependant phenomenon due to increasing ductile and brittle behavior at elevated and sub-room temperatures respectively. Fiber matrix debonding and transverse ply delamination, which are major causes of fatigue failure, are supposed to be temperature dependent.

Till date very limited work has been carried out to investigate the effect of temperature on the fatigue behavior of CFRPs. Engineering data related to fatigue performance under non-ambient temperatures (higher and lower than room temperature) is constantly sought by the designers. Proper characterization of fatigue damage and development of reliable fatigue life prediction methodologies pertaining to fatigue of CFRPs under non-ambient temperature is very much in demand.

The research work envisaged in the present study is an attempt to provide some meaningful answers to the above-mentioned issues. The objectives are to provide necessary engineering data, characterizing the damage, and examine the applicability of stiffness degradation based fatigue prediction methodology for woven fabric-reinforced plastic composites subjected to cyclic loading at elevated and sub-room temperature.

CHAPTER 2

LITERATURE REVIEW

During the last four decades, composites have become a material of intense research due to its increasing use in the engineering industry. Since engineering structures are frequently subjected to cyclic loading, during the past decades investigating fatigue performance, and developing fatigue life prediction methodologies, have been the subjects of study for a large number of researchers.

Sunderdas and Clark [1] presented a very comprehensive review of fatigue damage in advanced composite laminates. They reviewed fatigue process, data results, damage development, impact damage, and effects of joints, holes, and notches and have reviewed the damage inspection methods. Much of the experimental work has been involved with the determination of stress-life (S-N) behavior of the composite laminates. In general, the S-N curves of composite laminates are flatter than for metals as shown in Figures 2.1(a) and 2.1(b). For the specific case of the 0/90 type laminates the stage I degradation, namely ply cracking, developed very rapidly. Stage

II damage development consisted largely of the growth of longitudinal cracks and the nucleation of some delaminations. Stage III was characterized by significant increase in length of the longitudinal cracks and the coalescence of delaminations. The principal damage development process of woven laminates was shown to be the nucleation of fatigue cracks at tow cross-over points in the weave. The damage was found to be particularly evident in 0/90 lay ups. There was evidence to show that a +/-45 woven lay up has slightly improved tension-tension fatigue properties over conventional non-woven materials. The fatigue loading for woven carbon fiber composites with sharp notches showed that matrix shear cracking was observed to occur most rapidly, followed by the nucleation of delaminations at specific ply interfaces. The progressive degradation occurred with continued fatigue loading.

2.1 GENERALIZED FRACTURE BEHAVIOR OF CFRPs

Fatigue crack growth in short carbon fiber reinforced PEEK(Polyetherether ketone) has been investigated by Evans et al [3]. They studied the role of fiber volume fraction and interdependent parameters such as fiber arrangement, fiber preferred orientation, and fiber length on fatigue crack growth. Fatigue crack growth rates in compact tension specimens were found to decrease significantly with increasing fiber fraction when loading was parallel to mould filling direction (MFD). This effect was however, less marked for loading perpendicular to MFD.

Donti et al [4] studied the effects of pultrusion process variables on fatigue damage in graphite epoxy composites. The fractional factorial statistical design was used to characterize the effects of pultrusion process variables and their interactions

with the fatigue damage of pultruded graphite epoxy composites. The start and progress of damage due to the loading and influence of the material processing conditions were reflected by discernible changes in the loss factor, which is defined as the ratio of dissipation energy to stored at maximum displacement. The changes shown by the loss factor were used to characterize the effects of the processing variables on the cyclic damage.

Miyano et al [5] studied the influence of stress ratio on fatigue behavior in the transverse direction of unidirectional CFRPs. The dependence of flexural fatigue behavior upon stress ratio of two unidirectional carbon fiber-reinforced plastics was studied at several constant temperatures. They found that as the stress ratio decreased from one to zero, the flexural fatigue strength near room temperature decreased while the strength at temperatures close to glass transition temperature (T_g) increased. The fracture mechanism was found to change with increasing temperature. Below, glass transition temperature the composites failed in a cohesive fracture mode. However, near T_g the composite failed in interfacial fracture mode. It was found that the fatigue strength at room temperature depended strongly on stress amplitude, and strength was controlled by fatigue damage, while the strength near T_g depended on mean stress and therefore was controlled by creep damage.

The properties of short carbon fiber reinforced resin composites, such as strength, Young's modulus, and fracture toughness for various volume fractions of carbon fibers were studied [6] in detail. The results showed that the Young's modulus increased linearly with increasing volume fraction, whereas strength and fracture toughness increased at first and then peaked at a volume fraction of 0.25. For the two

short fibers reinforced thermoplastic (SFRTP) materials studied, the main energy absorbing mechanisms during fracture were homogenous and localized plastic deformation of the matrix, de-bonding of the fiber-matrix interface, and fiber pull-out. The contribution of each mechanism depends on the extent of strength and toughness between the fiber and matrix, and the fiber-matrix adhesive strength.

The effect of lay up sequence on the mechanical properties and fracture behavior of the advanced CFRP composites was examined. by Yoshiyuki and Morioka [7]. The mechanical properties were evaluated by three point slow bend and instrumented Charpy impact tests. V notch sub-size specimens (2mm X 2mm) with angle plies of 0, 45 and 90° between the 0° layers were used. The unidirectional laminate specimen exhibited high slow bend and Charpy impact energies, but the 0°/0° plies had a remarkable anisotropy of the mechanical properties. The mechanical properties of the orthotropic laminates (0°/90°) specimens significantly decreased but those of the (0°/90°/45°) specimen dramatically increased because large amounts of fiber were pulled out in the 45° direction. For quasi-isotropic laminates (0°/90°/+/-45°), there were marked benefits in the mechanical isotropy. However, their slow bend and charpy impact energies were, respectively, about 60 to 70 % of the (0°/0°) specimens.

Rochardjo et al [8] studied the effects of the fiber content on the microscopic and macroscopic fracture modes of unidirectional carbon/epoxy composite. Necked-in thickness direction specimens having a fiber volume fraction (V_f) ranging from 30% to 70% were tested in tension in the fiber direction. The effects of the fiber volume fraction (V_f) on the fracture appearance showed that a transition in fracture mode

occurred, from tensile fracture at the necked region at low V_f to interlaminar shear failure at high V_f. Scanning electron microscopy (SEM) of the specimen surface showed that, at low V_f, the specimen fractured with a fiber break dominated fracture, whilst, at high V_f, an interfacial damage dominated fracture was observed.

Fatigue behavior of carbon fiber reinforced polyetheretherketone (PEEK) laminated composite $[+/- 45]_{4s}$ was studied [9]. The static loading and tension-tension fatigue loading tests were conducted at various levels of stress amplitude to study the effects of stress amplitude on fatigue behavior. Two fatigue frequencies, 10 Hz and 1 Hz, were selected to study the effect of fatigue behavior. The effect of fatigue damage process on the specimen surface temperature change during fatigue test was investigated, and it was found that temperature rise would decrease the fatigue life.

Masaki hojo et al [10] examined the effects of matrix resin and fibers on the mechanisms and mechanics of delamination fatigue crack growth in unidirectional Carbon Fiber-reinforced Composite laminates. Tests were carried out under mode I loading at different stress ratios. The fatigue crack growth behavior of laminates tested was mainly controlled by the toughness of the matrix resin. It was found that the resistance against fatigue crack growth increased with the increase of the static fracture toughness. However, the ratio of the fatigue threshold to the static fracture toughness decreased with the decrease of the γ value. Where, the parameter γ, which indicated the relative contribution of the maximum stress to cyclic stress, was determined from the analysis of stress ratio dependency. Thus, the increase of the fracture toughness does not fully contribute to the fatigue crack growth resistance.

2.2 FATIGUE DAMAGE CHARACTERIZATION

Khan et al [11] studied the multi mode fatigue failure process in Plain weave CFRP composites. Enhanced dye penetrant X-ray Radiography, Scanning Electron Microscopy Optical Microscopy and edge replication techniques were employed to examine the fatigue damage mechanism. Unidirectional $[0]_{8s}$ and angle plied $[0,0,45,-45]_s$, $[45,-45,0,0]_s$ stacking sequences were used. It was found that in angle-plied laminates the fatigue fracture was a multi mode damage process including matrix cracking, fiber matrix debonding, fiber fracture and delamination. Delamination was found to be the dominant damage parameter. Whereas in unidirectional laminates the fatigue failure occurred in a more simple, yet a rather more catastrophic manner. In these laminates, instead of delamination, the predominant process was fiber fracture.

Dillon [12] used the scanning electron microscopy in the determination of fatigue growth mechanisms in carbon fiber reinforced PEEK APC-2 (a commercial name) laminates. He presented the general understanding of fatigue behavior of APC-2 by coherently describing the sequence of events leading to the failure of laminates of $[0]_s$ and $[0,90]_{4s}$ subjected to dynamic flexural fatigue. It was found that crack initiation occurs simultaneously at both faces of the fatigue sample. On the tensile side, random fiber breakage occurred with initially rapid crack propagation rates. Crack propagation slowed down as tensile failure approaches the neutral axis, leading to varying levels of fiber pull-out. On the compressive side, the crack progresses at a uniform rapid rate. Final failure occurred when tensile and compressive cracks met at the neutral axis.

A scanning acoustic microscope (SAM) that enabled inspection of internal defects at high resolving power by convergence of the acoustic wave was used by Akira Todoroki [13]. Delamination cracks in carbon fiber epoxy and carbon fiber PEEK laminated composite plates were examined. For carbon/PEEK, the delamination cracks were nearly straight compared to those in carbon/epoxy. The results of mode I and II testing of unidirectional carbon/epoxy composites, the delamination crack fronts in both modes had zigzag forms.

A micro-grid method [14] was used to measure displacements under tensile loading in 90° ply in CFRP cross ply laminates with only transverse cracks, and with both transverse cracks and delaminations. Micro-grids were printed on edge surface of CFRP cross ply laminates (T800H/363 1 carbon epoxy composite) by using the photo-lithography technique. Displacements both in the loading direction at the 0°/90° interface, and the middle plane between a pair of transverse cracks were measured. The crack opening displacement of the transverse crack was also measured. Measurements were also made for the laminates with not only transverse cracks but also with delamination at the tips of the transverse cracks.

Kim and Lee [15] estimated the damage of plain-woven carbon fiber reinforced plastics by using a new factor of acoustic emission and secant modulus during loading-unloading test. Acoustic emission signal and fracture process was monitored by AE measurement system and video microscope in real time during the test. High amplitude signal, middle amplitude signal, and low amplitude signal correspond to fiber breaking, debonding and matrix cracking respectively, in fracture process.

The static and dynamic response of fiber reinforced composite coupons with various levels of fiber surface treatment through strain measurement was investigated [16]. For this purpose, different surface treated fiber specimens were fatigue loaded. Continuous monitoring of stroke and load signals was carried out to measure phase lag & gain and obtain damping and dynamic modulus. The proposed approach made it possible to monitor continuously the fatigue damage evolution in any material system in real time without the use of an extensometer or strain gauge. This approach was an ideal candidate for studying damage under high temperature or extremely corrosive environments. The dynamic mechanical response under cyclic loading indicated that the damage and damage rate for 20% and 50% fiber surface treated specimens were almost the same. For 100% fiber surface treated specimens damage was however much more extensive and occurred at a faster rate than the other two.

Damage progress in quasi-isotropic CFRP laminates under tensile loading was investigated [17] microscopically. An optical microscope and soft X-ray radiography was employed to observe the onset and growth of transverse cracks and delaminations. To study the effects of toughened interlaminar layers, two material systems were used. One with toughened interlaminar layer CFRP and other one is without interlaminar layer. The toughened interlaminar layers contained tough and fine polyamide particles dispersed in the epoxy resin base. It was found that the toughened interlaminar layers suppressed delamination onset and growth.

The interlaminar fracture of a five-harness satin orthogonal woven fabric carbon epoxy composite laminate loaded in mode I, mode II and mixed mode were investigated [18]. Special emphasis was put on microscopic details of crack growth

and their relations to fracture resistance. For all fracture mode combinations, it was found that crack growth occurred in a non-planar region of topology determined by the weave pattern and relative positioning of the plies of adjacent to the crack plane.

2.3 FATIGUE DAMAGE MODELING AND LIFE PREDICTION

Gathercole and Adam [19,20] determined the fatigue response of T800/5245 carbon fiber epoxy composite in repeated tension, repeated compression, and mixed tension/compression at constant and variable stress levels over a wide range of R values. The results were analyzed in terms of constant life diagrams of the kind that can be used to provide design data and fatigue life prediction. This carbon fiber epoxy composite was tested with lay up sequence of $[(+/-45,0_2)_s]$ and fiber volume fraction (VF) of 69%. In the second part of this study variable load block like TTTT, TTCC, TCTC (T stands for tension and C for compression) were made and a computer program controlled the load sequence. Similarly, Takumura and Fuji [21] characterized the fatigue of woven CFRP laminates of T300-B series. Low and high cycle fatigue tests were performed with maximum stress of 480 MPa. They used scanning electron microscopy and acoustic emissions to analyze the fracture behavior. They found that for low cycle fatigue, fiber breakage started earlier but specimen failed without stiffness reduction. The observed high cycle fatigue failure process was divided in four stages. In the first stage, cracks do not occur and no significant reduction is determined. The traverse cracks occur in the 2^{nd} stage causing quasi-interlaminar delamination. The quasi-interlaminar delamination progressed further in

the third stage. In the final stage, an occasional fiber break occurred in warp bundles and the accumulation of this fiber break at some locations causes debonding in warp bundles. Residual strength and modulus decay was determined and used in the fatigue life prediction modeling.

The fatigue damage of composite laminates under service loading spectra was studied by Lee et al [22]. Residual stiffness degradation model, which proved to be capable of estimating the cumulative damage in composite laminates under constant loading, was used to investigate the fatigue damage of composite laminates under service loading spectra. An empirical failure criterion was proposed and fatigue life distributions for composite laminates subjected to different level of spectrum loading were theoretically derived. Fatigue tests were conducted on $[0/90/+/-45]_{2s}$ graphite epoxy laminates to generate statistically meaningful experimental data for the verification of theoretical approach presented.

Salvia and Vincent [23] modeled the fatigue damage in glass fiber reinforced polymers based on experimental observations subjected to deflection controlled flexural fatigue. The damage sequence was identified as transverse fiber and matrix superficial cracking on the tensile side, and delamination at the ends of the specimen. The damaged zone appeared to be a quasi-parallelepiped volume, which was claimed to have no contributions toward the stiffness of the specimen. In their fatigue damage model, the size of the damaged zone is expressed as function of the number of cycles and of a few empirical parameters.

The residual stiffness as a parameter to describe the degradation behavior of composite laminates was selected and a simple model, which contained residual

stiffness degradation equation and randomization of its parameters was proposed to predict the fatigue life [24]. A Morkov chain model was also employed. Both models can be used to predict the probability distribution of the degraded stiffness at a specified loading cycle. Experimental results verified the applicability of both models for tested Graphite epoxy laminates $[+/-45]_{2s}$.

Ochiai et al.[25] Studied the debonding process of multifilament unidirectional fiber reinforced composites. A new two-dimensional shear lag simulation method was developed to investigate the influences of residual stresses, frictional shear stress at debonded interface, and their interactions among broken components. It was found that debonding process hastened by interactions and growth rate of debonding, reduced with existence of frictional shear stress. Real time monitoring of dynamic strain and fatigue damage in a continuous unidirectional carbon fiber polymer matrix composite by measurement of electrical resistance in longitudinal direction was achieved [26]. The electrical resistance decreased reversibly upon tensile loading in every cycle, thus providing dynamic strain monitoring. This decrease in resistance was reported to be due to a reversible increase in the fiber alignment. Whereas the peak resistance irreversibly increased as the fatigue damage occurred due to breakage of carbon fiber. At 55% of the fatigue life, the peak resistance started to increase in spurts. At 89% of fatigue life, the peak resistance started to increase continuously from cycle to cycle, indicating the gradual breakage of fibers.

Shokreih [27] established a new model called the generalized residual material property degradation model. The model uses the experimental data from a unidirectional ply under uniaxial fatigue to predict the behavior of that ply in

multiaxial fatigue loading. The normalized residual strength used by Gathercole [18,19] and the new normalized fatigue life models were coupled into the generalized residual material property degradation model. This model is capable of considering fatigue damage under arbitrary stress ratios, without performing excessive amounts of fatigue testing.

Progressive failure from a circular hole in glass fiber-reinforced plastics under combined tension/torsion cyclic loading was investigated by Takemura [28]. The fatigue life was estimated based on the relationship between pseudo-crack-growth rate and energy release rate. The fatigue life of a plain weave glass fabric reinforced plastic (GRP) hole notched laminates under combined loading was estimated by using an equivalent damage length and a fracture mechanics approach. The energy release rate was used as a parameter for progressive failure.

Gamble et al [29] used a progressive damage model using finite element analysis to predict the development of damage in composite materials up to the final failure. The ABAQUS finite element code has been used to develop fully automated three-dimensional modeling of damage development in carbon fiber composites under tensile loading. This work covered the development of suitable meshes, identification of suitable criteria to control the onset and effects of local damage, and extending it the real geometries. Similarly, an experimental and numerical study of elasto-plastic behavior of thermoplastic matrix composite laminates under static and cyclic loads was presented by Kenny [30]. Off-axis and angle ply specimens from carbon fiber reinforced PEEK were tested under cyclic sinusoidal tensile loads and hysteresis loops were monitored. A micro mechanical model including parabolic criteria based on

plastic behavior of the matrix was adopted to study the non-linear behavior of composites. It was proposed that the mathematical model presented in their study can be used to predict the visco-elastic plastic response of the material and its influence on the fatigue life. The yielding threshold divides the fatigue behavior in two regions. In the first region, resin deformation is mainly elastic and the phenomenon is ruled by crack propagation. In the second region, the main damage is the plastic deformation and the higher friction between plies is responsible for temperature rise and thermo mechanical failure.

Boniface et al [31] studied the initiation and propagation stages of transverse ply cracking in cross ply laminates under quasi-static loading. Different ply thickness was studied. Two types of specimen coupons with polished edges, and coupons containing defects (notches) introduced into the transverse ply were used. In laminates, with thin transverse plies (less than 0.25mm) fully formed transverse cracks were observed at about the same strain in undamaged and notched laminates. In laminates with thicker transverse plies (greater than 0.25mm) the notched laminates showed fully formed transverse cracks at lower strains than the undamaged laminates. The multiple cracking was quantified by measuring crack density as function of strain, modulus, and Poisson's ratio. It was found that at large ply thickness, the cracking is initiation controlled while at small ply thickness it is propagation controlled.

Song [32] investigated the fatigue process of CFRP laminates of $[0°/90°]_s$ and the influence of damages occurring at fiber, matrix, and fiber/matrix interface on various critical strengths and the relationship between residual critical strength and failure. It was shown that fatigue life (fatigue strength) is a function of residual

critical strength and stresses occurring at each layer (0° and 90°) and interlayer. Residual critical strength decreases exponentially with dependence on fiber fracture crack density; transverse crack density and delamination crack density.

The effective crack growth model (ECGM) [33] was used to evaluate the residual strength of woven fabric composite laminates with circular holes. It was assumed that when the local normal stress reaches the tensile strength of un-notched laminate, damage initiate and propagates with increase in the applied load. It was found that the simulations from the ECGM correlated very well with the experimental data available in the literature. It was also found that for the notched woven fabric composite laminates, larger hole diameters or wider specimens result in greater damage zone sizes, i.e., the critical damage zone size is not laminate constant and it is dependent on the specimen geometry.

2.4 EFFECT OF TEMPERATURE ON FATIGUE RESISTANCE OF CFRPS

Fiber matrix bonding was investigated by Peters [34] as a function of the fiber surface treatment and cure temperature. Increased fiber-matrix bond strength and a reduction of defect size and number (through improved wetting) explained the positive influence of the fiber surface treatment on the transverse cracking. The bond strength for the material with untreated fiber is low and practically independent of the cure temperature in the range of 100° C to 190° C. A model taken from the literature, which described transverse cracking as influenced by defects, matrix ductility, and constraining effect, was applied to explain the effect of surface treatment in relation to the defect distribution and strength.

Miyano et al [35,36,37,38], in a series of experiments, studied the loading rate and temperature dependence on flexural fatigue behavior of satin woven CFRP laminates consisting of a high glass transition temperature resin matrix. The flexural static and fatigue behavior of this CFRP laminate was measured at various loading rates and temperatures below glass transition temperature of the matrix. A prediction method for long-term life of this laminate was proposed based on visco-elastic behavior of the matrix resin. It was found that not only flexural static strength but also flexural fatigue strength of this laminate depended on time and temperature even at temperatures lower than T_g. The reciprocation law of time and temperature was found to be applicable for both the flexural fatigue and static strength. It was verified experimentally [36] that the matrix controled the time and temperature dependency of CFRP. The time-temperature superposition principle for the visco-elastic properties of the matrix resin also held for the flexure strength of the CFRP laminates. A method was proposed to predict the flexure fatigue strength based on the experimental findings and considering the relationships among the static, creep, and fatigue flexural strength.

Boniface et al [39] studied the growth of matrix cracks in simple cross-ply laminates under quasi-static loading as a function of temperature and under thermal cycling conditions. It was shown that in CFRP laminates the total 90° ply strain for first ply failure under quasi-static loading (based on the sum of the thermal and mechanical strains) remained constant at approximately 1.5 % over the temperature range of –80° C to 200° C indicating a balance between those temperature dependant factors which tend to increase the cracking threshold with increasing temperature.

Murakami [40] studied the effects of carbon fiber contents, temperature and notch radius on fatigue behavior for Short Carbon Fiber-Reinforced Plastic (SCFRP). Fatigue strength increased with an increase in carbon fiber content and decreased with an increase in test temperature. It was found that fatigue strength of SCFRP depends little on the notch radius. The water absorption of the T800/924C carbon fiber epoxy composite system and its effect on the compressive behavior of unidirectional laminates tested in hot wet environment was examined [41]. The weight gains, maximum moisture contents, and through thickness diffusion coefficients of uni-directional laminates immersed in boiling water was reported. It was observed that failure of specimens tested in hot wet conditions always occur because of out of plane fiber micro-buckling. This was attributed to the reduction in matrix strength arising from elevated temperatures and environmental conditioning.

Nakamura et al [42] studied the influence of temperature on fatigue reliability for advanced carbon/glass fiber reinforced /PEEK composite. Attention was focused on the mechanism of the growth from mesocracks to macrocracks at elevated temperatures of 373K, 393K and 413K. All these temperatures were below glass transition temperature of PEEK (T_g for PEEK 415K). It was found that the fatigue life at elevated temperature decreased with increasing temperature. The influence of stress and temperature was represented by the N_f vs 1/T diagram and S Vs T(C+log t_r) diagram. Fatigue tests were carried out in high cycle and low stress range. From the results of SEM fractography the fracture occurring in a CF 15 (carbon fiber 15% by weight) material was found to be ductile, where as, that of GF 30 (glass fiber 30% by

weight) material was brittle It was reported that the temperature rise in the fatigue damage zone appeared to be closely related to the mesocrack formation process.

The static and dynamic mechanical properties of carbon fiber reinforced PEEK laminates subjected to long-term thermal ageing and cyclic treatment has been studied under three-point bending [43]. S/N curves were modeled using fatigue modulus degradation data. Laminates aged at high temperatures, for long time period (74 weeks), between the glass transition temperature and melting temperature showed a significant reduction in mechanical properties. However, for short ageing periods a crystal perfection process occurs, which enhanced the low stress level fatigue resistance of unidirectional and orthotropic laminates. The fully reversed fatigue behavior of a woven carbon fiber/polyamide resin laminate at room and elevated temperature was studied [44]. Non-destructive video edge view microscopy and destructive sectioning techniques were used to study the microscopic damage mechanism. The elastic stiffness was monitored and recorded throughout the fatigue life of a coupon. In addition, residual compressive strength tests were conducted on fatigue coupons with various degrees of damage as quantified by stiffness reduction. Experimental results indicated that the temperature only minimally influenced monotonic tensile properties. However, the monotonic compressive and fully reversed fatigue properties displayed greater reductions at elevated temperature. Similarly Cross ply cracking in specimens out of the laminate $(0/90_4/0)$ was investigated [45] at -100°C, 25°C, 60°C, 100°C. The thermal strain in the transverse ply at these temperatures was determined with the thermal expansion coefficients in fiber direction and transverse to the fiber of a unidirectional laminate. These thermal

expansion coefficients were found to vary approximately linearly with temperature. From the Weibull distributions and an available model for the transverse fracture strain distribution, it was found that at higher test temperature two phenomena influence the transverse fracture strain. These phenomena are the fracture strains of the matrix and the strength of the interface. First ply failure proved to be dominated by the increasing fracture strain of the matrix from -100°C to room temperature. Above room temperature, however, the influence of the decrease in interface strength dominates over the influence of the increased matrix fracture strain.

The long-term mechanical and thermal fatigue of an eight-harness satin woven composite system was investigated to study the inter-relationship between thermo-mechanical properties, namely the thermal expansion coefficient (TEC) and the compressive strength [46]. Qualitative trends in the experimental data generated by either thermal or mechanical loadings were shown to be similar to properties predicted by a shear lag based model. Measured compressive strength degradation was as large as 49% for this material undergoing mechanical fatigue cycling with TEC degradation as large as 61%. Experimental results showed that a correlation exists between TEC measurements and compressive strength. This correlation suggested that TEC measurements might be used as damage evaluation technique.

Carbon toughened resin epoxy composite has been investigated for influence of temperature and moisture content on the interlaminar delamination toughness in mode I, mode II, and mixed mode conditions [47]. Dry and moisture saturated specimens were tested over the temperature range –50°C to 100°C. Evaluation methods based on load/displacements, and, load measurements were employed. In

pure mode II the critical strain energy release rate was shown to drop with decrease in moisture content and increase in temperature. In mixed mode the critical strain energy release rate also decreases with moisture content, but no general trends in the dependence on temperature was observed. The critical strain energy release rate in pure mode I is unaffected by changes in moisture content and found to increase slightly at elevated temperatures.

Yoji and King [48] studied the effects of test temperatures on damage accumulation behavior and modulus reduction of Carbon Fiber epoxy cross ply laminates in conditions of fatigue and monotonic loading. Monotonic and fatigue tests were conducted at room temperature, low temperature (-40°C) and elevated temperature (100°C). They found that damage accumulation behavior varied as a function of test temperature. Theoretical models, based on shear-lag approach, predicted crack accumulation and Young's Modulus reduction satisfactorily.

Yoshihiko et al [49] studied the behavior of delamination crack propagation of a carbon fiber-reinforced polymer at high temperatures (200°C). Double cantilever specimen was used to investigate fracture toughness and slow crack propagation in creep and fatigue. It was found that CF/PEEK shows excellent fracture toughness up to 373 K, but fracture toughness decreased at higher temperatures. Crack propagation in high temperature fatigue is classified into two types, time dependant and cycle dependant. Crack propagation in these are controlled by stress intensity factor and stress intensity factor range respectively.

CHAPTER 3

EXPERIMENTAL

3.1 MATERIAL AND SPECIMEN GEOMETRY

The material used in this study was a prepreg plain weave woven carbon Fiber-reinforced Plastic with epoxy matrix. The fiber density in this Carbon Fiber-reinforced composite was 208 g/m^3. The high tenacity/high strength Carbon Fiber with 3000 filaments/yarn or tow was used in weave. The high strength fibers in the form of graphite had a density of 0.00017625 g/mm^3. The Young's Modulus, approximate elongation, and tensile strength of fibers were 235 GPa, 1.6% and 3.7 GPa respectively. The yarn twist was 15 TPM (turns/meter). The properties of the fabric, resin, and a single ply are given in table 1. The properties of the Carbon Fiber-reinforced composite were estimated using STRAN; software used for the analysis of mechanical properties of multilayer hybrid fiber composites.

300 X 300 mm panels were prepared in autoclave under vacuum bagging with 60 % volume fiber fraction. Curing temperature of 177°-200° C and curing pressure of

8 bars were used. The class 1 unidirectional $[0]_8$ and class 2 $[0,0,45,-45]_s$ fiber orientations were used. The test coupons for tensile tests were machined according to ASTM standard D-3039 [52] with dimensions of 220 X 30mm, having a thickness of approximately 1.8mm as shown in Figure 3.1. The fatigue test coupons were prepared similar to the work of Murakami et al [40] with reduced gage section width. This geometry was selected to localize the damage at the center of the gage section, which facilitated the observation of edge crack growth phenomenon damage via optical microscope. The end tabs of 30 X 25mm were prepared with same composite material and bonded with high strength epoxy, having effective temperature range of 0-250° F. the specimens with tabs were left to harden overnight and excessive epoxy was scrapped off for dimensional accuracy.

3.2 FATIGUE TESTING

The Instron 8501 material testing system was used to obtain tensile and fatigue data. The system is a closed loop servo-hydraulic, dynamic, single axis fatigue testing system. The machine is equipped with a hydraulically actuated self-aligning gripping system. To ensure the vertical alignment of the specimen specially machined metal inserts were used during the tests. Any preloading induced during clamping was adjusted to zero prior to testing by balancing of the load cell after clamping.

All tension and fatigue tests were carried out using a specialized **F**atigue **L**aboratory **AP**plication **S**oftware [FLAPS], which provided complete machine control, data acquisition, data reduction and analysis capability. All constant amplitude fatigue tests and position increment tensile tests were designed in FLAPS. Tensile tests were carried out under position control at a displacement rate of

1mm/min [ASTM D-3039]. The software logged position and corresponding load of the test with a constant position increment until fracture occurred at the ultimate tensile strength. The elastic modulus of the Carbon Fiber-reinforced composite was obtained by getting the load and position data throughout the test. The final stress value just before the fracture was selected as the tensile strength and the final actuator position gave the $\in_f$. The results of the tensile tests carried out at various temperatures are tabulated in table 2. The specimens were kept for some time in the environmental chambers before fatigue loading to stabilize the temperature variation in the specimen.

Fatigue tests conducted through FLAPS followed the tasks; initially a ramp to mean load level and then a sinusoidal loading with a frequency of 20 Hz at a stress ratio R = 0.1. The maximum cyclic stress ranged approximately from 60% to 80% of tensile strength of the composite. Data logging was done for the constant amplitude cyclic loading at a rate of 40Hz for track values of load and position. The interval of data logging was selected between 500-3000 cycles for different tests depending upon the expected life of that particular test specimen.

The fatigue tests carried out with manual setting of machine were used for view of edge crack growth phenomenon with optical-microscopic camera. The machine was hold for some time during the test to capture the edge view with 35mm camera equipped with optical microscope. These events were also recorded with high magnification JVC-Digital video camera. These video-graphs were digitized with the help of ATI Video player to capture the still images.

3.3 ENVIRONMENTAL CHAMBERS

In order to study the effect of temperature on fatigue and monotonic properties of Woven Carbon Fabric-reinforced composite two environmental chambers were designed; one for sub-room temperature testing and other one for elevated temperature testing.

The electrical heating tapes lined around the inner walls of a cylindrical Plexiglas chamber provided a uniform source of heat for elevated temperature testing. An insulation wall of Aluminum foil sandwiched with Styrofoam was attached on the inner side of the cylinder to minimize the heat loses. The heating tapes 10 x 2 inches were placed next to insulation wall in circular periphery for uniform temperature distribution around the specimen. A small window of 30 X 30mm was made in insulation wall to view the specimen edge. Thermocouple attached onto the surface of the test specimen provided continuous measurement of the test temperature, which was maintained at the desired level by a temperature controller. This controller was able to maintain the temperature with an accuracy of +/- 1°C.

The monotonic and cyclic testing at sub-room temperature was done in a specially designed double wall chamber. Two concentric cylinders of Plexiglas were used to make this chamber. The space between two cylinders was filled with glass wool and Styrofoam to minimize the heat transfer from outer environment. Similarly, top and bottom of this cylinder were also made of two layers of Plexiglas sheets sandwiched with Styrofoam. A small window of 30 X 30mm was made in insulation wall to view the edge of the specimen. 5/8 inch copper tubing was used to form a helical circuit around the specimen. A solution of 60% Methanol-40% water was used

as the refrigerant and circulated through these tubes. The methanol solution was maintained at desired temperature with the help of a cooling bath (POLYSTAT constant temperature circulation bath), which was capable to cool the solution up to – 45°C. This solution was pumped through copper tubing within the cylinder to provide a low temperature environment. In order to achieve low temperature efficiently two small CPU cooling fans were used inside the chamber to force the air over the copper tubes. The temperature on the specimen was measured by OMEGA J-Type thermocouple attached to the surface of specimen.

3.4 FATIGUE DAMAGE CHARACTERIZATION

The equipment used for non-destructive and destructive testing of the damaged Carbon Fiber-reinforced Composite specimens are given below

- Joel JSM T-300, Scanning Electron Microscope
- JVC Color Video Camera
- Questar QM 100 Optical Microscope

Joel JSM T-300 Scanning Electron Microscope was used to investigate the surface morphology of damaged Carbon Fiber-Reinforced Composite specimens. The damaged specimens were cut to the appropriate size with Buehler Isomet™ low speed diamond saw. A very fine coating of Gold was deposited on the fracture surface by vacuum deposition ion sputtering at 1-1.5 KV and at a vacuum of 0.1 Torr.

The optical examination of the specimen edges was carried out with optical microscope attached to a JVC industrial video camera and 35 mm still camera. The specimen, edges were metallographically polished to provide a clear view of the specimen edge. Manually polishing was done with increasing grit size from 240-600

grit emery papers. The sequence was followed in such a way that the 600 grit was used to polish for the last time along the direction of fibers which are along the length. 0.3 micron Alpha Alumna powder with water on a micro cloth was used as the final polishing step.

In the study of sequential damage it is essential to have a quick and reliable method of permanently recording in-situ damage during the entire period of fatigue loading from N = 0 to N_f. This objective was achieved by continuous videotaping of the events taking place at the specimen edge through the optical microscope + industrial video camera + continuous time recording VCR system. These video-graphs were then digitized with the help of ATI Video player software. In addition, a 35mm still camera was also used to capture the photographs of the specimen edge.

X-Ray radiography technique was used to examine internal damage features of the fatigued specimens. A special Zinc Iodide solution was used to infiltrate the damage zone and enhance the visibility of the damage on the radiographs. The composition of this solution was 60 gm Zinc Iodide (ZnI_2), 8 ml Water (H_2O), 10 ml Isopropyl Alcohol and 3 ml Kodak Photoflo-200. A hypodermic syringe was used to inject the dye at the edges of the coupons and in the damaged sites visible outside. Reasonable amounts were injected in, and excess amount removed with a clean cloth. It was useful to inject with certain tensile static load being applied on the coupon to allow the dye to penetrate deeper inside the cracks. A Seimens Polyphos-30 X-ray machine available at KFUPM medical center was used for this radiography. X-Rays at 40 kV with a rate of 0.2 mA/sec were used. The best X-rays with clear contrast had exposure distance from the source to the target coupons between 135-145 cm. The

radiographs were able to identify matrix crack, fiber fracture and delamination in the fractured specimen.

CHAPTER 4

ANALYTICAL MODEL FOR FATIGUE LIFE PREDICTION

The development of rational fatigue life prediction methods for a material involves:

a) Physical observation of the damage accumulation process and the formulation of an appropriate damage parameter;

b) Formulation of a damage accumulation model in terms of the damage parameter and empirical characterization of the model parameters using simple experiments;

c) Development of a damage accumulation procedure based on the damage parameter to predict life under fatigue loading;

d) Experimental verification of the life predictions.

This approach has proved to be successful for metallic structures for which crack size is the appropriate damage metric. Simple crack growth equations have been developed and experimentally characterized. These equations can be integrated, cycle by cycle, to predict life under general fatigue loading.

In contrast, Polymer Matrix Composite materials do not exhibit a single simple damage process since the damage accumulation process consists of a complex combination of matrix cracking, delamination and fiber fracture events. As a result, various life prediction methods have been proposed and used for polymeric matrix composite materials.

4.1 GENERAL BACKGROUND

The two macroscopic properties most often utilized as a measure of damage in polymeric woven composites are residual strength and residual stiffness. The theories based on residual strength degradation suffer from two major weaknesses. First, the remaining life cannot be assessed by non-destructive evaluations (NDE) and the second, they require extensive experimental characterization of each laminate and material system.

Various attempts have been made to overcome these problems. These attempts involve the formulation of fatigue theories based on damage parameters that lend themselves to measurement by NDE techniques and exhibit greater changes throughout fatigue life. One such parameter is the stiffness change, which changes monotonically throughout the fatigue life of composite laminates.

The recently proposed stiffness degradation fatigue theories are logical generalization of the residual strength degradation fatigue theories. These are based on the following assumptions.

The fatigue behavior and life of a laminate is controlled by the fatigue response of critical load carrying elements in the laminate. For a fiber-dominated laminate containing 0° plies, the critical elements are 0° plies. The fatigue behavior of the critical elements is governed by a fatigue theory based on residual strength degradation.

The stiffness changes of the laminate during cyclic loading causes internal load redistribution in the laminate, thereby, changing (usually increasing) the magnitude of the cyclic load imposed on the critical element. The primary advantage of residual stiffness is that it can be readily obtained through a fatigue test. Most of the researchers have focused on elastic modulus as a pertinent measure of the damage state. Poursartip et al [53] pointed out that elastic modulus is particularly attractive because as a fourth order tensor, it offers the possibility of distinguishing and monitoring different components of damage. Similarly, Wang and Chim [54] proposed a similar model based on stiffness degradation in short fiber composites. A parameter D (damage) was introduced to describe quantitatively the degree of homogenous fatigue damage. A power law relationship was found between the rate of the damage development and fatigue loading cycles. The exponent in the damage growth law was related to the maximum applied stress.

Hwang and Han [55,56] presented the concept of 'Fatigue Modulus', which was defined as a slope of applied stress and resultant strain at a specific fatigue cycle. The

fatigue modulus concept was based on the assumption that fatigue modulus degradation rate follows a power function of fatigue cycles. An attempt was also made to find the relationship between fatigue modulus and elastic modulus but a correlation was found for limited domains of fatigue cycles. Yet, due to experimental complexities it has some drawbacks.

4.2 MATHEMATICAL MODEL

The fatigue damage accumulation law proposed here incorporates a scalar representation for damage, but admits an anisotropic evolutionary law. This model predicts the current damage state (as quantified by current stiffness) and a remnant life of a composite that has undergone known cyclic loading at a given temperature. This damage model is dependant upon applied multi-axial stress state, which can be reduced to uni-axial stress state. The model is also a function of the maximum applied fatigue stresses, the mean stresses, and temperature. The model is characterized by using the uniaxial fatigue life and stiffness degradation data of the plain weave woven Carbon fabric-reinforced composite employed in this study. The stiffness degradation curves for Class 1 $[0]_8$ and Class 2 $[0,0,45,-45]_s$ have been shown in figures 4.1-5.

Since damage is not a physical quantity which can be measured directly. Its quantitative evolution is linked to the definition of the variable chosen to represent the phenomenon. The damage is defined as

$$D = 1 - \frac{E}{E_o} \qquad \{0 < D < 1\} \qquad 4.1$$

Where E_o is the elastic stiffness of the material if it has no damage and E is the current stiffness. This implies that initial damage is zero at a point where $E = E_o$, but if initial damage is not zero, than equation 4.1 becomes;

$$D_i = 1 - \frac{E_i}{E_o} \qquad \{D_i < D < 1\}$$

Where E_i corresponds to the elastic modulus of the material with damage D_i Thus, if the Young's Modulus E_o is known, any measurement of the residual elastic stiffness can be used to determine damage.

To describe the evolution of damage, a power law relationship is employed. The general form of the evolutionary law is expressed, as a power function in terms of ϕ which is a function that can account for multiaxial cyclic stress state, but it can also be used for the uniaxial stress state as in our present case. The evolutionary law is also a function of the current state of damage. The function ϕ is dependant on the maximum cyclic stress and cyclic mean stress. The damage rate is expressed as

$$\frac{dD}{dN} = A\frac{\phi^c}{B(D + D_i)^{\beta-1}} \qquad 4.2$$

Where D_i is the initial damage state and A,B and C are material constants. The functional dependence of ϕ is stipulated as the difference between a function F evaluated at two different stress states i.e.,

$$\phi = \left[F\left(\sigma^*_{max}, \sigma^*_U\right) - F\left(\sigma^*_{mean}, \sigma^*_U\right)\right] \qquad 4.3$$

The vectors σ^*_{max} and σ^*_{mean} have components dependant on the maximum cyclic stresses (σ_{Lmax}, σ_{Tmax}, τ_{LTmax}) and similarly cyclic mean stresses (σ_{Lmean},

σ_{Tmean}, τ_{LTmean}) respectively where L & T are longitudinal and transverse axis of the material. The vector σ^*_U represents respective ultimate values.

The function F in (4.3) defines the monotonic failure surface. Actually ϕ utilizes the monotonic failure function to obtain a scalar representation of the stress state. Therefore, when stress state moves closer to monotonic failure surface the damage rate accumulation increases. For monotonic failure function, we use Hill's failure theory. Utilizing Hill's definition for multiaxial failure, the function F is defined as

$$F = \left(\frac{\sigma_L}{\sigma_{LU}}\right)^2 + \left(\frac{\sigma_T}{\sigma_{TU}}\right)^2 - \left(\frac{1}{\sigma^2_{LU}} + \frac{1}{\sigma^2_{TU}} - \frac{1}{\sigma^2_{ZU}}\right)\sigma_L\sigma_T + \left(\frac{\tau_{LT}}{\tau_{LTU}}\right)^2 \qquad 4.4$$

This is reduced to Function F for uniaxial stress state (in present case)

$$F = \left(\frac{\sigma_L}{\sigma_{LU}}\right)^2$$

So the final form of stress state function ϕ is given as

$$\phi = \left[\left(\frac{\sigma_L}{\sigma_{LU}}\right)^2\right]_{max} - \left[\left(\frac{\sigma_L}{\sigma_{LU}}\right)^2\right]_{mean} \qquad 4.5$$

Hill's theory stipulates that for plane stress environment the monotonic failure initiates when F = 1.

Damage evaluation is obtained by integrating (4.2) at D = D_i, N = 0 ; D = D, N = N.

$$\int_{Di}^{D} \frac{dD}{dN} = A\int_{0}^{N} \frac{\phi^c}{B(D+D_i)^{B-1}}$$

$$B\int_{D_i}^{D}(D+D_i)^{B-1}dD = A\phi^C\int_0^N dN$$

Let $D+D_i = S$ which gives $dD = dS$ and the limits,

When $D = D_i$, $S = 2D_i$; $D = D$, $S = D + D_i$

$$B\int_{2Di}^{D+Di} S^{B-1}dS = A\phi^C\int_0^N dN$$

Integrating,

$$(D+D_i)^B - (2D_i)^B = A\phi^C N$$

$$(D+D_i)^B = A\phi^C N + (2D_i)^B$$

$$D = \left[A\phi^C N + (2D_i)^B\right]^{\frac{1}{B}} - D_i \qquad 4.6$$

At the end of fatigue life the damage parameter reaches a critical value i.e.,

$D = D_i + D_{critical}$ 4.7

Combining (4.6) and (4.7) and solving for N_f yields the estimates of the fatigue life of the composites as;

$$N_f = \frac{(D_{critical} + 2D_i)^B - (2D_i)^B}{A\phi^C} \qquad 4.8$$

The reduced form of the model when $D_i = 0$ is as;

$$N_f = \frac{(D_{critical})^B}{A\phi^C}$$

Since the stage II in stiffness degradation, is linear, and accounts for almost the entire fatigue life (as shown in figures 4.1-5), it is reasonable to model damage to this stage only. The linear behavior shows that current level of stress does not affect the degradation rate. In other words, the relationship of stress with damage accumulation

is linear. To eliminate the dependence of current level of damage, the constant B will be taken as equal to 1. The final equation for estimation of fatigue life becomes;

$$N_f = \frac{D_{critical}}{A\phi^C}$$

It was also found that modulus degradation behavior is independent of temperature so we can utilize all the fatigue data to find the values of the constants. The Log (stiffness degradation rate dD/dN) at all temperatures were plotted as a function of the log of stress state function ϕ as shown in Figure 4.6. The constant A represents the inverse log of the intercept and constant C represents the slope of the line. Regression analysis, of the data in Figure 4.6, yields the model constants for Class 1 $[0]_8$ material system as;

$A = 0.0578$

$B = 1$

and $C = 21.107$

The fatigue life data showed a significant shift in cycles to failure because of change in temperature. This temperature dependence is a result of change in material's tolerance to damage. To account for this temperature effect a parameter ***Critical Damage*** is defined that corresponds to the lowest stiffness value on the stage II portion of the modulus degradation curves as shown in figure 4.1. This critical damage indicates the normalized stiffness value at which damage accumulation shifted to catastrophic failure. This parameter indicates the ultimate limit of damage accumulation that occurs through the fatigue life. A linear relationship was obtained for $D_{critical}$ verses ϕ at all temperatures. It is evident from experimental values of $D_{critical}$ that it is function of both stress and temperature i.e., $D_{critical} = f(T, \phi)$. The linear

and independent relationship of temperature and stress factor ϕ was defined by Gyekenyesi [44] as:

$$D_{critical} = P(T) + Q\phi \qquad 4.9$$

Who used this model for fully reversed fatigue behavior. The above equation describing the critical damage was used for class 1 $[0]_8$ and class 2 $[0,0,45,-45]_s$ lay ups.

It was found that slopes of the regression lines fitted through the data points at different temperatures were almost same as shown in figure 4.7, but the intercept values were a bit scattered. To find a linear relationship, the intercepts in figure 4.7 were plotted against temperature as shown in figure 4.8. A linear regression provides the dependence of P on temperature. The final values of P and Q for class 1 $[0]_8$ and class 2 $[0,0,45,-45]_s$ are given in table 3.

CHAPTER 5

RESULTS AND DISCUSSION

5.1 MONOTONIC PROPERTIES

The results of all tensile tests are presented in tabular form in table 2. A graphical representation of conventional σ - $\in$ curve for Class 1 $[0]_8$ specimens tested at various temperatures (0°C, room temperature, and 100°C) is shown in figure 5.1. An examination of the test results for Class 1 $[0]_8$ indicates that there is slight improvement in elastic modulus at 0°C. This change is, although, just 5-6% of the modulus value over 100°C. The average values of elastic modulus at 100°C and room temperature are almost similar for Class 1 $[0]_8$. The tensile strength also shows a slight improvement at 0°C as compared to room temperature values.

Few tensile tests were also carried out at room temperature in transverse direction of the woven CFRP. It was found that monotonic properties are similar in

transverse direction for woven CFRP. These results indicate that woven laminates show similar mechanical properties in both longitudinal and transverse directions, and hence reduces the anisotropy of the laminate. It was also noted that monotonic properties of unidirectional Class 1 $[0]_8$ laminates are higher than the angle plied laminates (see table 2).

In Class 1 $[0]_8$ laminates longitudinal fibers are the only load carrying elements under monotonic loading. So the failure of the material starts from fiber fracture of least strength. The ever-increasing load causes these fibers to fracture randomly throughout the gauge section. What happens after fiber damage depends upon the applied stress and the remnant strength of the material. The fiber fracture is followed by the failure of the fiber/matrix interface. The strength of the interface is critical because it impedes the failure to next weaker fibers. Once this interface fails to stop the propagation of fracture then immediately other weaker fibers, which are in the vicinity break, they face a substantial increase in applied stress due to decrease in load carrying cross section. The number of broken fibers increases continuously until the gauge cross-section is substantially reduced and is no longer able to support the applied load any further. This incessant process results in the catastrophic fracture of the composite.

Since the fracture under tensile loading is mainly dependant on the strength and stiffness of the fibers, which show excellent thermal stability, therefore, temperature change is not expected to affect the monotonic properties of the composite. An examination of figure 5.1 indeed confirms that no discernible difference in the tensile strength and elastic modulus is observed at different

temperatures for Class 1 $[0]_8$. These results are in accordance with some previous findings [40,44,48].

The fiber/matrix interface is susceptible to temperature change. We can see a slight change in Elastic Modulus from 0° C to 100°C in Class 1 $[0]_8$ (table 2). At lower temperature, the fiber/matrix bonding becomes somewhat stronger, which thwarts the propagation of fiber breaking sequence for some time. But this change in fiber/matrix bond strength is minimal which is evident from the change in Elastic Modulus (E) values at non-ambient temperatures. It can thus be concluded that there is no significant effect of temperature on the monotonic properties of Woven Carbon Fabric-reinforced Plastics at elevated (below T_g) and sub-room temperatures.

Damage characterization of tensile specimens with Scanning Electron Microscope shows a discernable difference in fiber/matrix interface adhesion with temperature. Figure 5.2 (A) shows a flat fracture in Class 1 $[0]_8$ at 0°C, which is a characteristic failure pattern for uni-directional laminates. But a prominent feature to note here is that the fibers of weft bundle show a strong adhesion with matrix as evidenced by chunks of matrix that apparently remain glued to the fibers in the weft bundles. This observation is quite in agreement with the findings of Yoji Matsuhisa et al [48]. However at 100°C Figure 5.2 (B), a ductile fracture surface morphology and clean fiber surface indicates a weak fiber/matrix adhesion, and a more ductile cracking of the matrix. Lack of strong adhesion is expected to result in the inability of the matrix to transfer the load as effectively at elevated temperature as 0°C and results in producing a large amount of transverse cracks. At room temperature fiber/matrix interface behaves somewhat in between the above two cases as shown in figure 5.2

(C). These three figures indicate quite well that apart from matrix, temperature has no significant effect on the strength and stiffness of the composite.

5.2 FATIGUE TEST RESULTS

As discussed earlier, damage mechanism in CFRPs is actually a multimode phenomenon. The causative sequence of micro damage development in composite laminates can be thought of as a process of initiation and successive localization of the damage, which includes initiation of primary matrix crack, fiber fracture, local debonding, secondary cracking and delamination. Temperature is expected to play a significant role in such a damage initiation and localization process. In the following sections the results of fatigue testing carried out on Class 1$[0]_8$ and Class 2 $[0,0,45,-45]_s$ WCFRP laminates at various temperatures are presented and discussed.

5.2.1 GENERALIZED FATIGUE BEHAVIOR

The results of all the fatigue tests conducted in this study are provided in tabular form in tables 4 and 5, a graphical representation of the results in the form of S-N curves are provided in figures 5.3 and 5.4 for Class 1 $[0]_8$ and Class 2 $[0,0,45,-45]_s$, respectively. The lines drawn through the data points are the best-fit regression lines. As can be seen from these figures, the S-N curve is rather flat, which indicates that small increases in the stress levels brings about a severe reduction in fatigue life. A change in the maximum applied stress from 365 MPa to 410 MPa reduces the fatigue life from 2×10^6 cycles to just 83,254 cycles at 0°C. An examination of the fatigue results for both classes at non-ambient temperatures indicates that temperatures significantly affect the fatigue life of WCFRP. It is found that the fatigue life is inversely proportional to temperatures. An increase in temperature from the sub zero temperature of –20°C to +150°C severely

reduces the fatigue life of the Class 1$[0]_8$ laminates. This reduction in fatigue life is observed to be much more pronounced at high stress levels, and the effect gradually diminishes at low stress levels. At 100°C more than 2 orders of magnitude reduction in fatigue life is observed at 380 MPa as compared to room temperature. Compared to –20°C, the life at 100°C is lowered by as much as 4 orders of magnitude. At 150°C the fatigue strength is severely lowered from 400 MPa to 250 MPa at a life of 1 x 10^6 cycles. The detrimental effect of temperature on fatigue life gradually tapers off in the lower stress (high cycle) region. At the applied maximum stress of 365 MPa the fatigue life is lowered by only a factor of 5 as compared to an over 2 order of magnitude lowering of fatigue life at 380 MPa.

A decrease in fatigue life with increasing temperature, and improved fatigue life at sub-room temperature was also observed for Class 2 $[0,0,45,-45]_s$ laminates. The lowering of the fatigue life could be related to an apparent decrease in the fiber-matrix bond strength with increasing temperature. At sub zero temperatures (–20°C and 0°C) strong adhesion between the fiber and matrix makes it difficult for the transverse cracks to induce delamination parallel to the warp bundles. The evidence of the decrease in the fiber matrix bond strength with increase in temperature is presented later in the next section.

The results of fatigue tests carried out for class 2 $[0,0,45,-45]_s$ are shown in table 5. It can be seen that fatigue performance is significantly affected by change in ply stacking. Class 1 $[0]_8$ composites having all plies in the 0° direction show substantially high fatigue strengths as compared to class 2 $[0,0,45,-45]_s$ orientations (see tables 4 and 5). It highlights the effect of stacking sequence on fatigue life of

plain weave woven carbon fabric-reinforced composite. It was reported earlier that ultimate tensile strength of Class 2 $[0,0,45,-45]_s$ is lower than the Class $1[0]_8$ composites. Now we note that fatigue strength of Class 2 $[0,0,45,-45]_s$ is also lower than the Class $1[0]_8$, but it can be noticed that maximum applied stress for Class 2 $[0,0,45,-45]_s$ is a higher fraction of ultimate tensile strength i.e., 80-85%, whereas, in Class $1[0]_8$ it ranges from 75-80% of ultimate tensile strength.

5.2.2 FATIGUE DAMAGE DEVELOPMENT

The two main characteristics of WCFRP composites, which have a major influence on the manner in which fatigue damage occurs are the inhomoginity and anisotropy of the composite laminates. Inhomogenity contributes greatly to progressive deterioration by a damage localization process. Local damage events like matrix cracking, debonding, and, localized ply separation play the role of damage initiators. However, damage growth is severely inhibited by the presence of adjacent plies or adjacent matrix phases due to their different properties and responses. In fact, this constraint on damage growth forms the basis for a progressive localization and intensification of damage in a successively smaller volume of material as load cycling continues. This localization process is repeated throughout the laminates at different locations. The anisotropy also has a major influence on damage development. The most obvious effect is the influence of complex stress state associated with reinforcement phases. These reinforcements may be aligned or arranged in some geometric fashions, which result in a directional dependence of the mechanical properties of the composite systems.

Figure 5.5 schematically shows different stages of damage development in CFRPs. There are four basic stages in the composite laminates, primary transverse crack formation, secondary cracking, delamination, and fiber fractures. In all types of FRPs the matrix crack is expected to initiate in plies, which experience tensile stress excursions in directions parallel to the fibers. If these stress excursions, exceed in amplitudes to the level sufficient to cause failure of matrix material present between the fiber bundles, transverse matrix cracks are introduced. In Class 1 $[0]_8$ laminates these primary matrix cracks are produced in the entire section of the laminate. These primary matrix cracks are saturated at the end of stage I of modulus degradation curves (figures 4.1-5), but continuous cyclic loading causes secondary cracks in warp bundles at tow cross over points. These secondary cracks in warp bundles cause fiber debonding/splitting. This is the time when some delamination in warp and weft bundles starts growing. As soon as delamination starts growing the saturated primary matrix cracks, become unstable and start growing. The fiber splitting in warp bundles cause fiber fracture in warp bundles. This occurs so rapidly that laminates fail almost catastrophically and there is no significant decrease in stiffness. It is noted that fatigue fracture in Class 1 $[0]_8$ is almost flat, which also provides additional evidence of catastrophic failure of warp fiber bundles. Fracture surface morphology is similar to the work reported by Khan et al [11]. The temperature affects the fiber/matrix interface bonding and strength of matrix against tensile stress excursion in fiber bundles parallel to applied load. As we can see the modulus degradation curves are almost similar at all temperatures, thus the temperature seems to only affect the formation of primary matrix crack and delamination growth rates. This is why at

higher temperatures modulus degradation is more severe than at sub-room temperatures and the value of $D_{critical}$ is also lower that indicates the final stage of damage accumulation after some delamination.

An optical photomicrograph in Figure 5.6 shows multiple cracks in off-axis plies and the induced delamination in Class 1$[0]_8$ composite system. Figure 5.7 shows a transverse matrix crack that has induced delamination in Class 1$[0]_8$ composite specimen. Figures 5.8 presents an optical view of the edge of a Class 1$[0]_8$ specimen fatigued at room temperature. Figure 5.8 (A,B) show the ply delamination at 50 and 70% of fatigue life, respectively.

In class 2 $[0,0,45,-45]_s$, the initiation process is somewhat different due to the presence of angle plies. The series of damage events that take place in class 2 $[0,0,45,-45]_s$ are mainly initiated by shearing of 45° plies. Initially Transverse Matrix Cracks (TMCs) appear through the weft of 0° fiber bundle, which is at 90° to the loading direction. These TMC travel inward from the edge of the composite and this process proceeds with cyclic loading similar to Class 1 $[0]_8$ shown in figure 5.7. Subsequently the fibers in the 45° ply start splitting in the transverse direction. Upon further cyclic loading these cracks link up with the neighboring 90° weft cracks, which are actually at –45° to the applied load. When these cracks merge, they start to jog to other similar cracks creating ultimately a major edge delamination. This delamination grows in both directions parallel and perpendicular to the applied load. This delamination growth is much faster and more severe at the points where stacking sequence changes, e.g. in class 2 $[0,0,45,-45]_s$ severe delamination is observed (Figure 5.22) between 0° and 45° plies. The final failure of 0° plies is similar to unidirectional Class 1 $[0]_8$

laminates as shown in the Figures 5.21. The damage mechanism is accelerated or retarded by temperatures but there were no major change in damage events. The fiber/matrix interface that is supposed to be dependent on temperature, plays a role in formation of primary matrix cracks.

The second major type of micro-damage event, which occurs in damage development of Class 1 $[0]_8$, is local delamination. This local delmination causes the intersection of primary, and secondary cracks. Such evidence on a microscopic scale has been substantiated by X-ray radiographs shown in Figure 5.9-13. The third and the most critical event is the consequence of above mentioned two events. This is the fiber splitting in 0° plies which is immediately followed by fiber fracture of warp bundle in almost a flat plane.

Hence, the causative sequence of micro damage development, in a fiber reinforced composite laminate under tensile fatigue loading, can be thought of as a process of initiation and successive localization. It includes initiation of primary matrix cracks, local debonding, secondary cracking, fiber fractures, and local delamination which becomes more and more concentrated in a small region around the intersection of primary and secondary cracks.

5.2.3 DAMAGE CHARACTERIZATION THROUGH X-RAY RADIOGRAPHY

In order to study the internal damage, enhanced dye penetrant X-ray radiography was conducted on a number of specimens fatigued at various temperatures. Fatigued specimens were injected with a solution of ZnI_2 in 2-Propanol and water with a hypodermic syringe (details are given in chapter 3). The Zinc Iodide

provided the needed opacity to the X-rays and enhances the contrast. Radiographs were taken by Seimens Polyphos-30 equipment operating at 40 KV and 0.02 mA/sec with Kodak TME (100NIF) film.

Figures 5.9-12 show X-ray radiographs of Class 1 $[0]_8$ composite laminate specimen after fatigue testing at various temperatures. Figure 5.9 shows the difference of fatigue failure at room and sub-room temperatures at the same applied stress. Figure 5.9 (a, b and c) represents the failure at room temperature, -20°C, and 0°C, respectively. As is evident from the radiographs, noticeable amount of ply delamination occurs in the specimen fatigue at room temperature, whereas, at –20°C and 0°C, the failure occurs without discernible ply delamination. In order to make sure that the delamination found in the specimen fatigued at room temperature shows the damage that actually occurs during the cyclic loading and is not related to the final stages of tensile failure, a few run out specimens were also examined. As can be seen from figure 5.10 evidence of ply delamination is obvious in the run out specimens suggesting that ply delamination occurs during cyclic loading predominantly at room temperature. Figure 5.11 represents the change in damage behavior at three different temperature levels (0°C, 24°C, 100°C) for Class 1$[0]_8$ specimens. Figure 5.11 (a, b and c) show the specimens failed at different stress levels at 100°C, while; 5.11d and 5.11e show specimen at room temperature and 0°C, respectively, at the same stress level as in 5.11a. A clear change in the damage behavior can be noted, and the effect of temperature on ply delamination is evident for Class 1$[0]_8$. Figure 5.12 shows the specimen tested at 150°C i.e., above Glass Transition (T_g) of epoxy matrix. A very severe matrix degradation and ply delamination can be noted.

The results of these X-ray radiographs can be summarized as follows: the damage sequence in Class 1 $[0]_8$ is almost same at all test temperatures. The primary matrix cracks are the initiators of fracture at all test temperatures. The local debonding, which is actually a reason for delamination growth at cross over points, is significantly affected by temperature. At lower temperatures, the delamination growth is almost negligible and final fracture is very catastrophic by fracture of fibers in warp bundles. At higher temperatures, local debonding and delamination growth is higher and laminates fail after noticeable modulus degradation as discussed in the preceding sections. At temperature higher than Glass Transition (T_g) of epoxy resin, severe matrix degradation occurs, which appreciably reduces fatigue life.

Figure 5.13 (a,b,c) shows the results of class 2 $[0,0,45,-45]_s$ specimen fatigue tested at 0°C, room temperature, and 100°C, respectively. The fracture occurs due to extensive delamination. At 100°C the delamination between 0° and 45° plies is much severe at room temperature. At 0°C the amount of ply delamination further decreases, and the final fracture appears to be much flat, indicating that fiber fracture is more dominant than delamination at 0°C.

5.2.4 DAMAGE CHARACTERIZATION THROUGH FRACTROGRAPHY

Fracture surface morphology of fatigue fractured specimens was studied by Scanning Electron Microscope (SEM). The complexity of woven structure and damage in class 2 $[0,0,45,-45]_s$ are shown in figure 5.14. It was found that the damage process in class 2 $[0,0,45,-45]_s$ is much complex than the Class 1 $[0]_8$. The simpler

damage mechanism in Class 1 $[0]_8$ is mainly dominated by transverse matrix cracking and fiber fracture, as seen in figure 5.15.

In Class 1$[0]_8$ transverse primary matrix cracks are formed because weft fiber bundles are non-load carrying members and the only load carrying element in these bundles is the surrounding matrix. These transverse matrix cracks (TMCs) start growing with cyclic loading, but final fracture of laminate takes place when some of these cracks linkup together and cause a sudden increase in damage accumulation rate. These TMCs in weft bundles initiate catastrophic fiber fracture in warp bundles as shown in Figure 5.15. Figure 5.16 indicates that before the final failure primary cracks at cross over points initiate local debonding and local delamination. Further evidence of the local debonding and delamination is provided in figure 5.17 and 5.18. The final damage event, which occurs just before final fracture, is fiber splitting in warp bundles initiated by local delamination as shown in figure 5.19. The local debonding and fiber splitting some times caused cracking of weft bundles in vertical plane as shown in figures 5.20-21.

Figure 5.16 also shows cusp formation, which indicates that a significant amount of shear occurs during transverse matrix crack. The orientations of these peel cusps are assumed to indicate the direction of crack propagation. The coarseness of these cusps suggests the extent of ply separation and fiber/matrix interface strength.

Figure 5.22 shows a complete delaminated region between 0° and 45° plies in class 2 $[0,0,45,-45]_s$ CFRP specimen. The fracture can be observed to have occurred after extensive delamination. Similarly 45° and –45° fiber bundles can be seen separated due to substantial interfacial delamination due to shearing of the plies (see

figure 5.23). Figure 5.22 also indicates that 0° plies fail in almost a flat fracture manner similar to the fracture in Class 1$[0]_8$. Whereas, the fiber bundles of angle plies fracture in a manner that creates a serrated fracture surface. Figure 5.24 shows the low magnification view of fiber breakage and interfacial delamination in angle plies. It can be noted that fractured fibers carry few matrix debris on the surface indicating fiber/matrix debonding before fracture.

It has been discussed earlier that temperature does not affect the sequence of events in both class of laminates. It only affects the damage initiation and damage accumulation rates. The two main damage players are the matrix behavior as a whole and fiber/matrix interfacial strength. The change in matrix damage with temperature is presented in Figures 5.25-27. These figures show matrix crack at –20°C, room temperature, and 100°C respectively for Class 1$[0]_8$ specimens. Presence of smaller hackles and a rather flat fracture surface indicate that the ductility of the matrix is appreciably reduced at 0°C, and –20°C (see figure 5.25). A more ductile matrix cracking with blunt crack and undulations on matrix surface (figure 5.27) provides evidence that the matrix behaves in much more ductile manner at 100°C.

The fiber/matrix interface strength is also a function of temperature. Figures 5.28-31 show fracture surface morphology of the matrix surrounding the weft bundles, for –20°C, 0°C, 100°C, and 150°C, respectively for Class 1 $[0]_8$ laminates. The small cusps on fracture surface in figure 5.28 and 5.29 show that a strong interfacial bonding existed between matrix and the fibers at 0°C and –20°C. On the other hand, in figures 5.30 and 5.31 the size of cusps indicates a weak fiber-matrix bonding at 100°C

and 150°C. In fact at 150°C, fibers seem to have completely debonded from matrix and tore off at final failure (figure 5.31).

Similarly, the effect of temperature on fiber/matrix interface strength of warp fiber bundles at various test temperatures shown in figures 5.32-35. Figure 5.35 show that almost a complete degradation of the matrix has occurred at 150°C. Figure 5.34 shows the clean surface of warp fibers, whereas; figure 5.32 and 5.33 showing small pieces of matrix with fibers indicating strong interfacial bonding. The week interfacial strength causes extensive delamination in Class 1 $[0]_8$, while; at lower temperature only local delamination occurs as shown in figure 5.36 and 5.37 respectively.

5.3 FATIGUE LIFE PREDICTION

The analytical model described in chapter 4 was used to predict the fatigue life of plain weave woven Carbon Fiber-reinforced Composite Plastic subjected to cyclic loading at various temperatures. As it was mentioned earlier, that the analytical model was based on Elastic Modulus degradation that accounts for fatigue damage accumulation during the cyclic loading. The parameter $D_{critical}$ that was introduced in chapter 4, indicates the least stiffness value in stage II. At the end of stage II final failure occurs and specimen lasted only 2-5% of total life. A series of fatigue tests were carried out at non-ambient temperature ranging from –20°C to 150°C to generate the experimental fatigue data.

5.3.1 STIFFNESS DEGRADATION RATE

The Stiffness Degradation was used as the basis for predictive model. Figures 4.1-5 are showing typical modulus degradation curves for class 1 $[0]_8$ and class 2 $[0,0,45,-45]_s$, which are normalized by initial modulus. As it is explained in figure 4,

the Modulus Degradation curve can be divided in to three stages. The first damage stage refers to the first 5-10% of fatigue life. This was followed by a linear second stage (constant degradation rate), which constitutes the majority of fatigue life. As final failure approaches, a dramatic increase in damage rate occurs in class 2 $[0,0,45,-45]_s$ as shown in figure 4.1. However, in Class 1 $[0]_8$ final failure occurs without such increase in damage rate. This increased damage rate is indicated by the sudden loss in modulus prior to failure.

The modulus degradation curves obtained at various stress levels and temperatures are generally similar and vary little in nature with changes in temperature, stress, or change in lay-up of composite. The temperature dependence of the modulus degradation rate with temperature is reflected in the change in the slope of stage II.

The stage I of Modulus Degradation curve indicates that maximum degradation in the stiffness occurs during this stage, but this stage is not very significant, because it accounts for only 5-10% of the total fatigue life. This reduction is attributed to several events that mark the early part of fatigue life. The first event that takes place is the straightening of the warp fiber bundles, which contributes to the strain in longitudinal direction. Second, the formation of transverse matrix cracks in the weft bundles and third, the shearing between the warp and weft bundles at cross over points. The cumulative contribution of all the above three events cause the longitudinal strains to sharply increase and hence lowers the modulus sharply. At the end of stage I, transverse matrix cracking saturates, and local debonding and local delamination begins at tow cross over points. This causes the onset of stage II. The

progress of the damage occurs at a constant rate and thus results in a constant rate of modulus degradation constituting the linear stage II portion in the modulus vs. number of cycles curve. As can be seen (from figure 4.1-5) stage II accounts for about 90% of the total fatigue life.

In stage II, matrix cracks, which were created in stage I continue growing. These matrix cracks in weft bundles cause delamination between warp and weft bundles at the crossover points. Delamination and matrix cracking is thus the dominant phenomenon in stage II. It is clear from Modulus Degradation curve for Class 1$[0]_8$ that failure is catastrophic in nature and stage III is indiscernible. The major contribution towards failure is strictly matrix cracking, interply delamination coupled with fiber splitting in 0° plies, and then sudden failure of these fiber bundles resulting in complete fracture. In class 2 $[0,0,45,-45]_s$ the final failure is indicated relatively early in fatigue life where the stiffness degradation is relatively gradual due to longitudinal crack growth and interply delamination of warp and weft bundles of 0° and +/- 45° laminas. In class 2 $[0,0,45,-45]_s$ the increase in the damage rate in the last 5% of fatigue life accounts for extensive delamination and fiber bundle splitting in warp bundles. In Class 1 $[0]_8$ this phenomenon is quite sudden and change in Modulus Degradation occurs so rapidly that it could not be recorded.

Figures 4.2-5 show the Modulus Degradation for Class 1 $[0]_8$ at various test temperatures. Modulus Degradation behavior is quite similar at all temperatures but slope and length of stage II is different. The slope of stage II is shallower at 100°C than at room temperature and sub-room temperatures. Furthermore, the location of stage II in Modulus Degradation curve is also different at various temperature ranges.

At 100°C the stage II starts at lower modulus values than room and sub-room temperatures. This phenomenon accounts for lower $D_{critical}$ values used in predictive model. It can be explained due to higher fibers/matrix displacement and matrix cracking in early part of fatigue life.

Figure 5.38 shows a comparison of Modulus Degradation in specimens tested at 0°C and 100°C at the same stress levels. Notice that normalized moduli degrade at different rates. The degradation rate for coupon tested at 100°C is higher than at 0°C. That is why coupon tested at 100°C failed much earlier than the coupon tested at 0°C temperatures. In the analytical model used in this investigation, $D_{critical}$ accounts for such an observation. Our methodology discussed in chapter 4 involves the stage II of Modulus Degradation, because this stage accounts for the major portion (about 90%) of the total fatigue life.

5.3.2 DAMAGE RATE

The damage rate dD/dN as obtained from Modulus Degradation data is plotted against the stress range $\Delta\sigma$ on a log-log scale for Class 1 $[0]_8$ (figures 5.39-41) and class 2 $[0,0,45,-45]_s$ (figures 5.42-44) for different temperatures. As can be seen from these figures, slight increment in the applied stress range causes a substantial increase in the damage rate. This clearly points at the sensitivity of WCFRP to fatigue damage by small changes in the applied stress levels. It can also be noted that damage rate for Class 1 $[0]_8$ is less sensitive than class 2 $[0,0,45,-45]_s$ at same temperature. A discernible increase in damage rate is, however, observed at elevated temperatures. The range of damage rate at elevated temperatures is higher than the sub-room temperatures. It shows the dependence of fiber/matrix interface strength on damage

rate. At higher temperatures the bond strength of this interface is deteriorated, which causes an increase in damage rate. At temperatures of 0°C or –20°C interfacial bonding is much stronger and, thus, the damage rate is lower than at elevated temperatures.

5.3.3 LIFE PREDICTIONS

The analytical model presented in chapter 4 was employed for predicting the fatigue life of CFRPs at various temperatures. The model is dependent upon some empirical material constants, which were obtained from experimental data. The details of these constants have been discussed in chapter 4. Stress factor ϕ, $D_{critical}$,and material constants A, B, C, P & Q are obtained from Figures 4.6-8. In addition to this, stress factor ϕ and $D_{critical}$ are obtained from equations 4.5 and 4.9 respectively. These relationships/parameters are different for each class of composite laminates.

The predicted lives obtained for Class 1 $[0]_8$ are reasonably good (within a factor of 2 to 3) for all temperatures considered in this investigation. Due to inherent nature of variability in fatigue a factor of two scatter in the experimental fatigue data is quite normal, and thus the predictions, which lie within a factor of 2, could be considered quite reasonable. The graphs in Figures 5.45-48 show plots of predicted fatigue lives verses experimental fatigue lives for specimens tested at various temperatures for Class 1 $[0]_8$. It can be seen that for Class 1 $[0]_8$ laminates tested at 0°C and –20°C the predicted fatigue life values lie mostly within a factor of 2 in both the conservative and non-conservative regions. At ambient conditions, in general, and at higher temperature (100°C) in particular, the data points lie mostly in the non-conservative band (but still mostly within the factor of 2).

As mentioned above our model is based on using linear portion of stage II in Modulus Degradation curve. This linear portion of modulus degradation curve represents the major portion (90%) of the fatigue life for high cycle fatigue situation. In this situation the initial drop in modulus (stage I) becomes insignificant because it represents only a relatively small portion of total fatigue life. However, in the case of low cycle (high stress) fatigue stage I represents a relatively larger portion of the fatigue life and should become significant. In fact in this fatigue region the use of the value B = 1 (which is quite justified for high cycle fatigue) can not be fully justified for low cycle fatigue case.

The second noticeable trend in predicted values are non-conservative region for data points at 100°C in particular. The parameter $D_{critical}$ is responsible for incorporating the effect of temperature in predicted value. We are taking a linear dependence of temperature while evaluating parameters P and Q for $D_{crcitical}$. At higher temperatures, the polymeric resin starts exhibiting visco-elastic behavior, which cannot be accurately modeled using the present approach. The predicted results for class 2 $[0,0,45,-45]_s$ shown in figures 5.49-51 are also reasonably good at all temperatures.

CHAPTER 6

CONCLUSIONS AND RECOMMENDATIONS

6.1 CONCLUSIONS

The following conclusions can be drawn from the analytical and experimental work carried out in this study.

- The monotonic properties of plain weave woven carbon fabric-reinforced plastics were found to be independent of temperature.
- The fatigue life of plain weave woven carbon fiber fabric-reinforced composite decreased with increase in test temperature from –20°C to 150°C. No discernible difference was noticed in the damage accumulation sequence, however, temperature had a strong influence on the damage accumulation rate
- The fiber/matrix interface strength was found to be a function of temperature

- Class 1$[0]_8$ WCFRP had higher fatigue life as compared to class 2 $[0,0,45,-45]_s$, which highlights the effect of stacking sequence on fatigue life of plain weave woven carbon fabric-reinforced composite
- Class 1 $[0]_8$ WCFRP showed lower stiffness degradation accompanied with small delamination, abundant matrix cracks, and catastrophic fiber fractures at the end of fatigue life.
- Delamination in class 2 $[0,0,45,-45]_s$ WCFRP was the major damage mode and was influenced significantly by the test temperature.
- A major decrease in fatigue life was noted at test temperature above Glass Transition (T_g) of matrix resin.
- Stiffness degradation model successfully predicted the fatigue life of WCFRP at all temperatures, and excellent predictions within a factor of 2 were obtained.

6.2 FUTURE WORK SUGGESTIONS

It is evident from the literature survey and from the results of this study that our understanding of fatigue phenomenon in woven CFRPs is still in its early stages. Substantial room for continued research exists to generate, analyze and understand the fatigue damage and development of reliable fatigue life prediction methodologies, especially under non-ambient

Following are few areas in which further research is needed:

- Comparison of fatigue response of woven and non-woven CFRPs, both at ambient and non-ambient test temperatures.

- Study of fatigue behavior of different weaves e.g., plain, satin etc both at ambient and non-ambient temperatures.
- Study of fatigue behavior at varying temperatures including the effect of different humidity levels.
- Effect of variable and random amplitude loading
- Effect of changing the processing parameters such as matrix resin, curing pressure and temperature during manufacturing and their effect on fatigue response at various non-ambient conditions.
- Incorporation of stress ratio and frequency effect into the Stiffness Reduction Model

Table 1: Neat epoxy resin and single ply prepreg mechanical and physical properties

Neat Epoxy Resin		Single Ply Prepreg	
Specific Gravity v	1.335 gm/cm^3	Tensile Strength σ_{uts}	848 MPa
Glass Transition T_g Dry	121°C	Elastic Modulus E	58 GPa
Tensile Strength σ_{uts}	80 MPa	Tensile strain $\in_t$	10.09%
Elastic Modulus E	3.24 GPa		
Tensile Strain $\in_t$	5.2%		
Fracture Toughness K_{IC}	$1.65Mpa(m)^{1/2}$		

Table 2: Tensile data for Class 1 $[0]_8$, and Class 2 $[0,0,45,-45]_s$ CFRP laminates

	Class 1 $[0°]_8$				Class 2 $[0,0,45,-45]_s$	
	Test at Room Temperature	**Test at 0° C**	**Test at 100 ° C**	**Transverse at Room Temperature**	**Longitudinal**	**Transverse**
Modulus GPa	43.1	44.3	36	39.1	32	
	37.3	40.4	45	38.4	32.2	33.3
	35.5				30.4	
	39.6				29.8	
	40.8					
	39.1					
Average	**39.2**	**42.3**	**40.5**	**38.8**	**31.1**	**33.3**
σ_{uts} MPa	489	580	552	537	347	
	483.4	486	472	607	412	413.55
	493.1				365	
	504				395	
	534.8					
	576					
Average	**513**	**533**	**512**	**572**	**380**	**414**

Table 3: Material constants evaluated from modulus degradation curves.

Model Constants	Mathematical Significance	Class 1 $[0]_8$	Class 2 $[0,0,45,-45]_s$
Material Constant **A**	Slope (dE/dN)	0.057	0.000131
Material Constant **B**	Linearity	1	1
Material Constant **C**	Inv Log (Intercept)	21.107	12.916
Material Constant **P** for Temperature dependence of $D_{critical}$	Intercepts $D_{critical} \sim \phi$	-0.0023(T) + 0.0316	-0.0032(T) – 0.13
Material Constant **Q** for Temperature dependence of $D_{critical}$	Slopes $D_{critical} \sim \phi$	1.39	1.57

Table 4: Experimental fatigue data for Class 1 $[0]_8$ CFRP

Room Temperature		*-20°C*		*0° C*		*100° C*		*150°C*	
Stress MPa	**Cycles**	**Stress MPa**	**Cycles**	**Stress MPa**	**Cycles**	**Stress MPa**	**Cycles**	**Stress MPa**	**Cycles**
350	1,685,000	380	1,711,085	365	2,000,000	350	2,000,000	250	1,796,325
365	1,200,365	390	608,586	365	2,663,254	365	1,156,340	260	932,561
380	875,200	390	856,235	380	863,258	365	896,325	265	463,254
380	676,580	400	223,456	380	1,356,328	370	658,320	270	67,823
390	259,634	400	153,663	390	397,870	370	543,817		
400	44,356	410	81,403	400	146,235	375	176,728		
400	1,200			410	83,254	380	425		
400	9,107								
410	292								
410	957								

Table 5: Experimental fatigue data for Class 2 $[0,0,45,-45]_2$ CFRP

Room Temperature		*0° C*		*100° C*	
Stress MPa	**Cycles**	**Stress MPa**	**Cycles**	**Stress MPa**	**Cycles**
315	1986323	320	1465329	290	2365215
320	1376258	330	1120365	300	1639850
330	963528	335	828963	310	1025638
335	756383	340	312582	315	763965
340	386325			320	423658
345	165327			325	298632

Table 6: Experimentally observed and predicted life data for Class 1 $[0]_8$ CFRP

Max. Stress MPa	Room Temperature		Max. Stress MPa	-20°C		Max. Stress MPa	0°C		Max. Stress MPa	100°C	
	Experimental Lives	Predicted lives		Experimental Lives	Predicted lives		Experimental Lives	Predicted lives		Experimental Lives	Predicted lives
350	1,685,000	4,491,759	380	1,711,085	1,044,607	365	2,000,000	2,144,986	350	2,000,000	3476,938
365	1,200,365	2,021,515	390	608,586	635,563	365	2,663,254	2,144,986	365	1,156,340	1583,754
380	875,200	939,479	390	856,235	635,563	380	863,258	994,546	365	896,325	1583,754
380	676,580	939,479	400	223,456	391,605	380	1,356,328	994,546	370	658,320	1227,211
390	259,634	573,111	400	153,663	391,605	390	397,870	605,824	370	543,817	1227,211
			410	81,403	244,202	400	146,235	373,704	375	176,728	954,129
						410	83,254	233,291	380		

Table 7: Experimentally observed and predicted life data for Class 2 $[0,0,45,-45]_s$ CFRP

Max. Stress MPa	Room Temperature		Max. Stress MPa	0°C		Max. Stress MPa	100°C	
	Experimental Lives	Predicted lives		Experimental Lives	Predicted lives		Experimental Lives	Predicted lives
315	1,986,323	1,447,322	320	1,465,329	1,313,009	290	2,365,215	2,565,344
320	1,376,258	1,203,278	330	1,120,365	912,232	300	1,639,850	1,760,641
330	963,528	838,620	335	828,963	763,456	310	1,025,638	1,221,284
335	756,383	702,901	340	312,582	640,625	315	763,965	1,021,070
340	386,325	590,651				320	423,658	855,796
345	165,327	497,560				325	298,632	719,011

Table 8: Stiffness reduction and damage rate data for Class 1 $[0]_8$ CFRP

Room Temperature				-20°C			
Max. Stress MPa	*Normalized Modulus Reduction*	*Stress Amplitude Δσ MPa*	*Damage Rate dD/dN*	*Max. Stress MPa*	*Normalized Modulus Reduction*	*Stress Amplitude Δσ MPa*	*Damage Rate dD/dN*
350	0.8596	157.5	3.28E-08	380	0.84058	171	1.17E-08
365	0.86147	164.25	6.86E-08	390	0.869	175.5	1.14E-07
380	0.8853	171	8.81E-08	400	0.9044	180	5.26E-07
390	0.8934	175.5	7.75E-07	410	0.902174	184.5	5.22E-07
0°C				100°C			
Max. Stress MPa	*Normalized Modulus Reduction*	*Stress Amplitude Δσ MPa*	*Damage Rate dD/dN*	*Max. Stress MPa*	*Normalize d Modulus Reduction*	*Stress Amplitude Δσ MPa*	*Damage Rate dD/dN*
365	0.857	164.25	1.82E-08	350	0.7681	157.5	1.22E-08
380	0.862	171	3.33E-08	365	0.7753	164.25	2.38E-08
400	0.90	180	3.55E-07	370	0.8115	166.5	4.21E-08
410	0.9523	184.5	1.45E-06	375	0.8442	168.75	6.51E-08

Table 9: Stiffness reduction and damage rate data for Class 2 $[0,0,45,-45]_s$ CFRP

0°C				100°C				Room Temperature			
Max. Stress MPa	Normaliz-ed Modulus Reduction	Stress Amplitud e Δσ MPa	Damage Rate dD/dN	Max. Stress MPa	Normaliz-ed Modulus Reduction	Stress Amplitude Δσ MPa	Damage Rate dD/dN	Max. Stress MPa	Normaliz-ed Modulus Reduction	Stress Amplitude Δσ MPa	Damage Rate dD/dN
320	0.9189	144	1.96E-07	280	0.7189	126	8.15E-08	320	0.786	144	2.33E-07
330	0.9517	148.5	4.81E-07	290	0.7428	130.5	2.72E-07	330	0.8023	148.5	2.97E-07
335	0.9681	150.75	1.27E-06	300	0.763	135	3.73E-07	335	0.8265	150.75	3.05E-07
340	0.98	153	4.09E-06	310	0.79	139.5	7.76E-07	340	0.8532	153	1.94E-06
				315	0.8014	141.75	1.71E-06				

a)

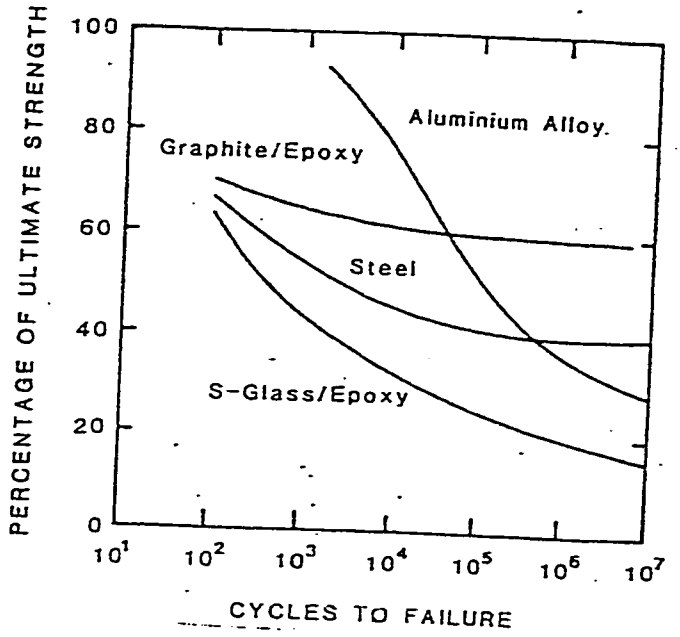

b)

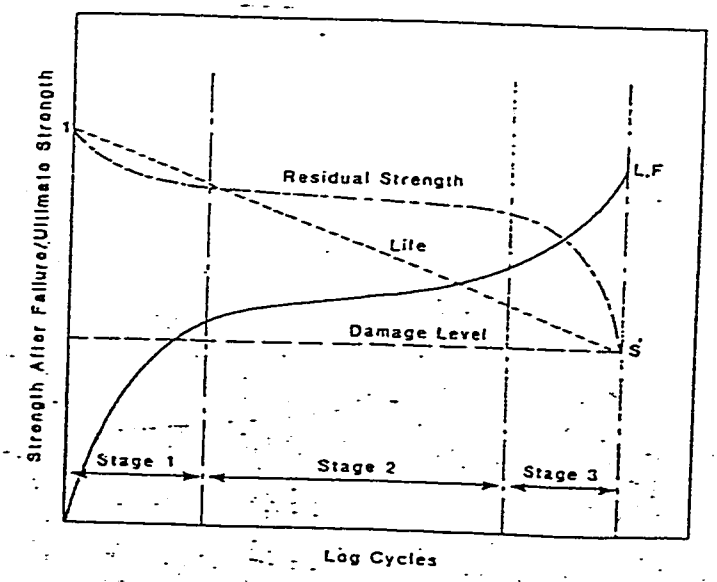

Figure 2.1: a) Tension-Tension Fatigue life characteristics of composite materials and typical metals.
b) Strength reduction and damage development in CFRPs [1]

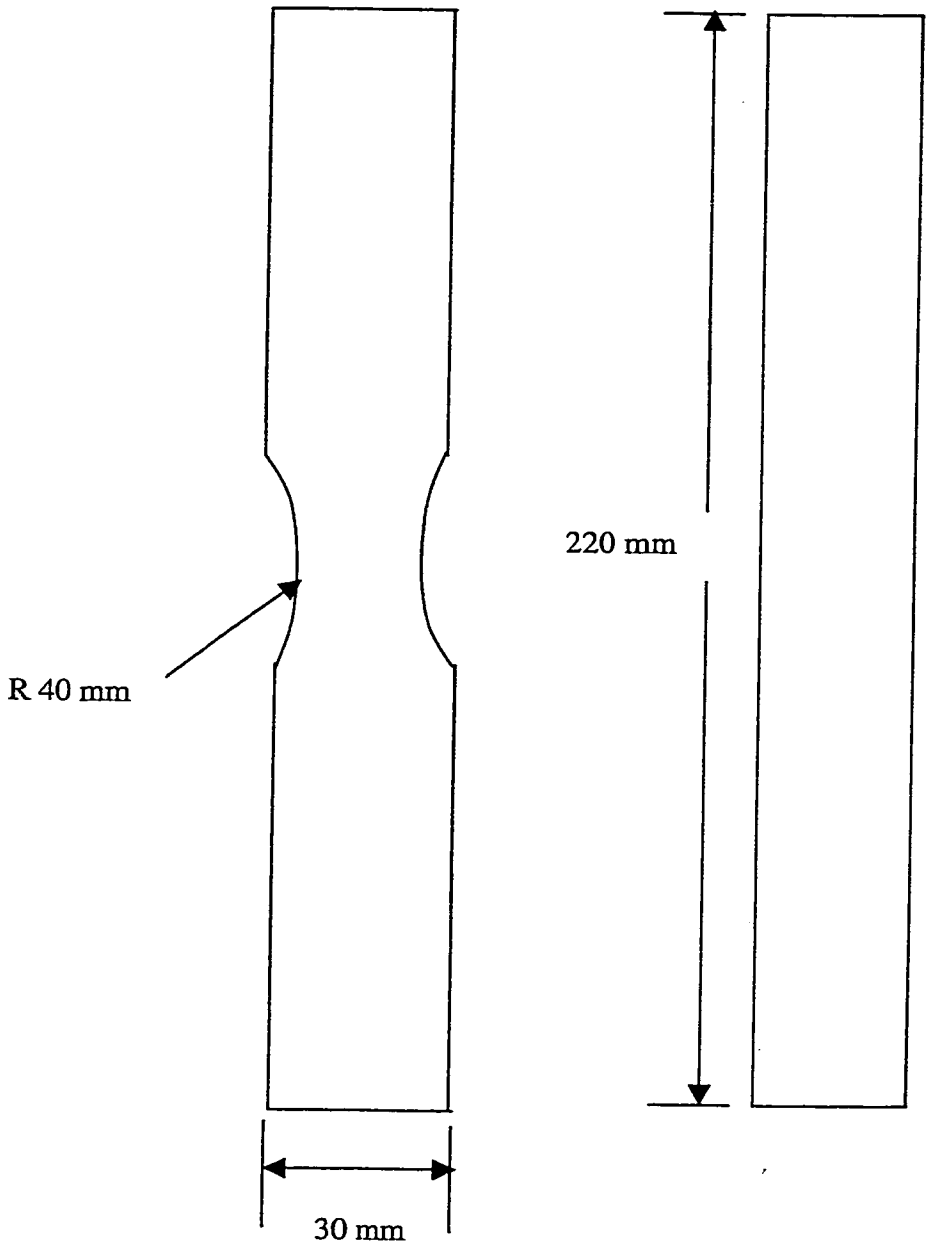

Figure 3.1: Carbon Fiber-reinforced Composite coupons for Fatigue (A) and Tensile Tests (B)

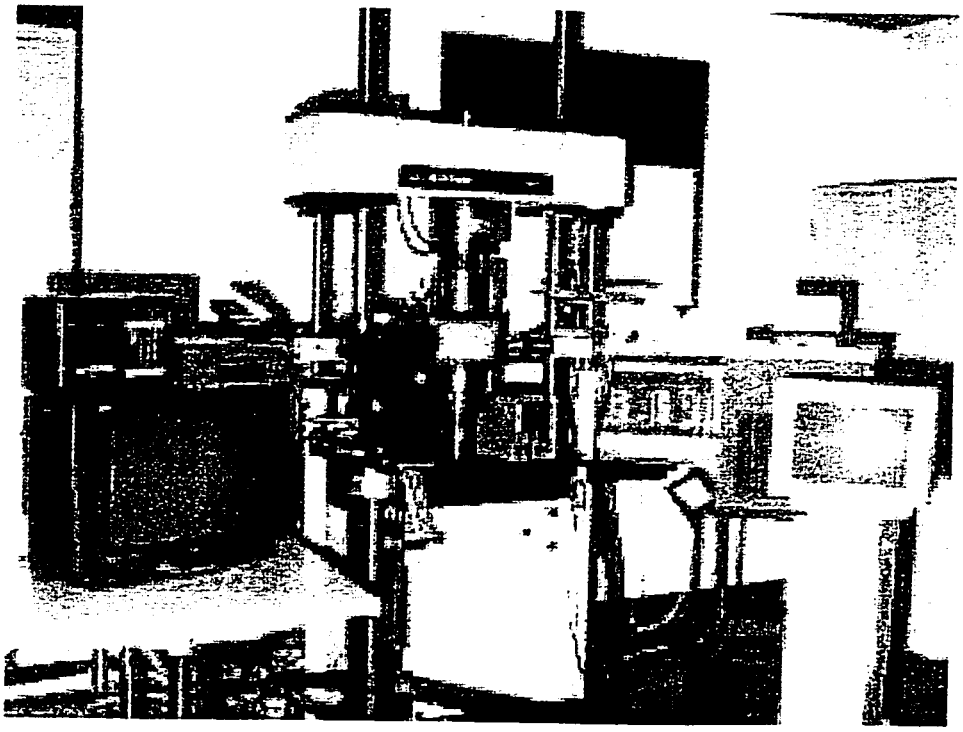

Figure 3.2: Instron 8501, servo-hydraulic material testing system

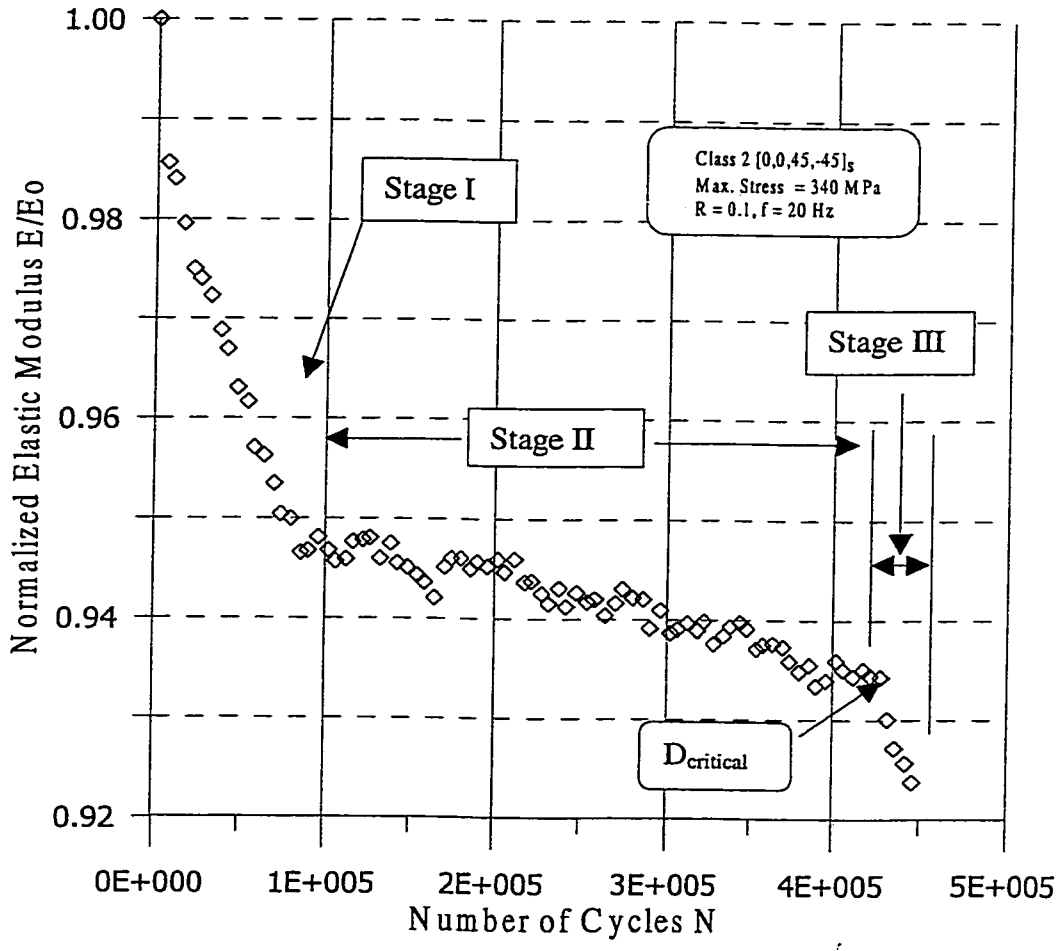

Figure 4.1: Elastic Modulus degradation with number of fatigue cycles for Class 2 $[0,0,45,-45]_s$ WCFRP at 0°C

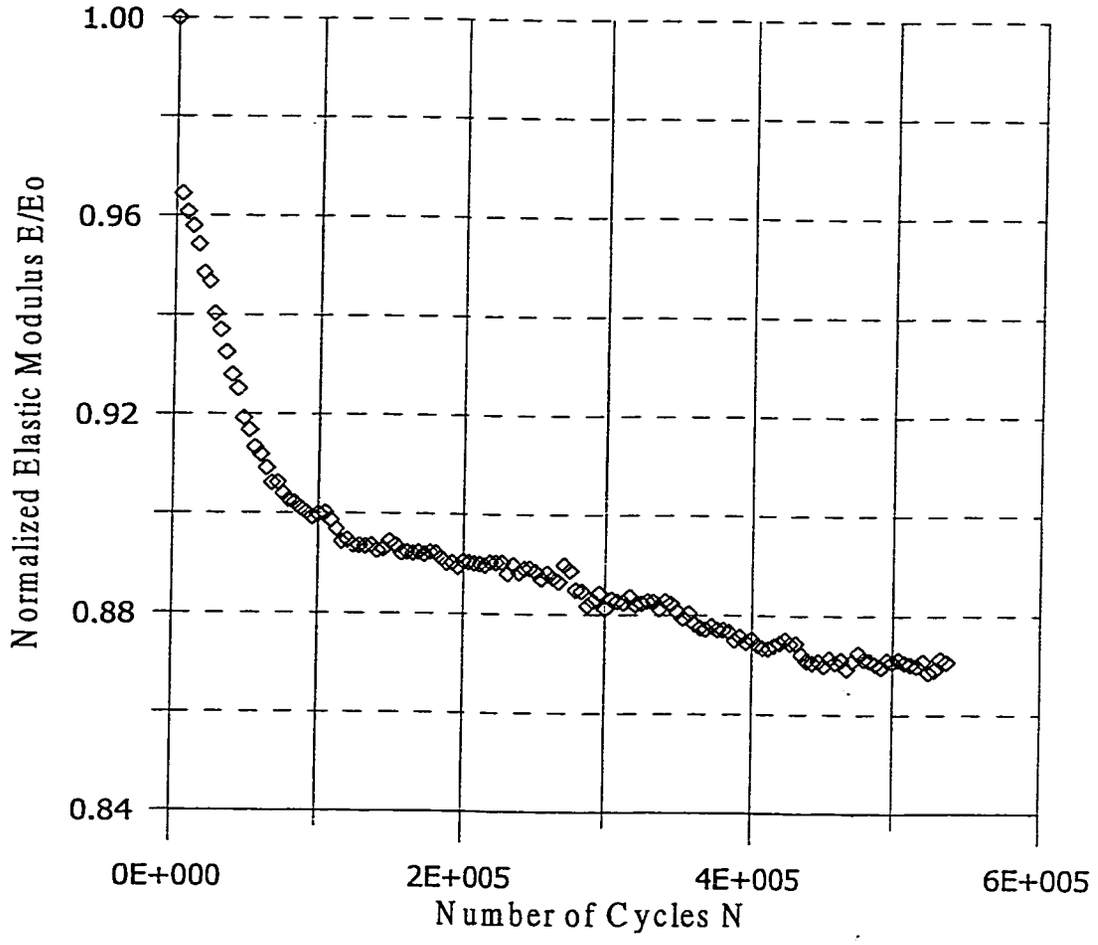

Figure 4.2: Elastic Modulus Degradation with number of Fatigue cycles for Class 1 $[0]_8$ WCFRP at -20°C

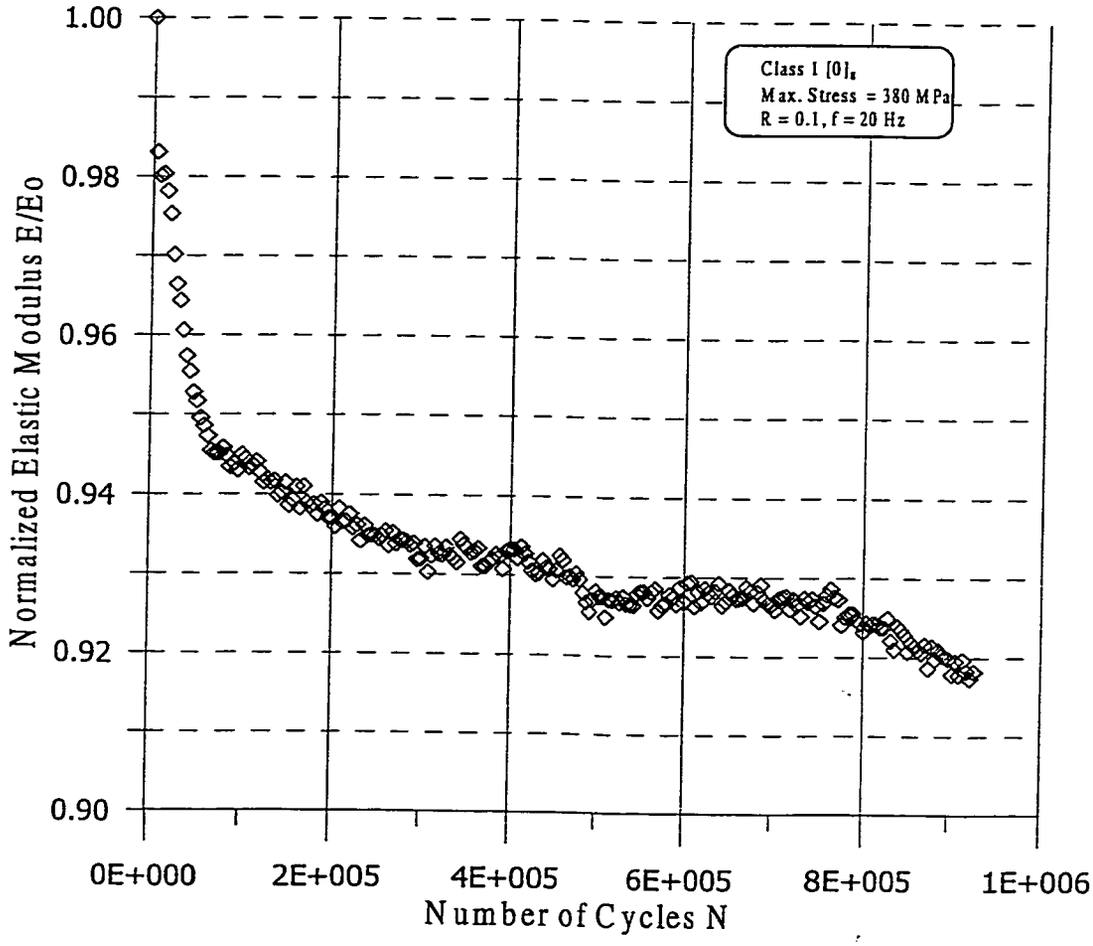

Figure 4.3: Elastic Modulus degradation with number of fatigue cycles for Class 1 $[0]_8$ WCFRP at 0°C

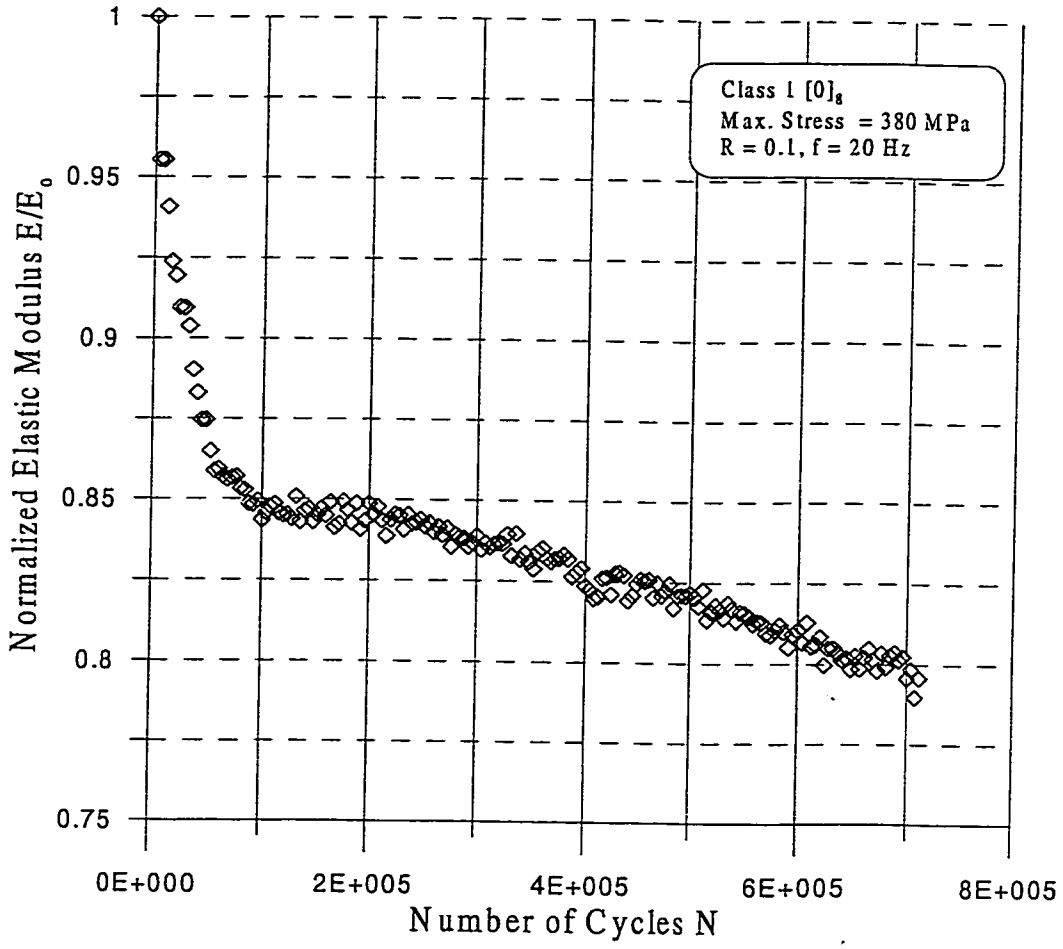

Figure 4.4: Elastic Modulus Degradation with number of Fatigue cycles for Class 1 $[0]_8$ WCFRP at Room Temperature

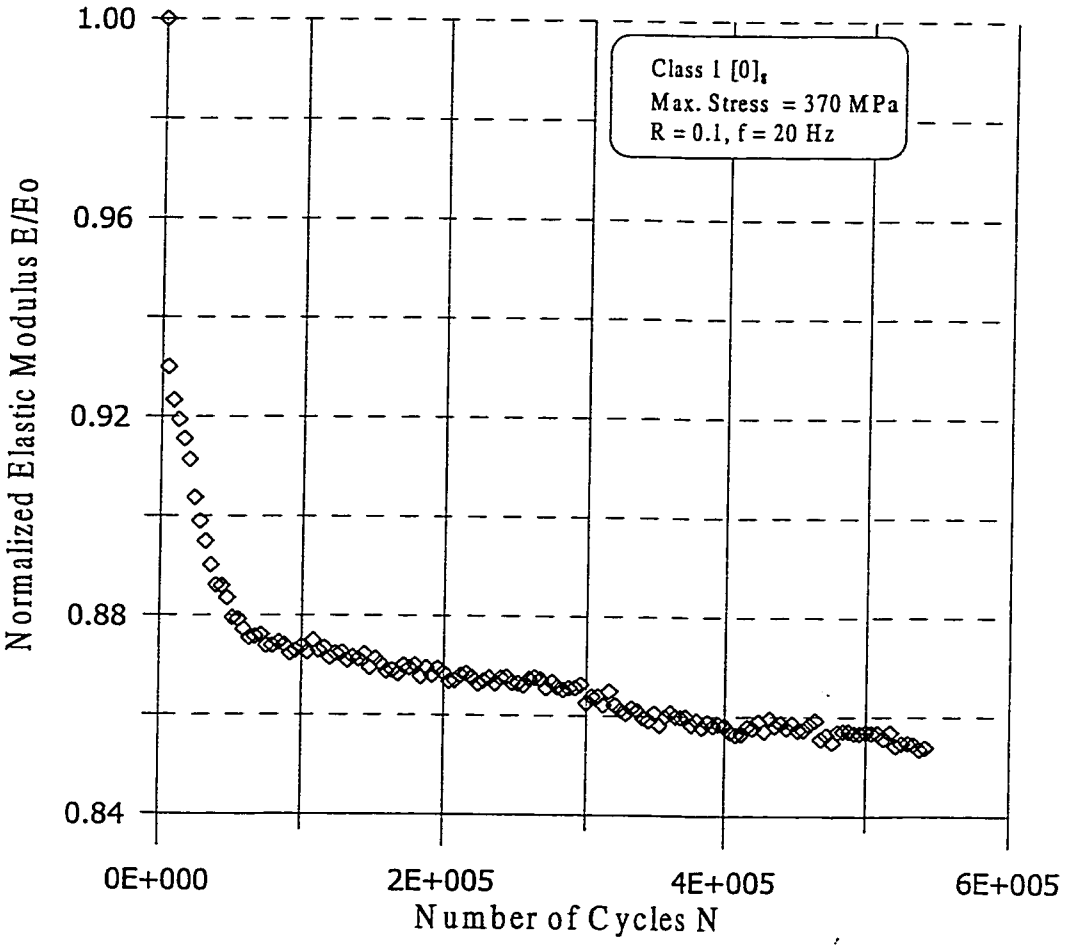

Figure 4.5: Elastic Modulus Degradation with number of Fatigue cycles for Class 1 $[0]_8$ WCFRP at 100°C

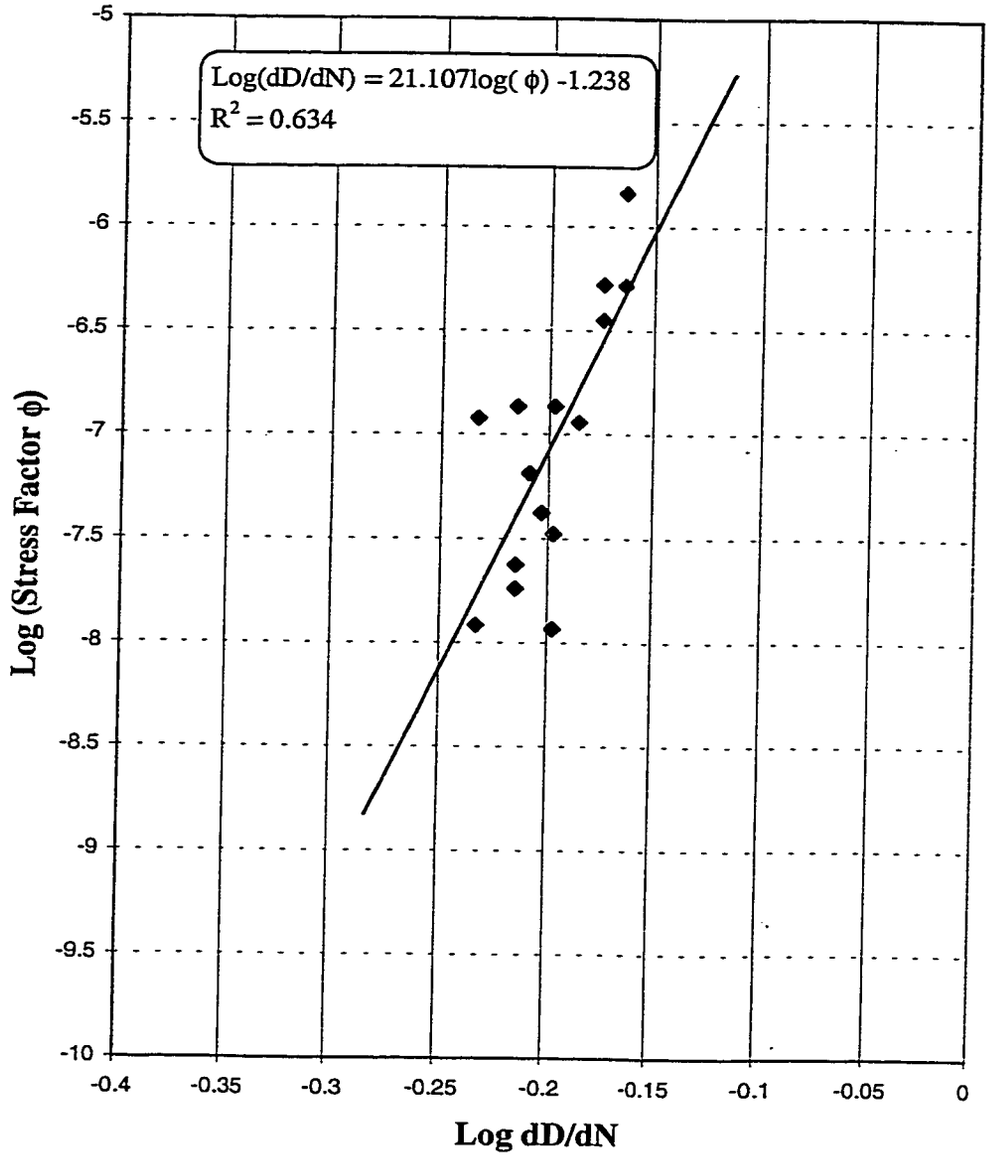

Figure 4.6: Log (dD/dN) and Log (ϕ) for finding Material Constants A C for Class 1 $[0]_8$ CFRP

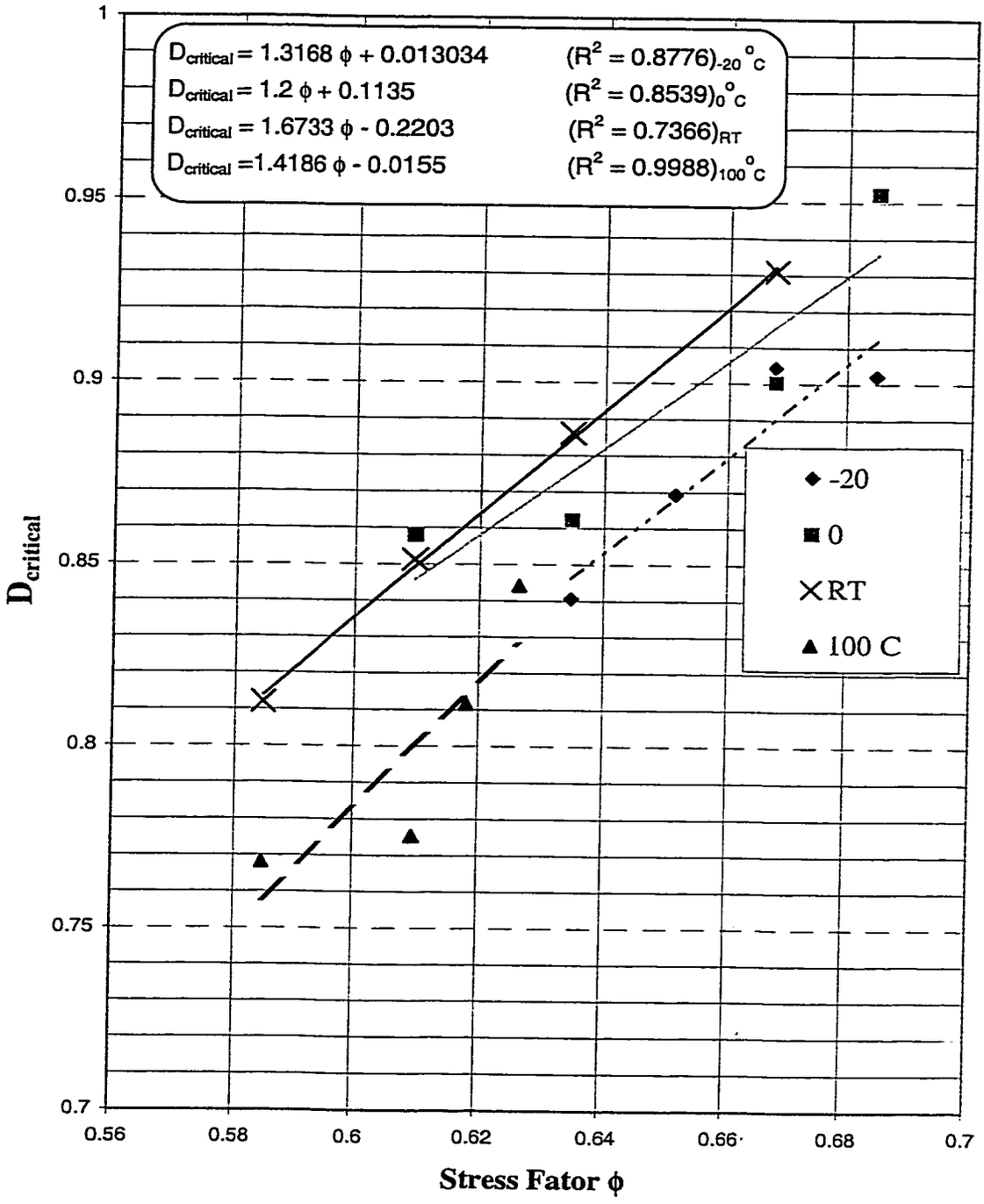

Figue 4.7: $D_{critical}$ verses stress factor ϕ to find material constants P and Q

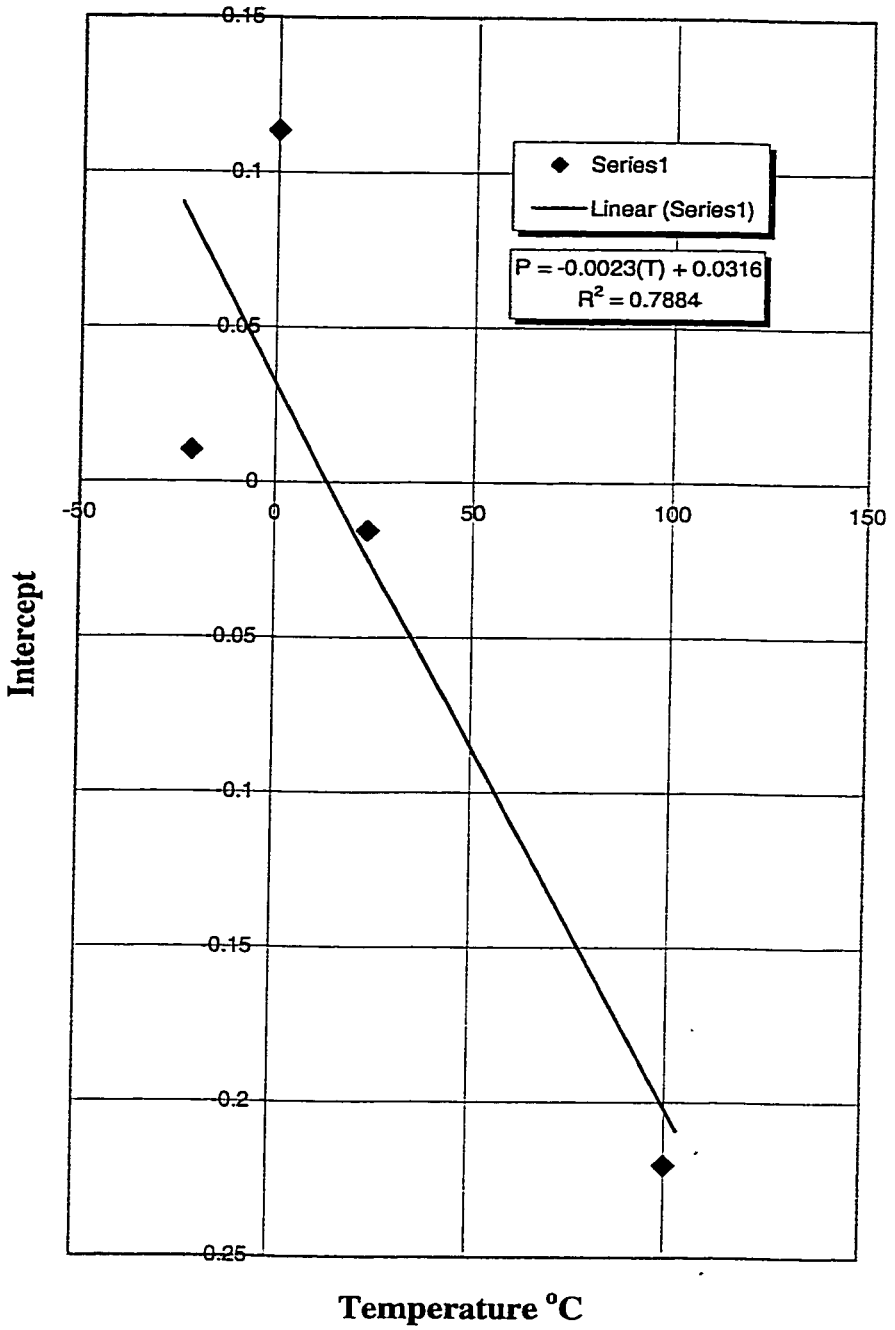

Figure 4.8: Plot to find the final temperature dependant for obtaining Material Constant P

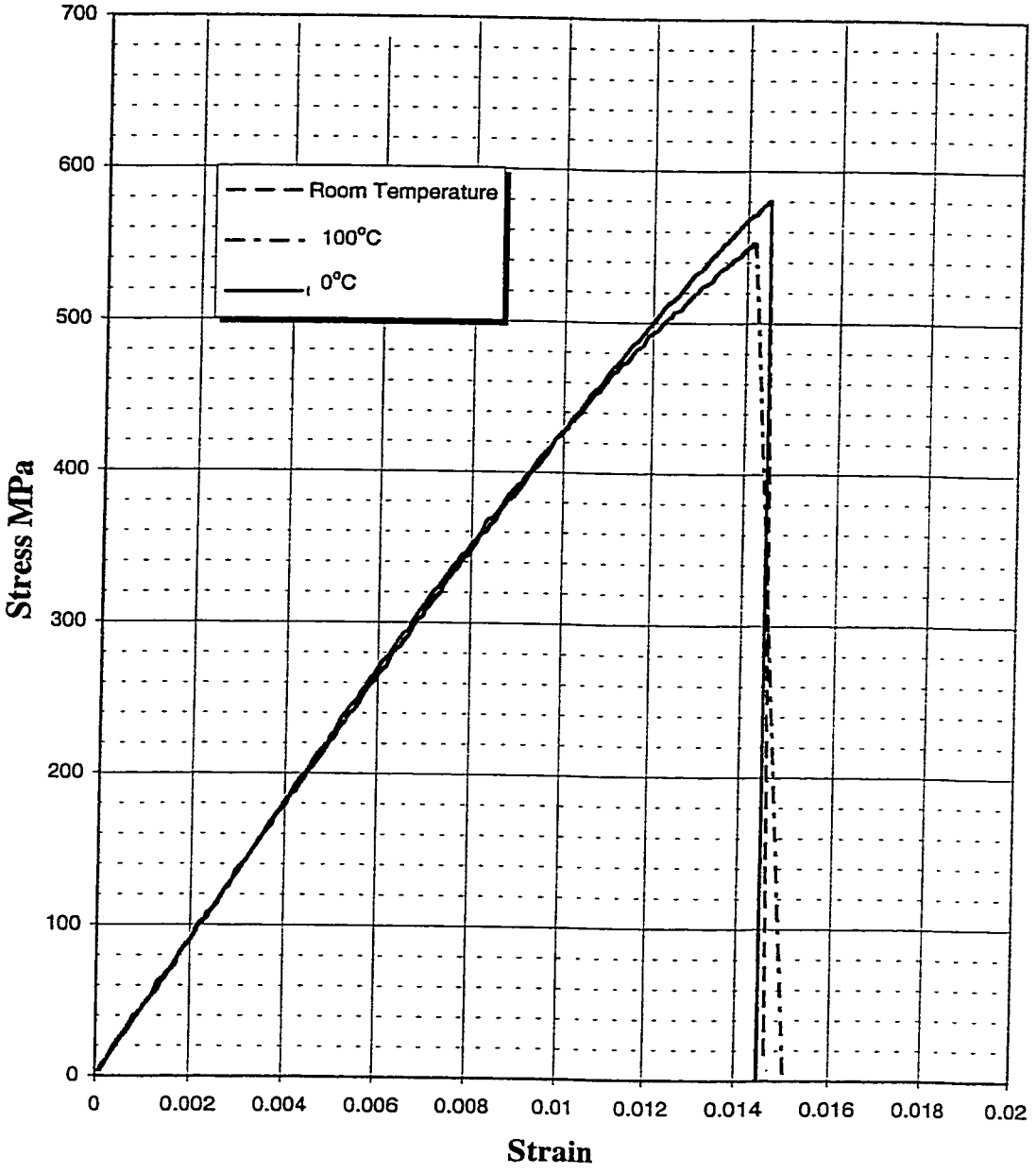

Figure 5.1: Monotonic Tests results for Class 1 $[0]_8$ WCFRP at different temperatures

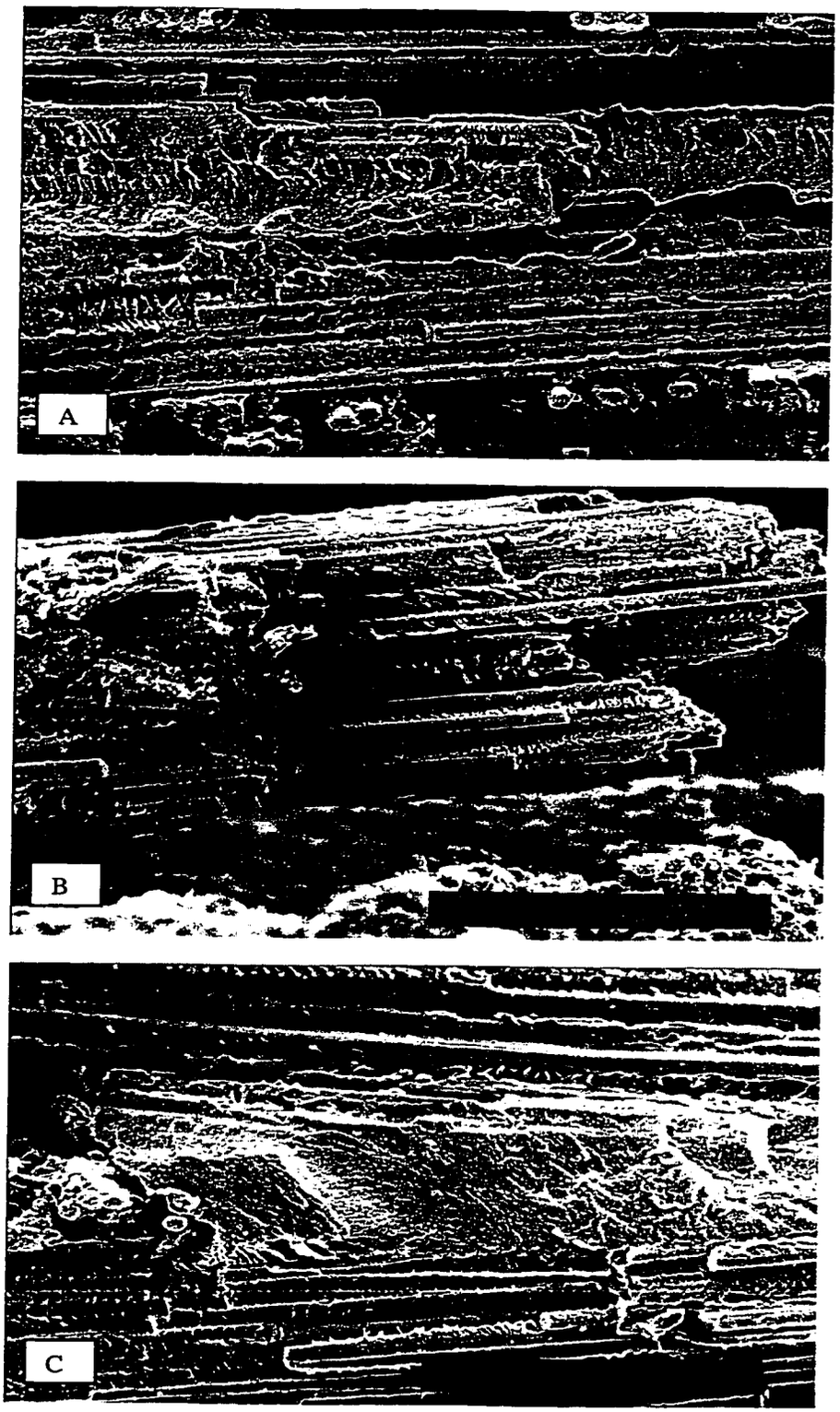

Figure 5.2: SEM Micro-photographs of Class 1 $[0]_8$ specimens fractured under monotonic tensile loading at (A) 0°C, showing strong matrix/fiber bonding than at (B) 100°C and (C) Room Temperature

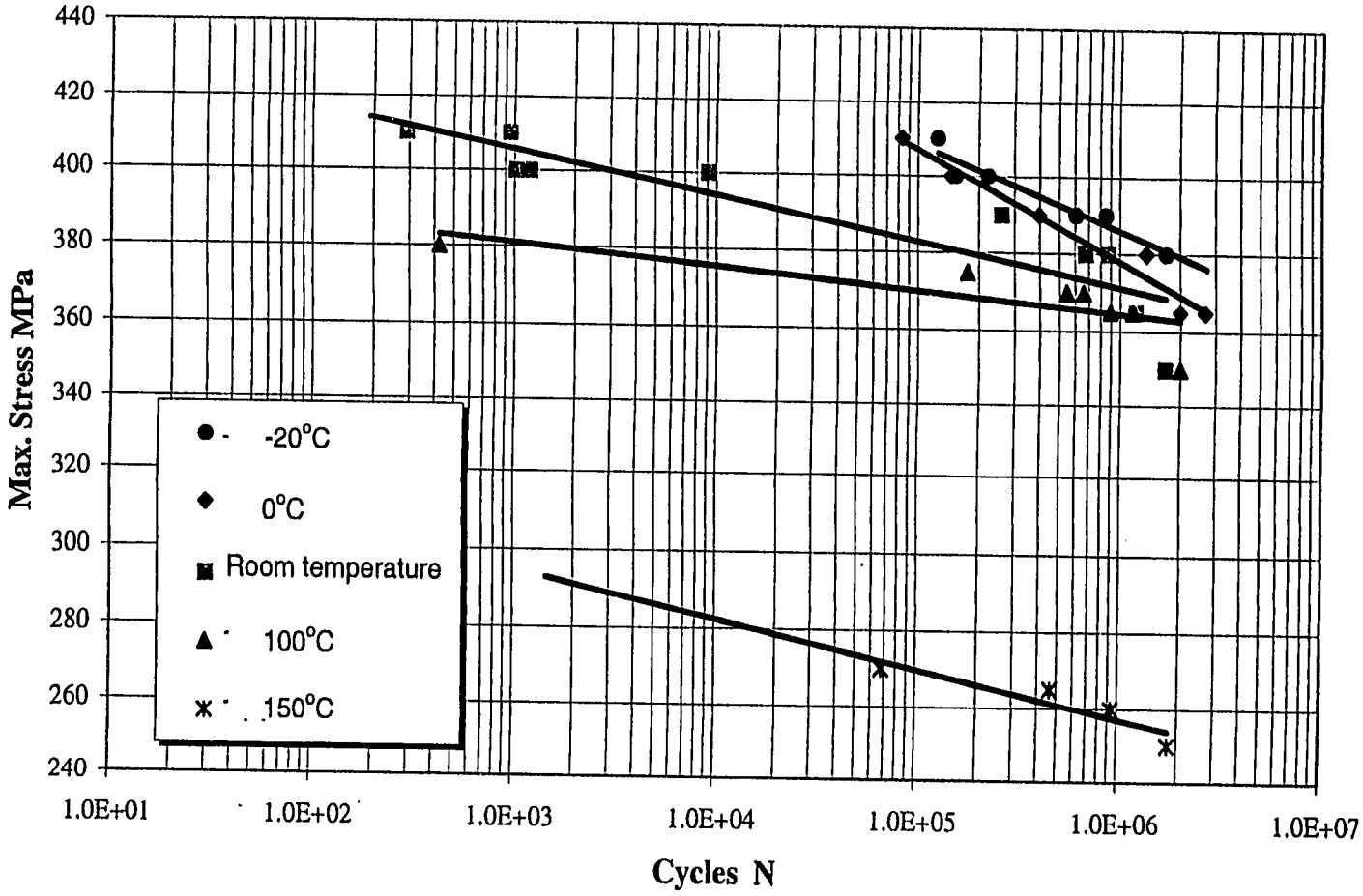

Figure 5.3 : S-N Curve for the experimental fatigue data at various test temperatures for Class 1 $[0]_8$ WCFRP

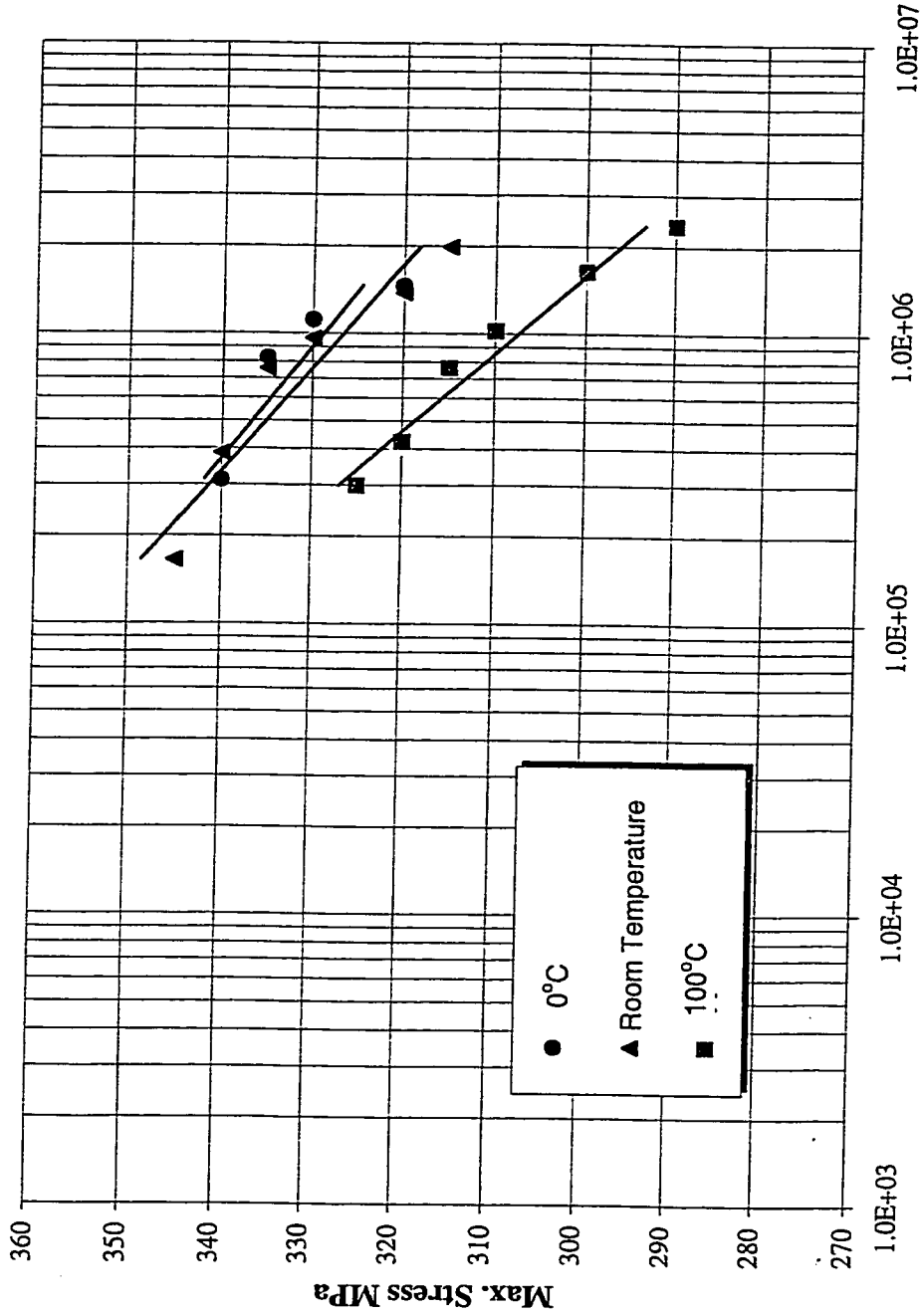

Figure 5.4 : S-N Curve for the experimental fatigue data at various test temperatures for Class 2 $[0,0,45,-45]_s$ WCFRP

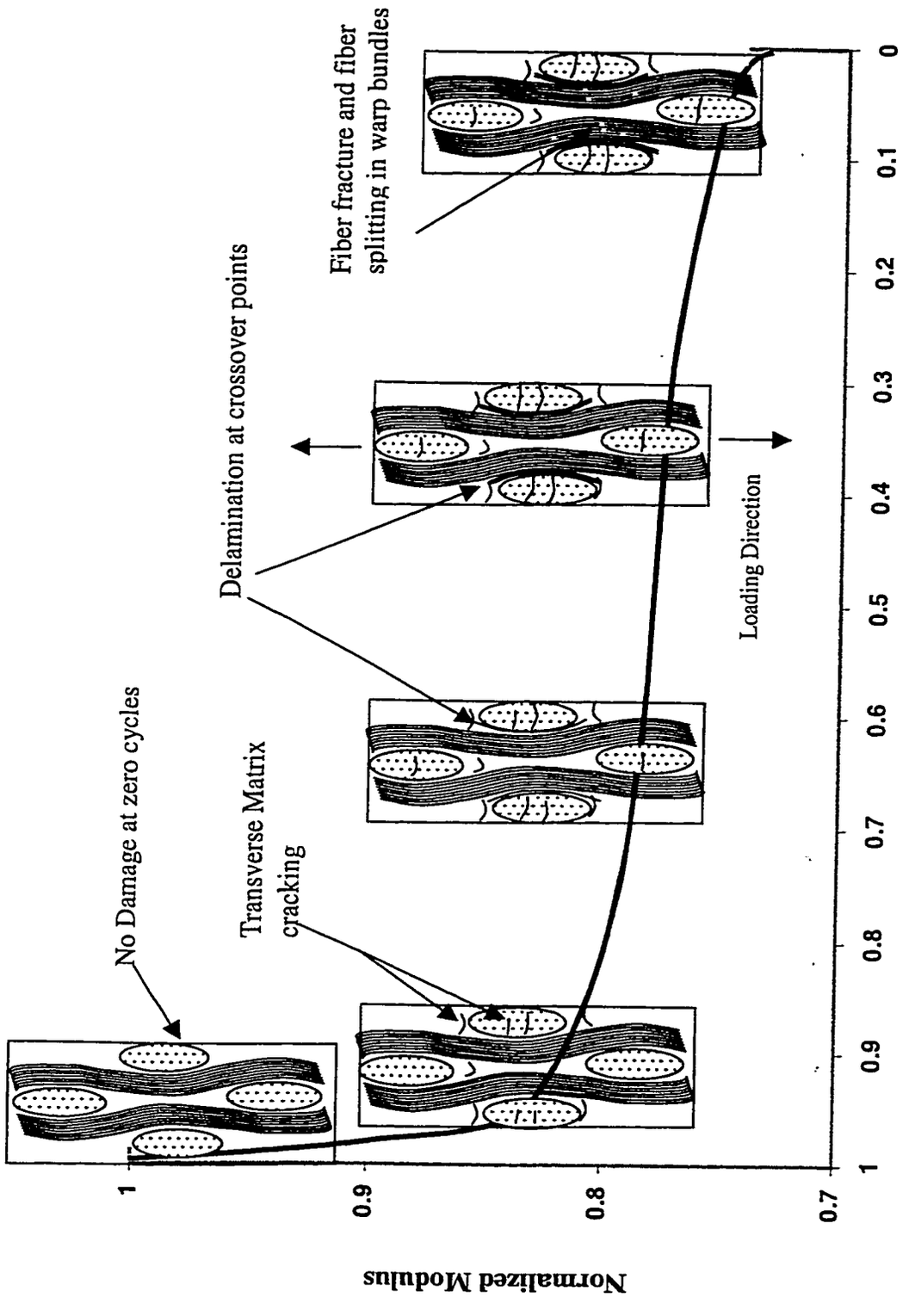

Figure 5.5: Schematic representation of damage development with modulus degradation during the fatigue life of a WCFRP specimen

Figure 5.6: Photomicrograph showing multiple cracks in off-axis plies and delamination in Class 1$[0]_8$ WCFRP

Figure 5.7: Photomicrograph showing matrix crack and delamination in Class 1$[0]_8$ WCFRP

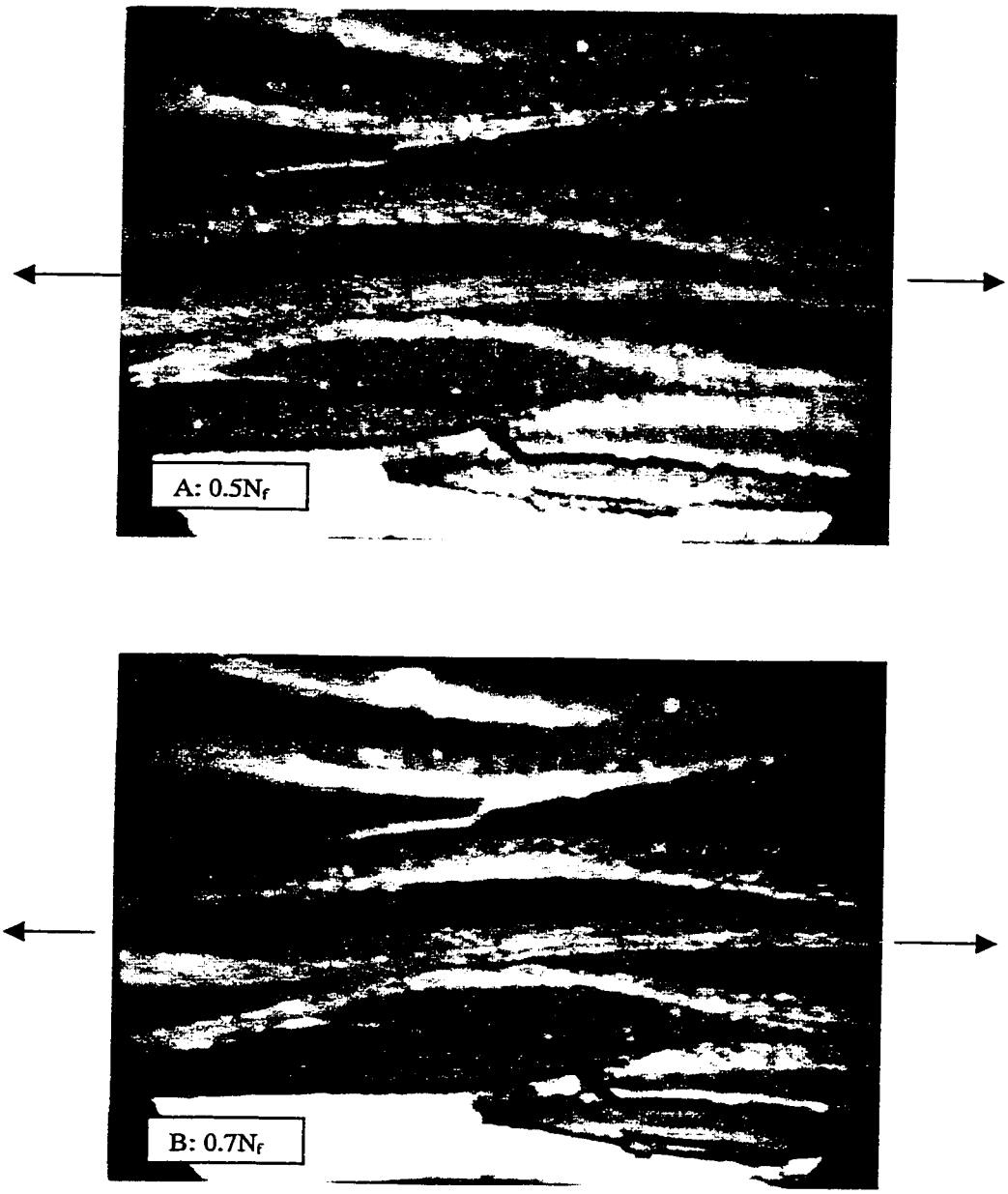

Figure 5.8: Edge delamination growth in Class 1 $[0]_8$ specimens at room temperature at (A) 50% and (B) 70% of Fatigue Life

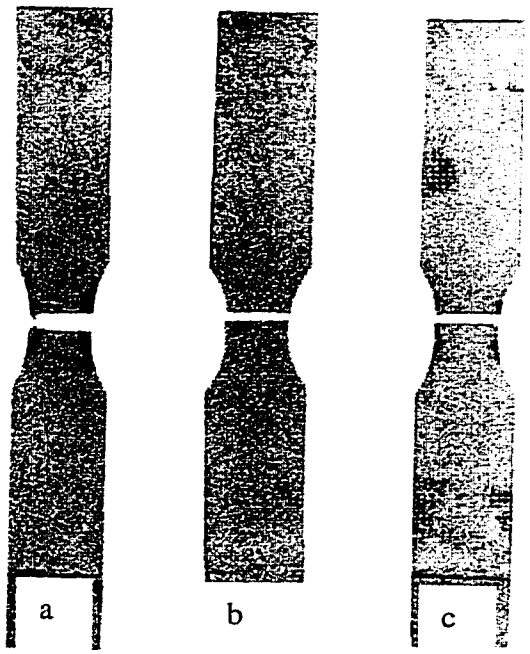

Figure 5.9: X-ray Radiograph indicating the failure at (a) Room temperature, (b) -20°C and (c) 0°C for Class 1 $[0]_8$ WCFRP

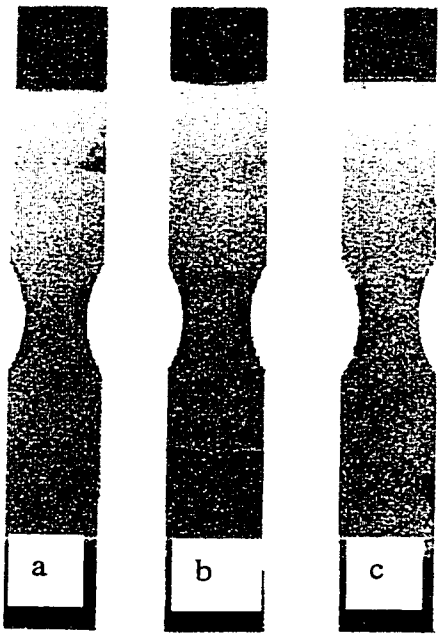

Figure 5.10: X-ray Radiograph indicating run-out specimens at (a) 0°C, (b) Room temperature, (c) -20°C for Class 1 $[0]_8$ WCFRP

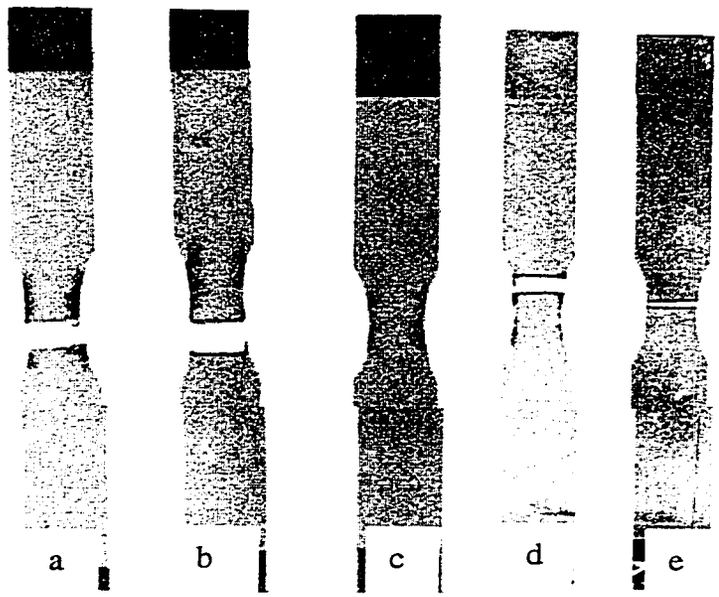

Figure 5.11: X-ray Radiograph showing the fatigue fractured specimens for Class 1 $[0]_8$ WCFRP, (a,b,c) at different stress but 100°C, (d,e) show specimen at room temperature and 0°C at same stress level as in (a) respectively

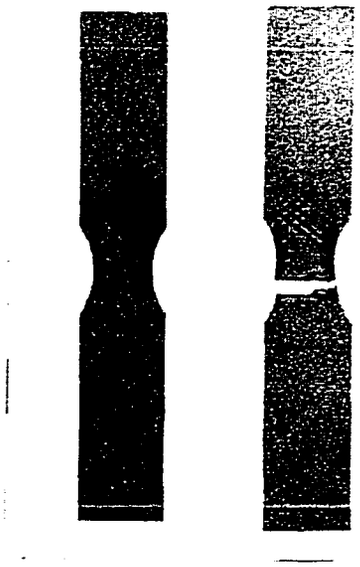

Figure 5.12: X-ray Radiograph representing Damage behavior at 150°C (above T_g) in Class 1 $[0]_8$ WCFRP

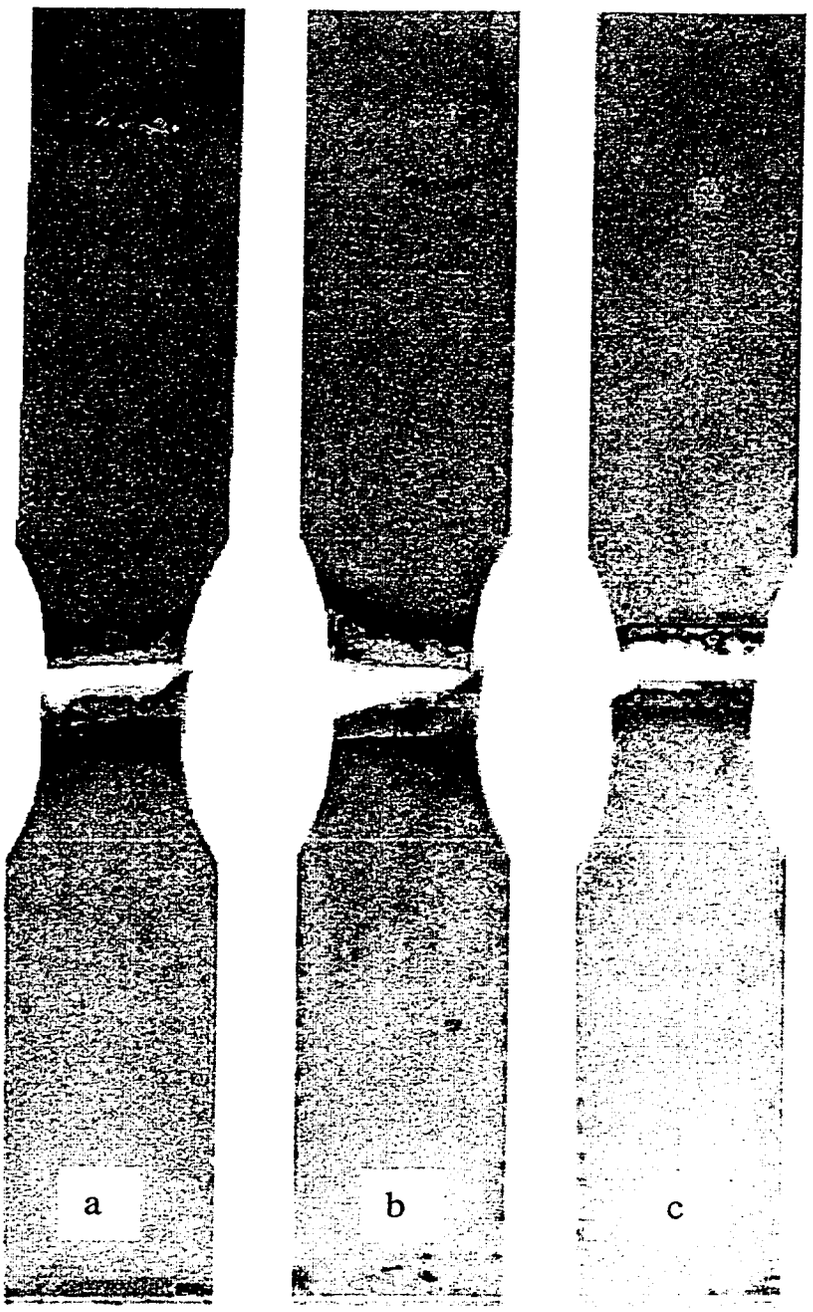

Figure 5.13 X-ray Radiograph (a,b,c) showing the results of class 2 $[0,0,45,-45]_s$ WCFRP specimen tested at 100°C, Room temperature,and 0°C

Figure 5.14: SEM Micrograph showing the complexity of woven structure and damage mechanism in class 2 $[0,0,45,-45]_s$ WCFRP

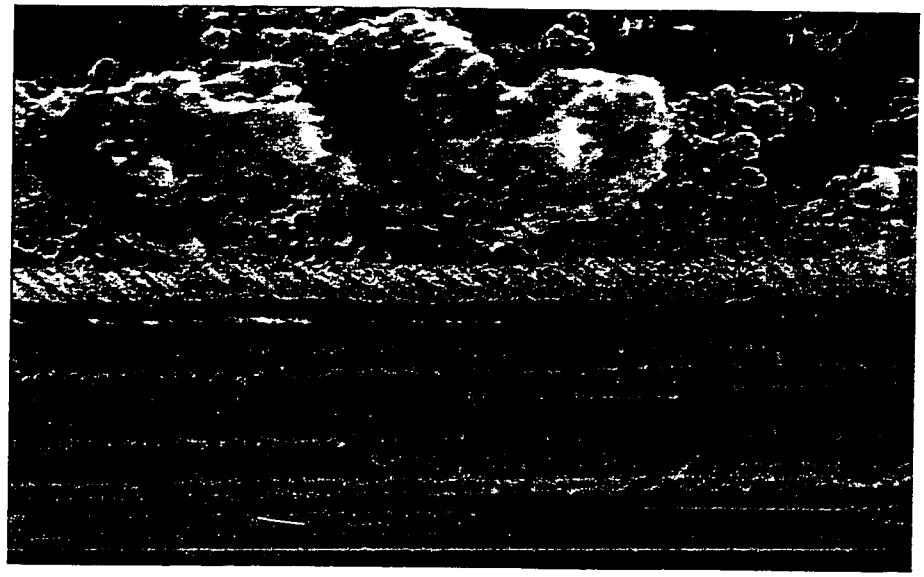

Figure 5.15: SEM Micrograph showing Catastrophic fiber fracture in Warp bundles of Class 1 $[0]_8$ WCFRP

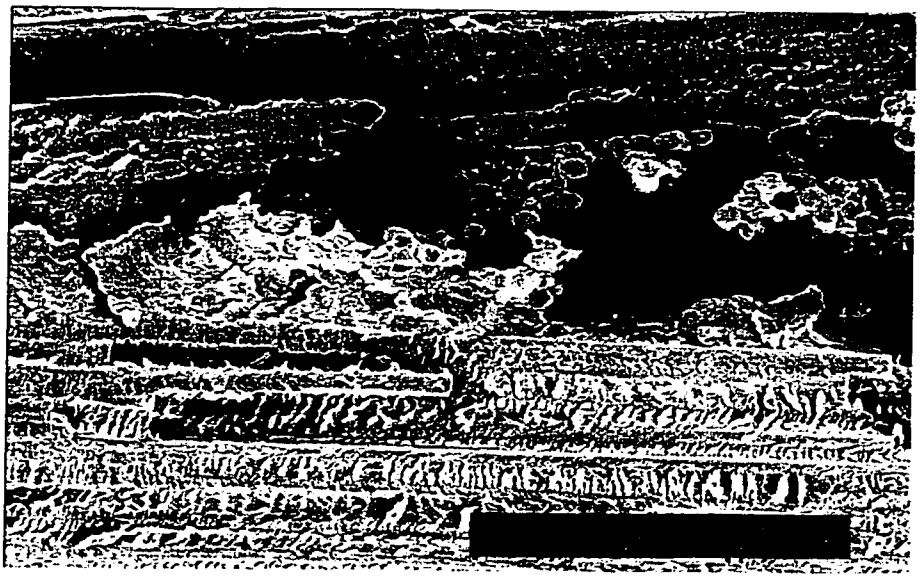

Figure 5.16: SEM Micrograph showing local debonding in Class 1 $[0]_8$ WCFRP

Figure 5.17: SEM Micrograph Showing local delamination at cross over points in Class 1 $[0]_8$ WCFRP

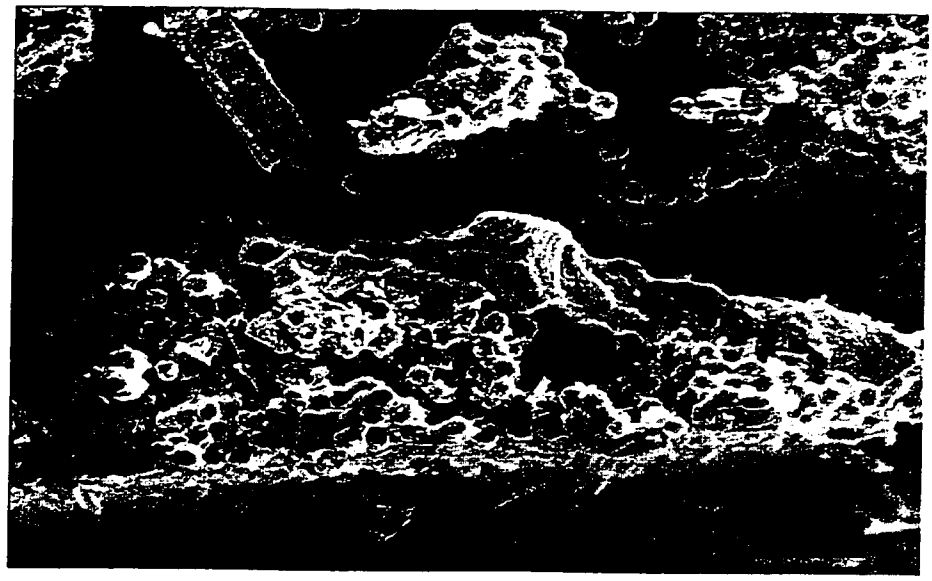

Figure 5.18: SEM Micrograph showing Delamination between two Warp plies in Class 1 $[0]_8$ laminates.

Figure 5.19: SEM Micrograph showing fiber splitting in warp bundles of Class 1 $[0]_8$ WCFRP

Figure 5.20: SEM Micrograph showing cracking of weft bundles in Class 1 $[0]_8$ WCFRP

Figure 5.21: SEM Micrograph showing cracking of weft bundles initiated from fiber splitting of warp bundles in Class 1 $[0]_8$ WCFRP

Figure 5.22: SEM Micrograph showing complete delaminated region between 0° and 45° plies in class 2 $[0,0,45,-45]_s$ WCFRP specimen.

Figure 5.23: SEM Micrograph showing interply delamination in angle plies of class 2 $[0,0,45,-45]_s$ WCFRP

Figure 5.24: SEM Micrograph showing macroscopic view of fiber breakage and interfacial delamination in angle plies of class 2 $[0,0,45,-45]_s$ WCFRP.

Figure 5.25: SEM Micrograph showing pure matrix cracking at –20°C in Class 1 $[0]_8$ WCFRP

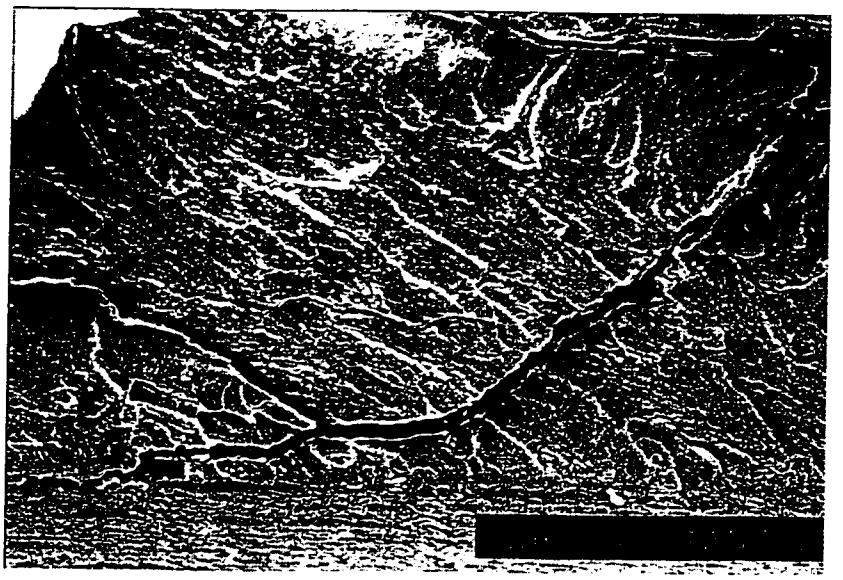

Figure 5.26: SEM Micrograph showing pure matrix cracking at Room Temperature in Class 1 $[0]_8$ WCFRP

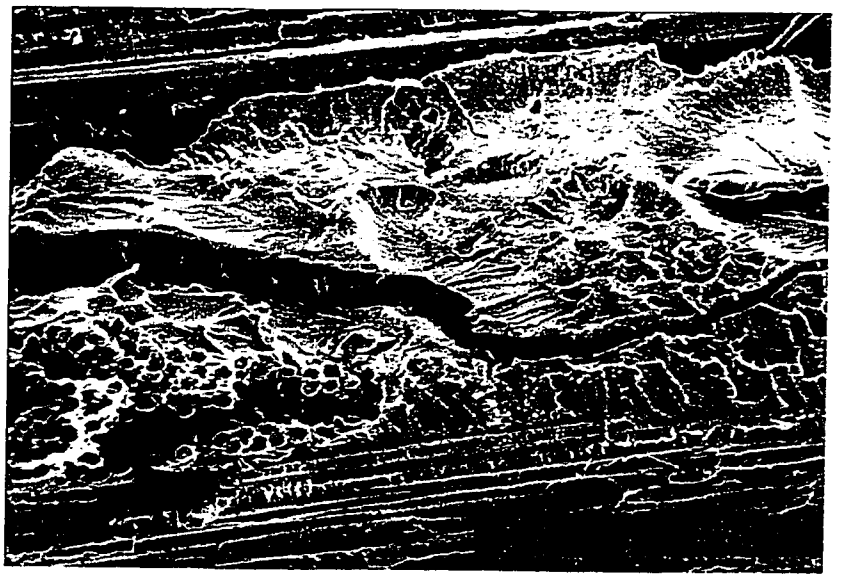

Figure 5.27: SEM Micrograph showing pure matrix cracking at 100°C in Class 1 $[0]_8$ WCFRP

Figure 5.28: SEM Micrograph showing matrix crack surface in weft bundles for –20°C in Class 1 $[0]_8$ WCFRP

Figure 5.29: SEM Micrograph showing matrix crack surface in weft bundles for –20°C in Class 1 $[0]_8$ WCFRP

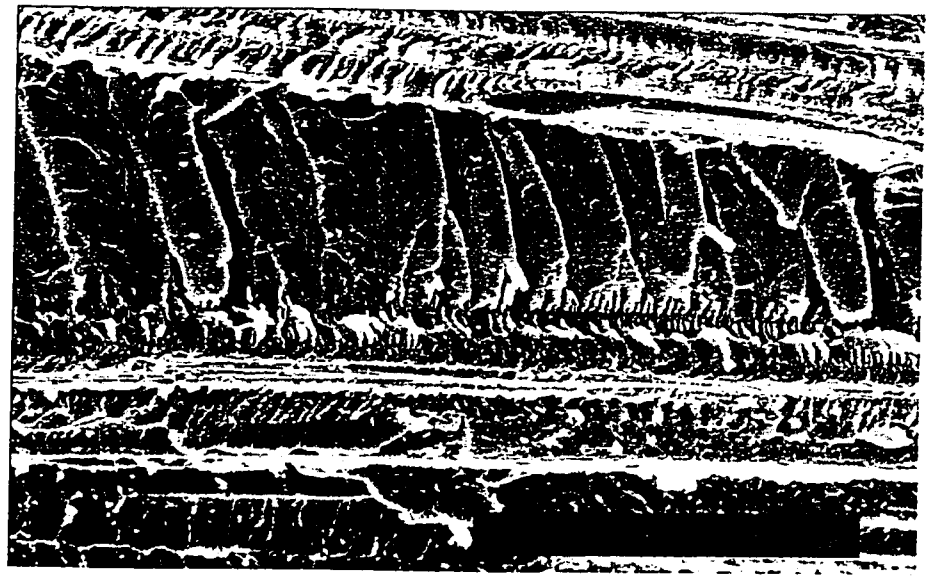

Figure 5.30: SEM Micrograph showing matrix crack surface morphology in weft bundles for 100°C in Class 1 $[0]_8$ WCFRP

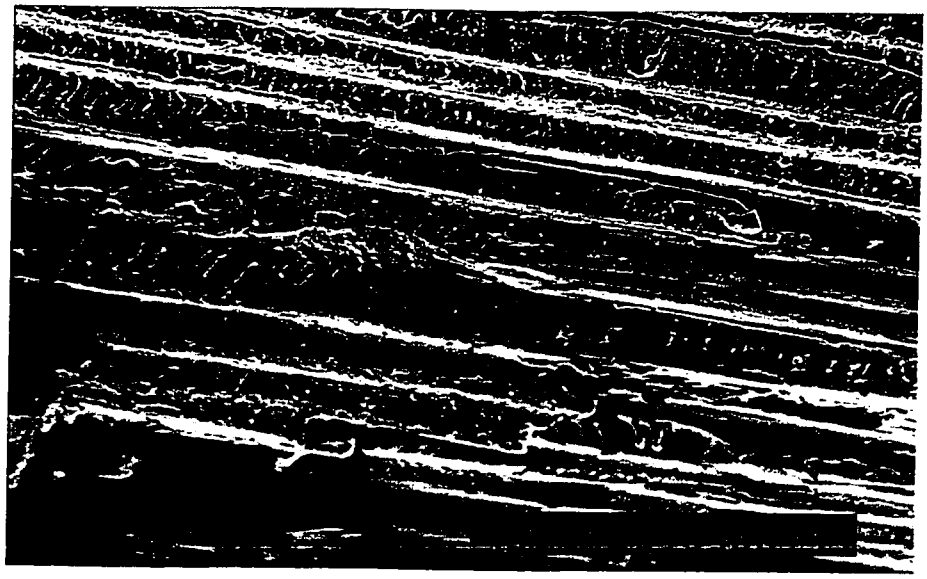

Figure 5.31: SEM Micrograph showing matrix crack surface in weft bundles for 150°C in Class 1 $[0]_8$ WCFRP

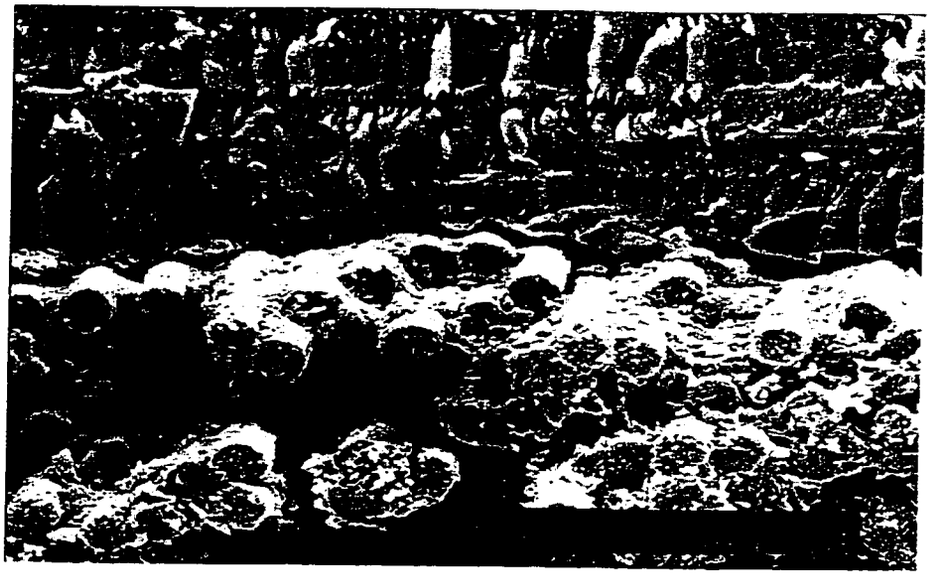

Figure 5.32 SEM Micrograph showing the effect of temperature on fiber/matrix interface strength of warp fiber bundles at 0°C in Class 1 $[0]_8$ WCFRP

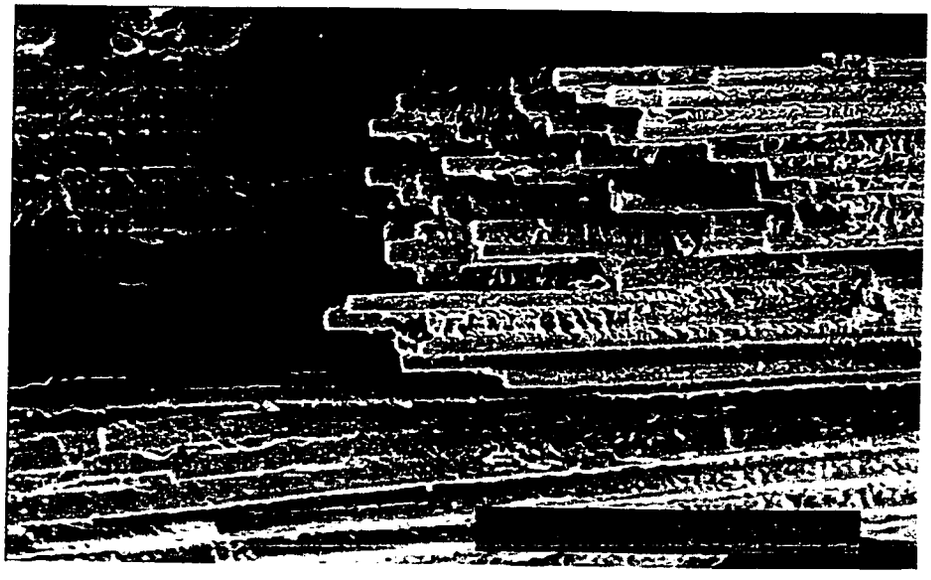

Figure 5.33: SEM Micrograph showing the effect of temperature on fiber/matrix interface strength of warp fiber bundles at 24°C in Class 1 $[0]_8$ WCFRP

Figure 5.34: SEM Micrograph showing the effect of temperature on fiber/matrix interface strength of warp fiber bundles at 100°C in Class 1 $[0]_8$ WCFRP

Figure 5.35 SEM Micrograph showing the effect of temperature on fiber/matrix interface strength of warp fiber bundles at 100°C in Class 1 $[0]_8$ WCFRP

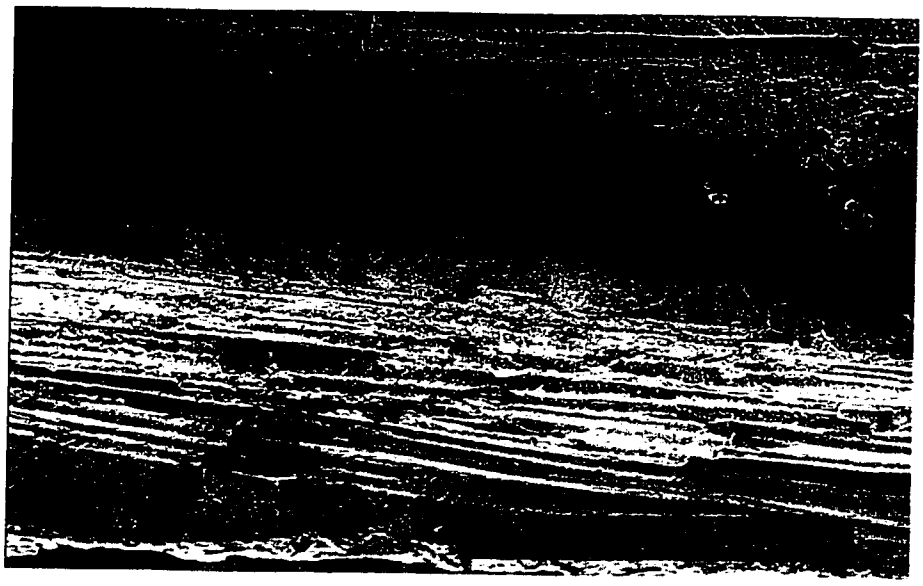

Figure 5.36: SEM Micrograph Showing the week interfacial strength caused extensive delamination in Class 1 $[0]_8$ WCFRP at 150°C

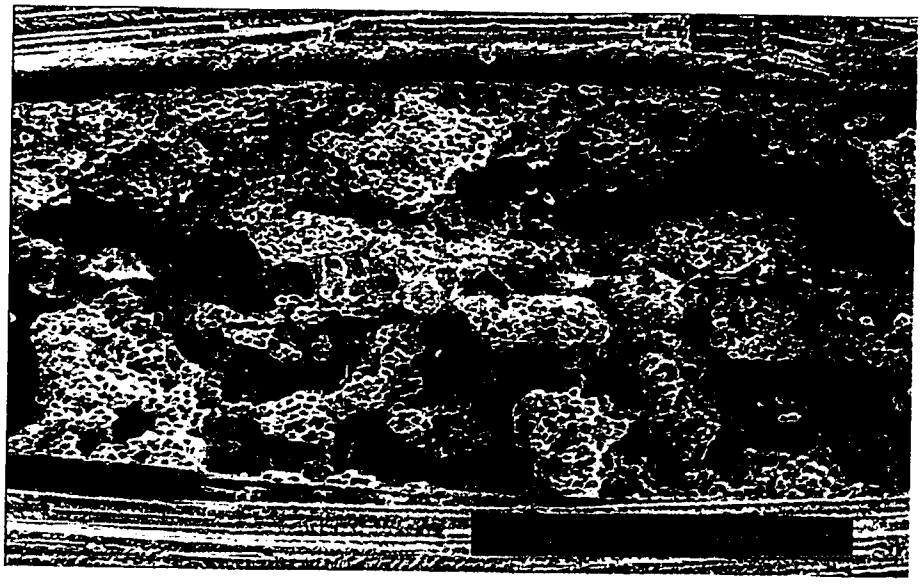

Figure 5.37: SEM Micrograph showing local delamination caused by strong interfacial strength at lower temperatures in Class 1 $[0]_8$ WCFRP

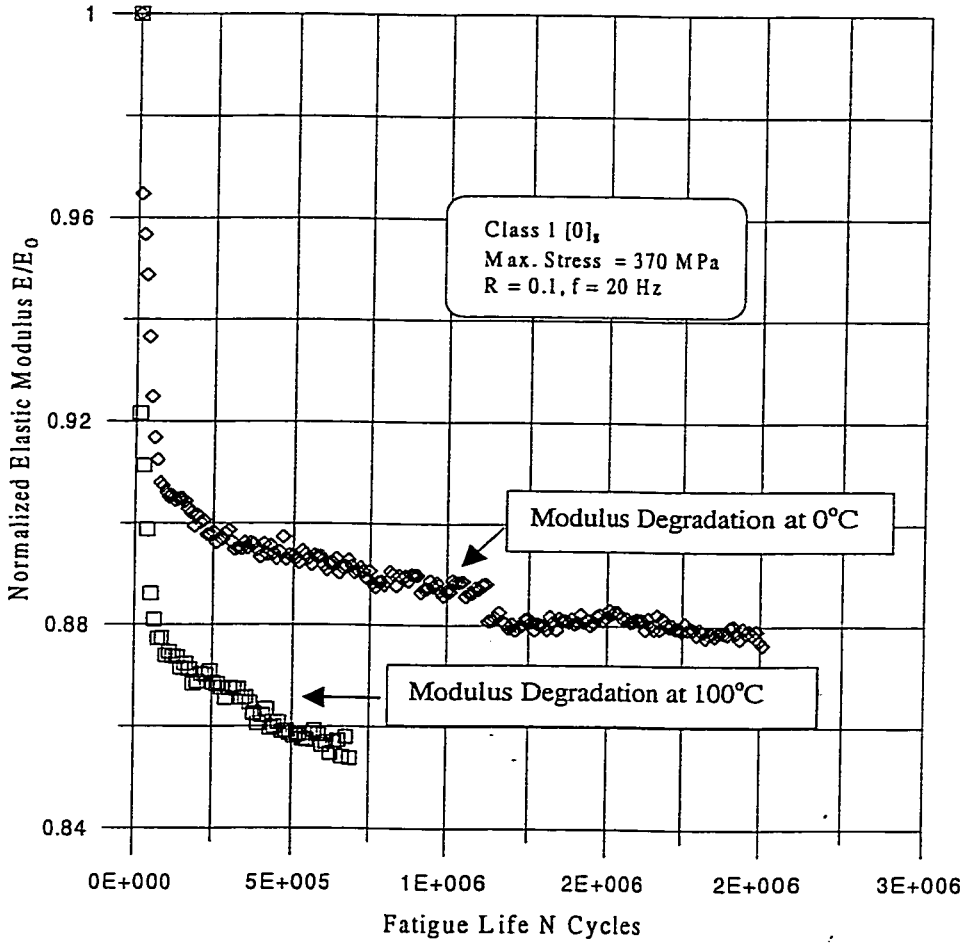

Figure 5.38: Modulus degradation with number of cycles at 100°C and 0°C at same stress level in Class 1 $[0]_8$ WCFRP

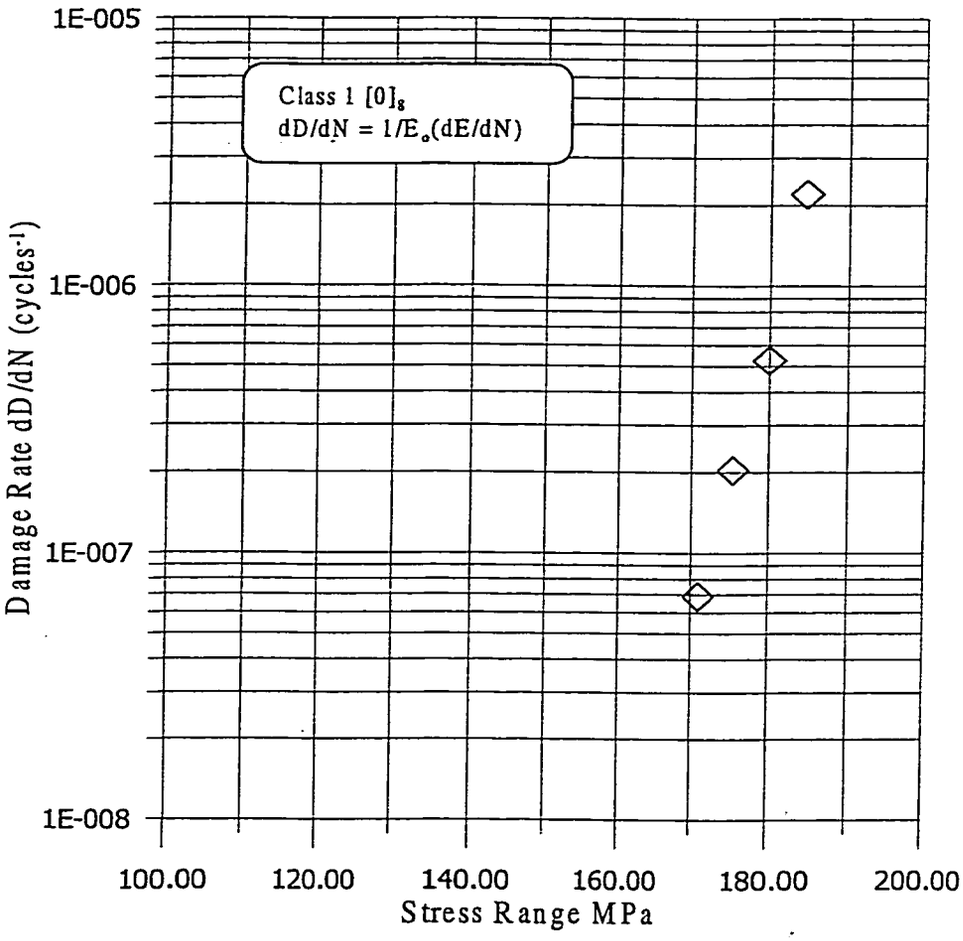

Figure 5.39: Damage Rate as a Function of Applied Stress Range for Class 1 $[0]_8$ WCFRP at -20°C

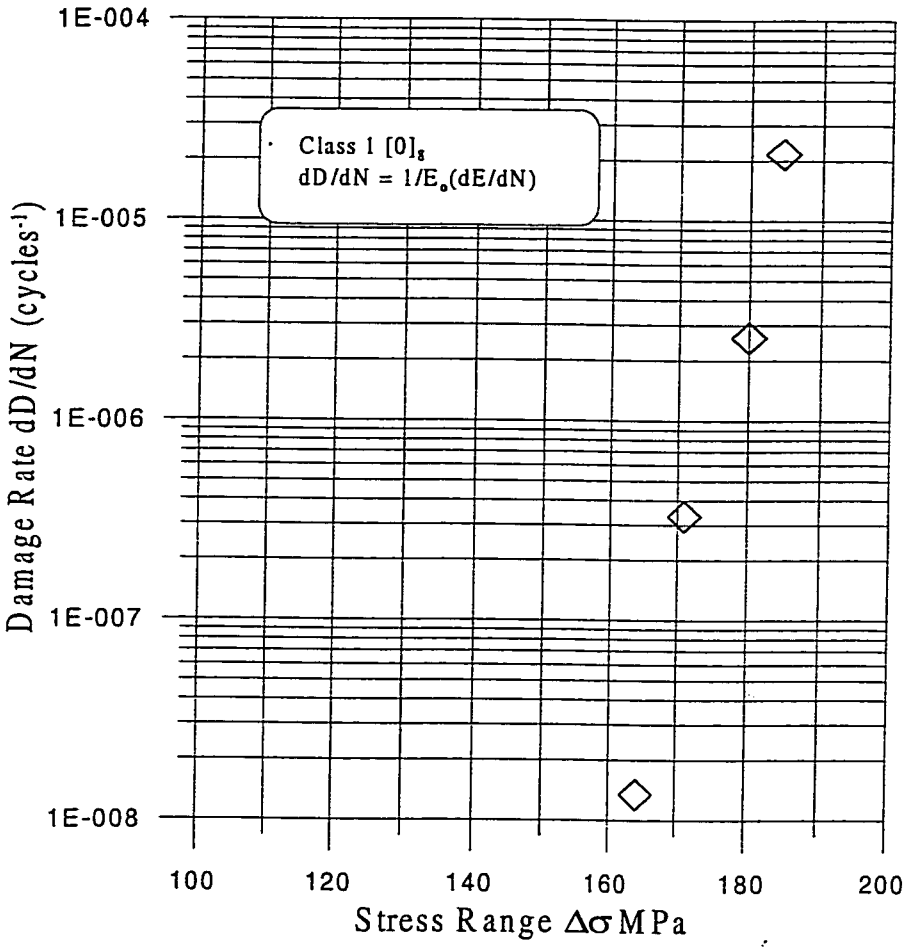

Figure 5.40: Damage Rate as a Function of Applied Stress Range for Class 1 $[0]_8$ WCFRP at 0°C

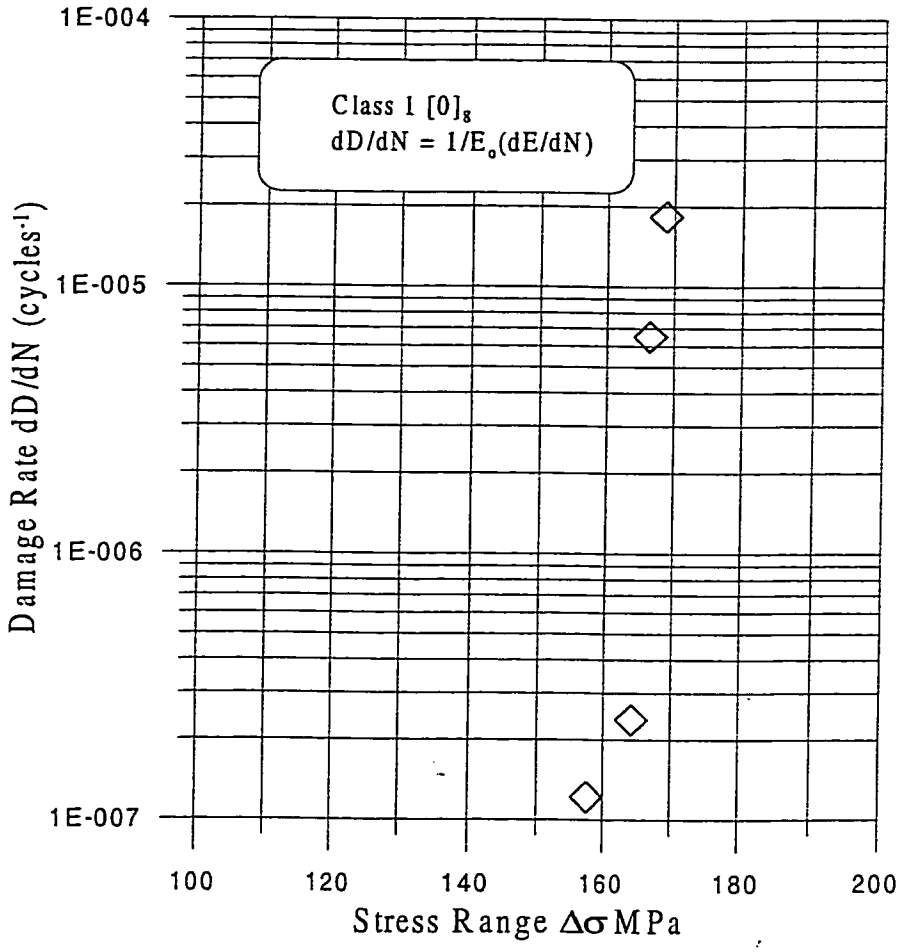

Figure 5.41: Damage Rate as a Function of Applied Stress Range for Class 1 $[0]_8$ WCFRP at 100°C

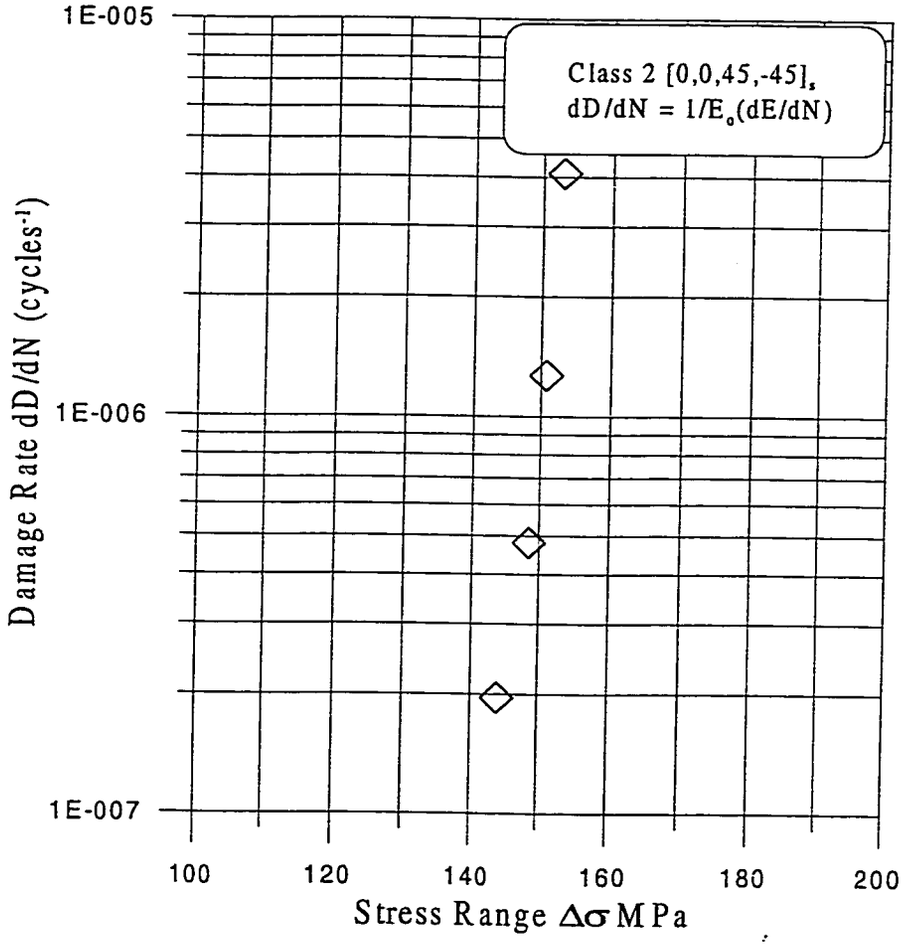

Figure 5.42: Damage Rate as a Function of Applied Stress Range for Class 2 $[0,0,45,-45]_s$ WCFRP at 0°C

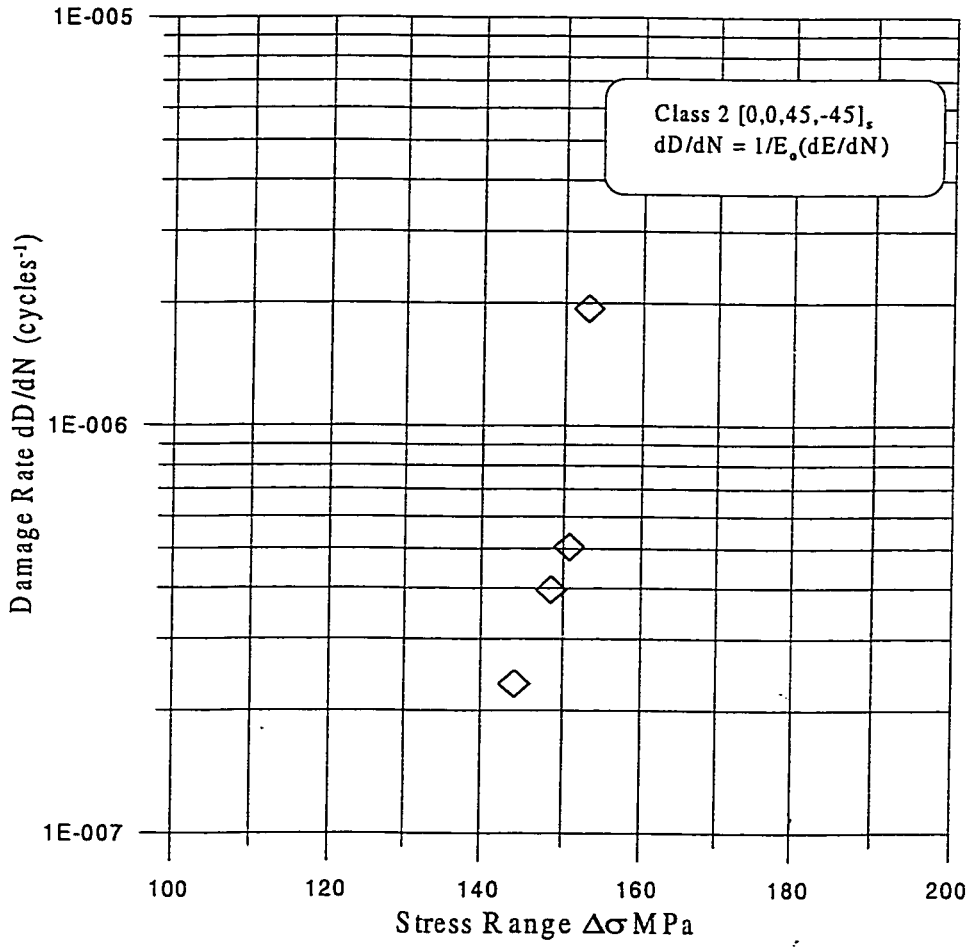

Figure 5.43: Damage Rate as a Function of Applied Stress Range for Class 2 $[0,0,45,-45]_s$ WCFRP at Room Temperature

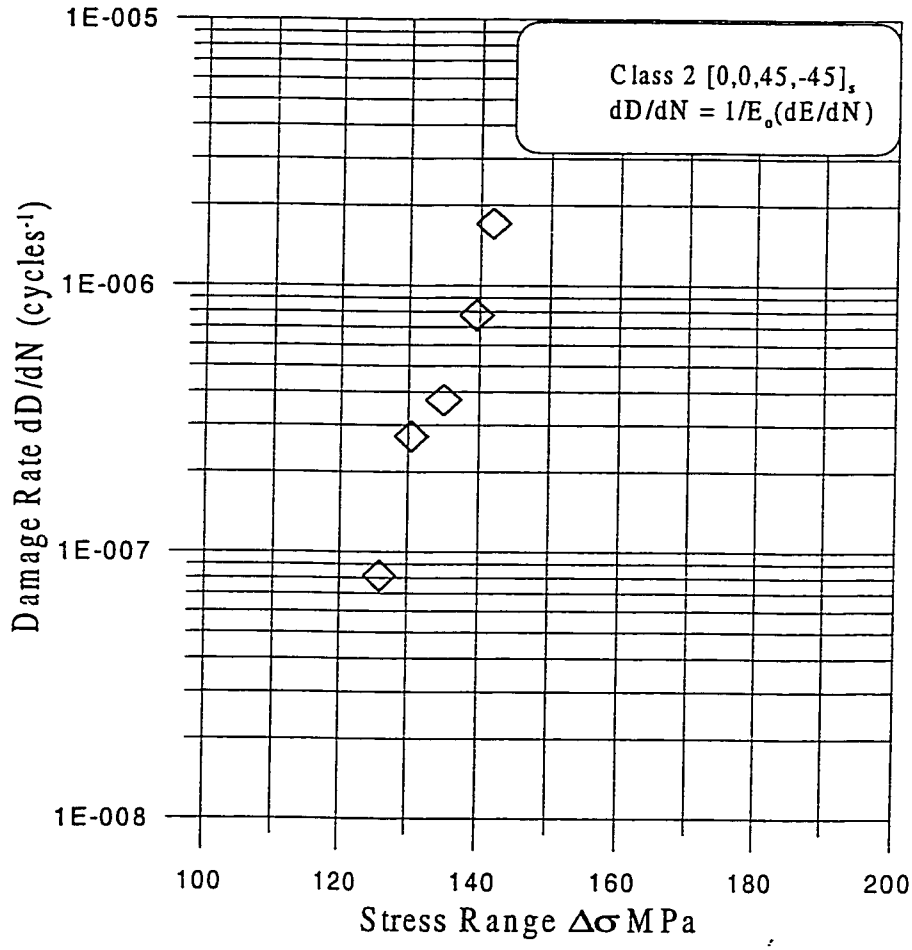

Figure 5.44: Damage Rate as a Function of Applied Stress Range for Class 2 $[0,0,45,-45]_s$ WCFRP at 100°C

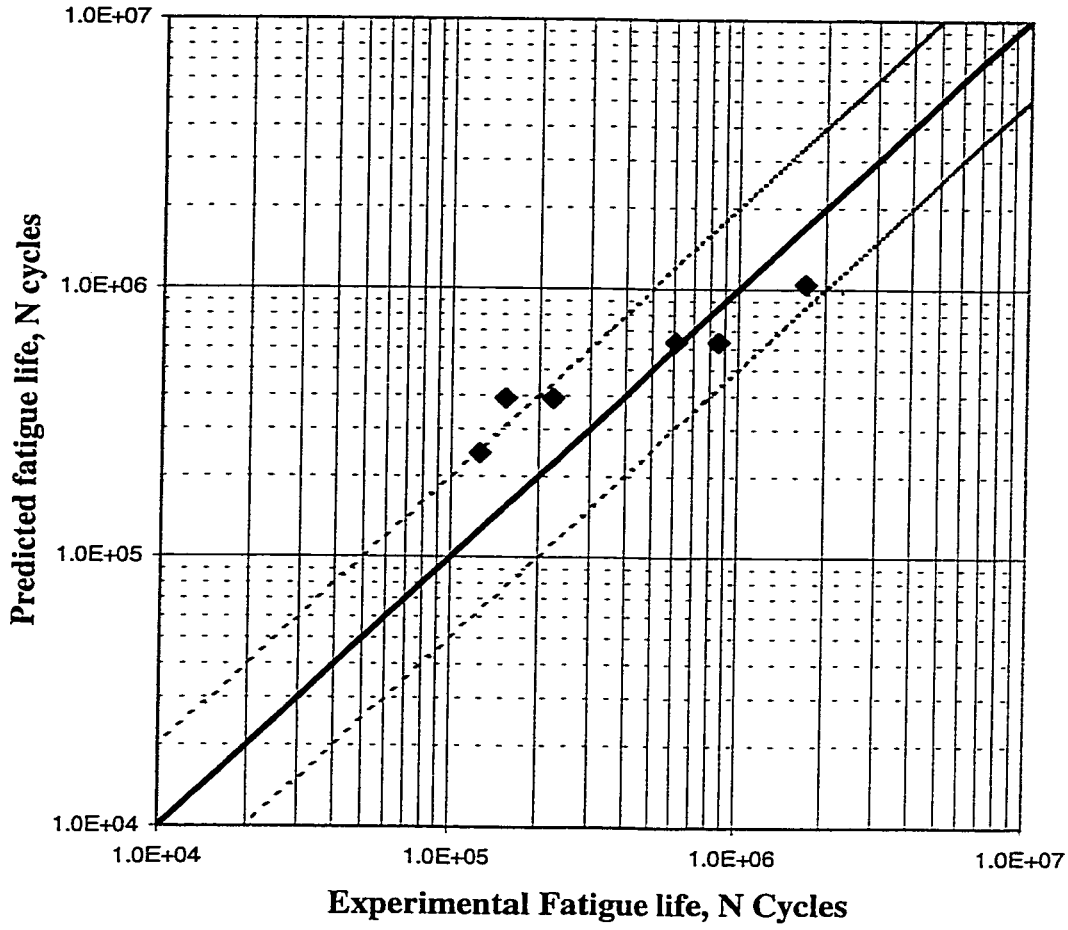

Figure 5.45: Comparison of Experimental and predicted Fatigue lives at -20°C in Class 1 $[0]_8$

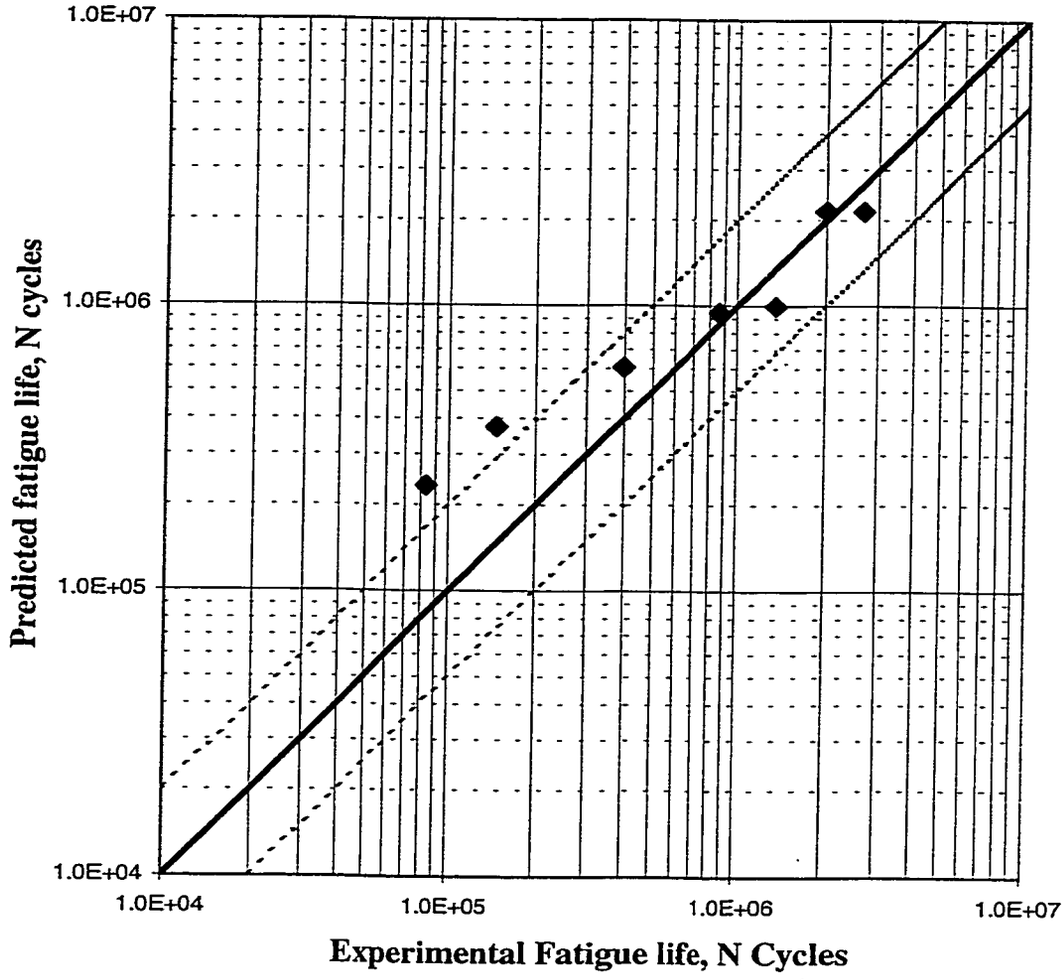

Figure 5.46: Comparison of Experimental and predicted Fatigue lives at $0^{o}C$ in Class 1 $[0]_8$

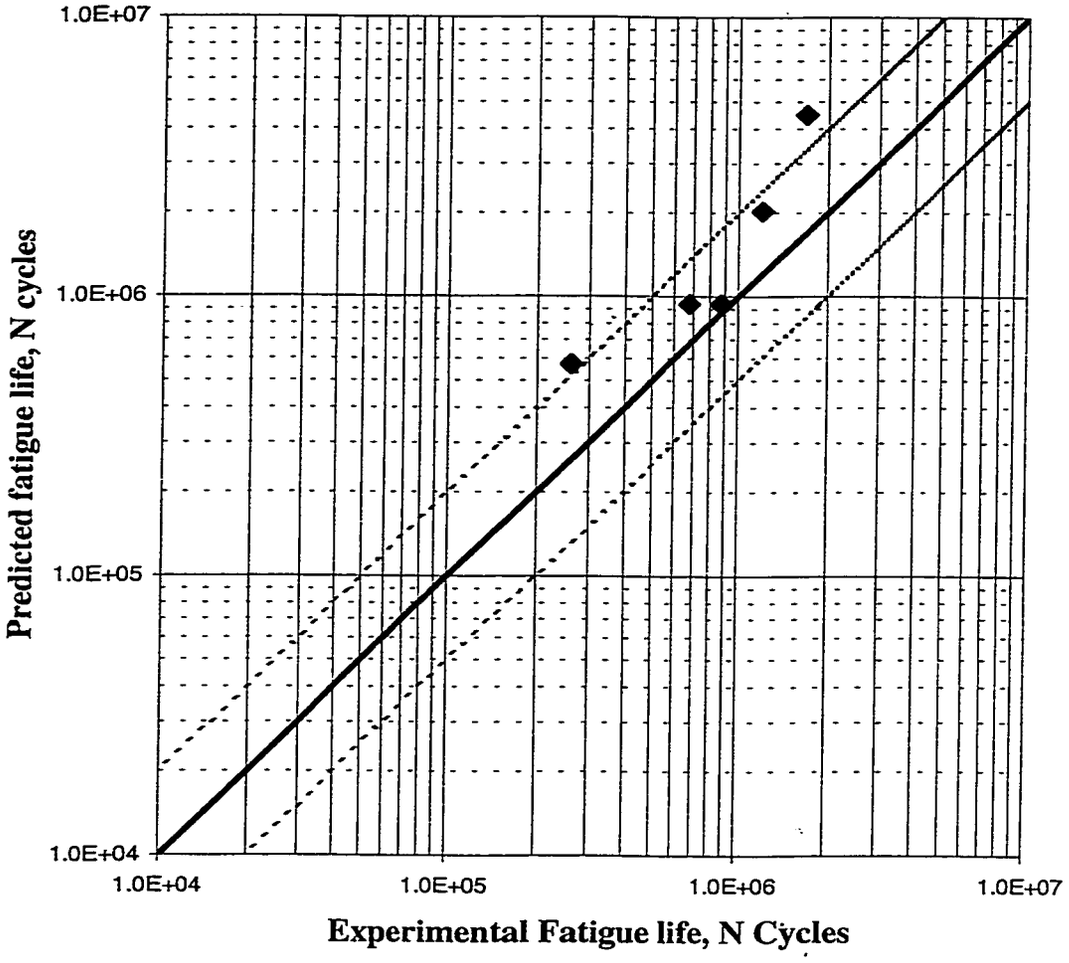

Figure 5.47: Comparison of Experimental and predicted Fatigue at Rom Temperature in Class 1 $[0]_8$

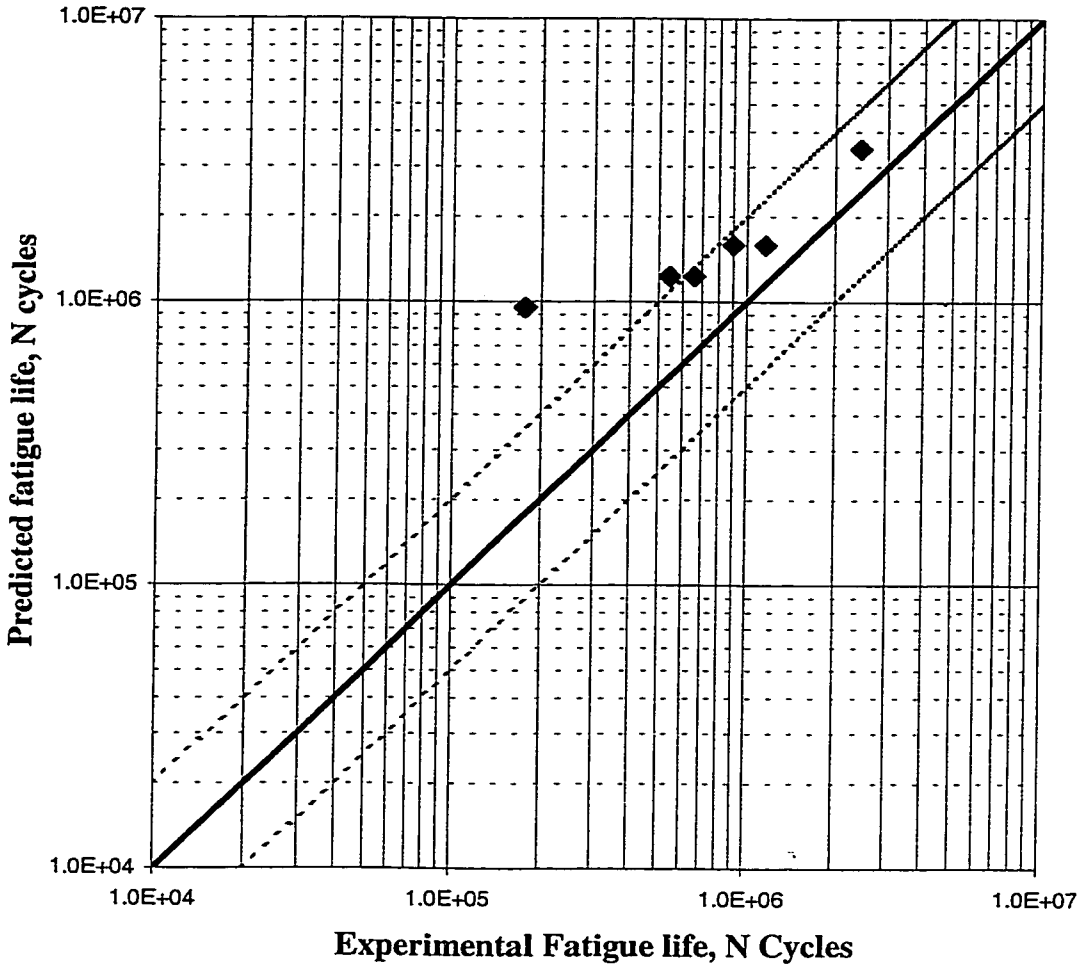

Figure 5.48: Comparison of Experimental and predicted Fatigue lives at 100°C in Class 1 $[0]_8$

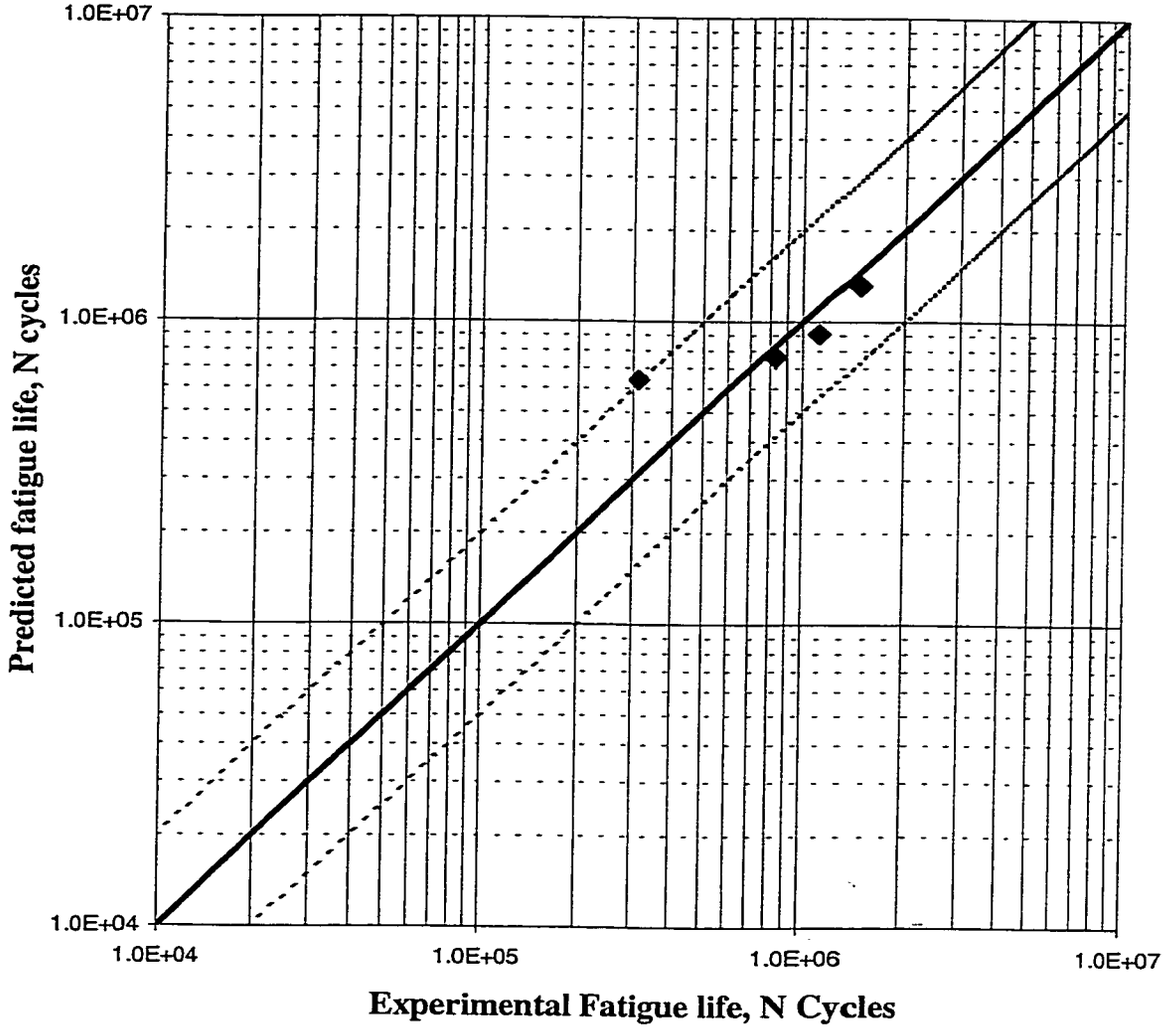

Figure 5.49: Comparison of Experimental and predicted Fatigue lives at 0°C in Class 2 $[0,0,45,-45]_s$

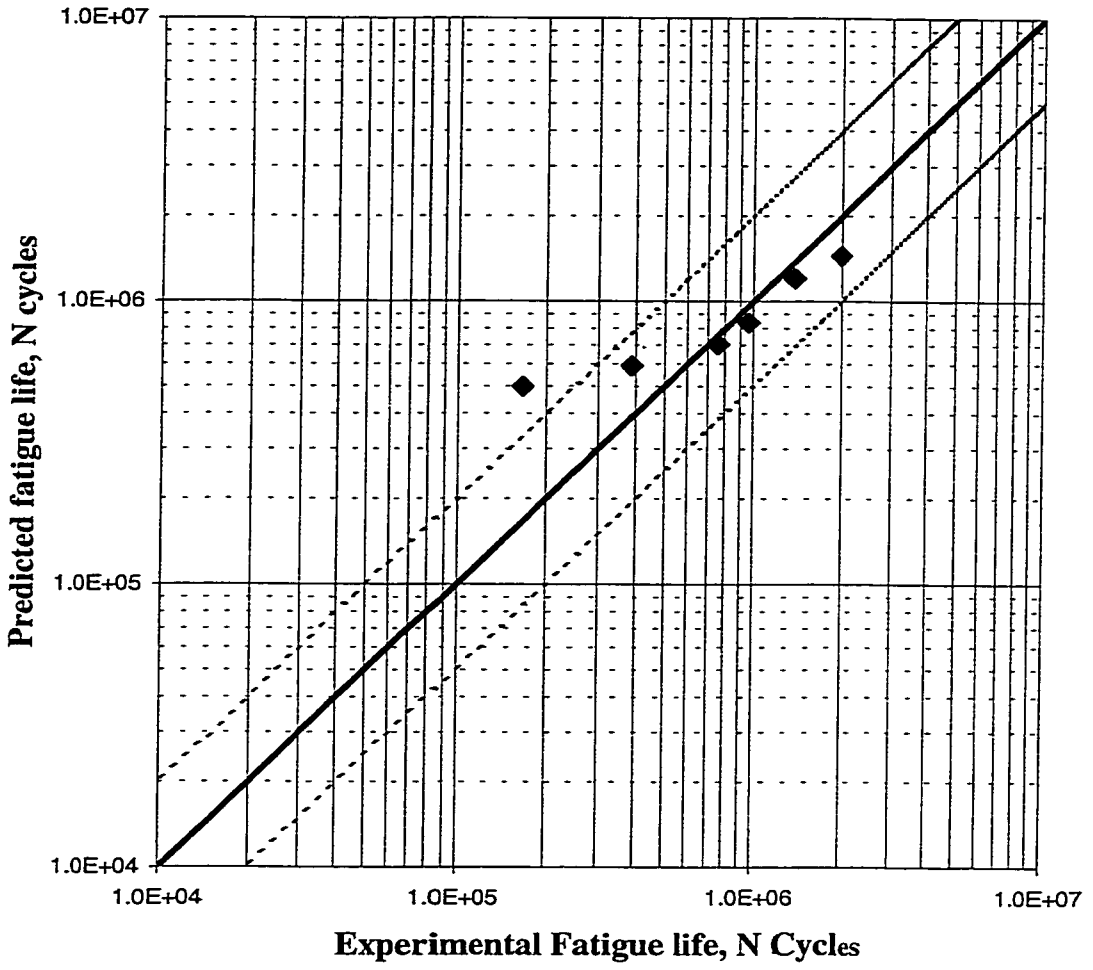

Figure 5.50: Comparison of Experimental and predicted Fatigue at Room Temperature in Class 2 $[0,0,45,-45]_s$

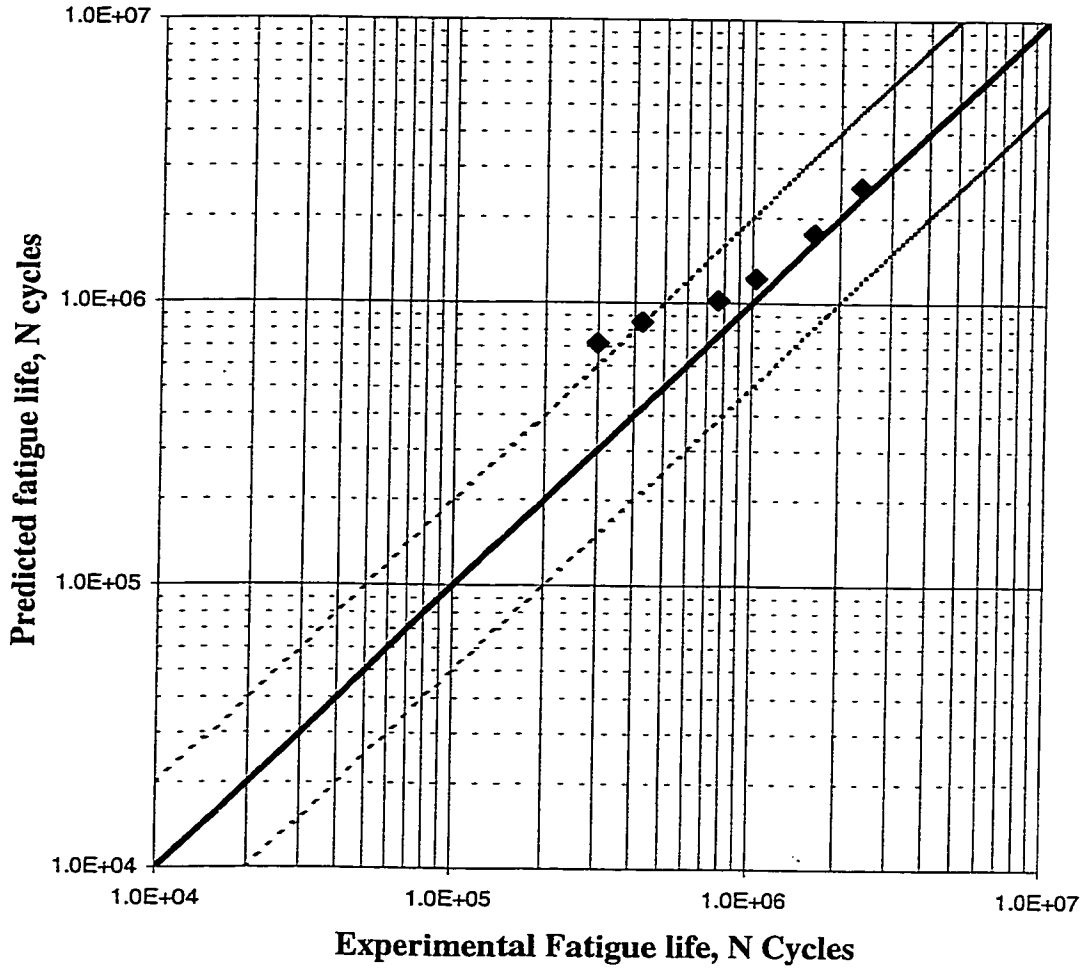

Figure 5.51: Comparison of Experimental and predicted Fatigue at 100°C in Class 2 $[0,0,45,-45]_s$

References:

1. Saunders, S. and G. Clark, "Fatigue Damage in Composite Laminates" Materials Forum, 17, 1993, p 309-331.

2. Mahfuz. H., Maniruzzaman, M., Krishnagoplan, J., Haque, A., Ismail, M., Jellani, S.; "Effect of Stress Ratio on Fatigue Life of Carbon-Carbon Composites" Theoretical and applied fracture mechanics, No 24, 1995, p 21-31.

3. Evans W. J., Isaac, D. H., Saib, K. S.; "The Effect of Short Carbon Fiber Reinforcement on Fatigue Crack Growth In Peek" Composites, part A 27A, 1996, p -547-554.

4. Parasad Donti R., Vaughan, J. G., Mantena, P. R.; "Effect of Pultrusion Process Variables on Cyclic Loading Damage of Graphite Epoxy Composites" Cyclic deformation, Fracture and non destructive evaluation of advanced materials: Second vol, ASTM STP 1184, 1994, p 301-314.

5. Yasushi Miyano, Nakada, M.; McMurry; " Influence of Stress Ratio on Fatigue Behavior in The Transverse Direction of Unidirectional CFRPs" Journal of Composite Materials, v 29, n 14, 1995, p 1808-1822.

6. Lin G. M. and Lai J.K.L. " Fracture Mechanism in Short Fiber Reinforced Thermoplastic Resin Composites" Journal of Materials science, v 28, 1993, p 52405246.

7. Yoshiyuki Tomita and Kojiro Morioka "Effects of lay-up sequence on mechanical properties and fracture behavior of advanced CFRP laminate composites" Materials science and Engineering, A234-236, 1997, p 778-781.

8. Rochardjo, H. S. B., Komotori, J., Shimizu, M., Miyano, Y.; "Effects of fiber contents on the longitudinal tensile fracture behavior of uni-directional carbon /epoxy composites" Journal of materials processing technology, v 67, 1997, p 89-93.

9. Ma, C. C., Kuo, H. C., Chang, M. J., Ong, C. L., Wu, I. C., Sheu, M. F. Tai, N. H.; "Fatigue behavior of carbon fiber reinforced Polyetheretherketone (PEEK) laminated composites" 38th International SAMPE symposium May 1993, p 1628-1639.

10. Masaki Hojo, Ochiai S.; Gustafson,C.; Tanaka K., "Effect of Matrix Resin on Delamination Fatigue Crack Growth in CFRP Laminate" Engineering Fracture Mechanics Vol 49,No. 1, pp. 35-47 1994.

11. Khan.Z,; Sulaiman,F.S.; Farooqi,J.K.; "Fatigue Damage Characterization in Plain weave Carbon-carbon Fabric Reinforced Plastic Composites" Journal of Reinforced Plastics and Composites, Vol 17, No. 15, 1998.

12. Dillon G. and Buggy M. " Damage Development during Flexural Fatigue of Carbon Fiber Reinforced Peek" Composites, Vol 26, 1995, pp 355-370.

13. Akira Todoroki, Kobayashi, H., Lee, J. G.; "Image Analysis of Delamination Cracks in Carbon Fiber Composites by Scanning Acoustic Microscopy" Composites science and technology, Vol 52, 1994, pp 551-559.

14. Nobuo Takeda, Oghira, S., Suzuki, S., Akira, K.; " Evaluation of Microscopic Deformation in CFRP Laminates With Delamination by Micro Grid Methods" Journal of composite materials, Vol 32, n 1, 1998, pp 83-100.

15. Sang Tae Kim and You-Tae Lee "Characteristics of Damage and Fracture Process of Carbon Fiber Reinforced Plastic Under Loading-Unloading Test By Using AE Method" Material Science and Engineering, A234-236, 1997, pp 322-326.

16. Elahi M, Reifsnider, K. L., Swain, R. E.; "Influence of Fiber Matrix Interface on Dynamic Response of CFRPs" Cyclic deformation, fracture and non-destructive evaluation of advanced materials: Second Vol, ASTM STP 1184, 1994, pp 255-264.

17. Nobuo Takeda et al "Effects of Toughened Interlaminar Layers on Fatigue Damage Progress In Quasi-Isotropic CFRP Laminates" International journal of fatigue, 21, 1999, pp 235-242.

18. Nidal Alif, Carlsson Leif, A., Gillespie, J. W. Jr.; "Mode I, mode II, and Mixed Mode Interlaminar Fracture of Woven Fabric Carbon/Epoxy" Composites materials: testing and design, thirteenth volume, ASTM STP 1242, 1997, pp 82-106.

19. Gathercole N., Adam, T., Reiter H., Harris, B "Life Prediction For Fatigue of T800/5245 Carbon Fiber Composites: Constant Amplitude Loading" Fatigue, Nov. 1994, Vol 16, pp 523-532

20. Adam, T., Gathercole N., Reiter H., Harris, B.; "Life Prediction for Fatigue of T800/5245 Carbon Fiber Composites: Variable Amplitude Loading" Fatigue, Nov. 1994, Vol 16, pp 533-546.

21. Kenichi Takemura and Toru Fuji., "Fatigue Damage and Fracture of Carbon Fabric/Epoxy Composites Under Tension-Tension Loading", JSME International Journal, Series A, Vol 37, n 4, 1994, pp 472-480.

22. Lee L. J., Fu. K. E., Yang, J. N.; "Prediction of Fatigue Damage and Life for Composite Laminates Under Service Loading Spectra" Composites Science and Technology, 56, 1996, pp 635-648

23. Salvia M. and Vincent L. "Modeling of Flexural Fatigue Behavior in Ud-Glass-Fiber -Reinforced Polymer" Composites Science and Technology, 56, 1996, pp 797-802.

24. Wen-Feng Wu, Lee, L. j., Choi, S. T.; "A Study of Fatigue Damage and Fatigue Life of Composite Laminate" Journal of Composites Materials, Vol 30, n 1, 1996, pp 123-137.

25. Shojiro Ochiai, Okumura, I., Tanaka, M., Hojo, M., Inoue, T.; " Influences of Residual Stresses, Frictional Shear Stress at Debonded Interface and Interactions among Broken Components on Interfacial Debonding In Unidirectional Multi-Filamentary Composites" Composite interfaces, Vol 5,n 4 , pp 363-381.

26. Xiaojun Wang and Chung D. D. L."Self Monitoring Carbon Fiber Polymer Matrix Composites" SPIE, Vol 2716, pp 259-266.

27. Mahmood M Shokreih and Larry B. Lesser "Residual Strength and Fatigue Life of Unidirectional Composite Plies Under Multiaxial Fatigue Loading" 26~ international SAMPE technical conference, Oct. 1994, pp 303-314.

28. Kenichi Takemura and Toru Fujii " Fracture Mechanics Evolution of Progressive Fatigue Damage in Circular Hole Notched GRP Composite under Combined Tension/Torsion Loading" Composites Science and Technology, Vol 52, 1994, pp 527534.

29. Keith Gamble, Piling, M., Wilson, A.; "An Automated Finite Element Analysis of The Initiation and Growth of Damage in Carbon Fiber Composite Materials" Composite structures, Vol 32, 1995, pp 265-274

30. Kenny J. M. and Marchetti M." Elasto-Plastic Behavior of Thermoplastic Composite Laminates under Cyclic Loading" Composite structures, Vol 32, 1995, pp 375-382.

31. Boniface L., Smith, P. A., Bader, M. G.; " Transverse Ply Cracking in Cross-Ply CFRP Laminates— Initiation and Propagation Controlled ?" Journal of Composite Materials, Vol 31, n 11, 1997, pp 1081-1111.

32. Dong-Yeul Song and Nobuo Otani "Fatigue Life Preidiction of Cross Ply Composite Laminates" Material Science and Engineering, A238, 1997, pp 329-335.

33. Akbar Afaghi Khatibi and Lin Ye "Notched Strength and Effective Crack Growth in Woven Fabric Composite Laminates With Circular Holes" Journal of Reinforced Plastics and Composites, Vol 15, April 1996, pp 344-359.

34. Peters P. W. M. " Influence of Cure Temperature and Degree of Surface Treatment on Transverse Cracking and Fiber/Matrix Bond Strength In CFRPs" Journal of composite materials, Vol 28, n 6, 1994, p 507-524.

p

35. Yasushi Miyano, McMurry, M. K., Enyama, J., Nakada, M.; "Loading Rate and Temperature Dependence on Flexural Fatigue Behavior of a Satin Woven CFRP Laminate" Journal of Composite Materials, Vol 28, n 13, 1994, pp 1250-1260.

36. Miyano Y., McMurray, M. K., Muki, R.; "Some Remarks on Static, Creep and Fatigue Flexural Strength of Satin Woven CFRP Laminates" Numerical Methods in Structural Mechanics, AMD-Vol 204, 1995, pp 69-82.

37. Yasushi Miyano, Kanemitsu, M., Kunio, T., Kuhn, H. A.; "Role of Matrix Resin on Fracture Strengths Of Unidirectional CFRP" Journal of composite materials, Vol 20, Nov 1986, pp 520-538.

38. Miyano,Y.; Nakada, M.; McMurry, M.K.; Muki, R.; "Prediction of Flexural Fatigue Strength of CFRP Composite Under Arbitrary Frequency, Stress ratio and Temperature" Journal of Composite Materials, Vol 31, No.6, 1997.

39. Boniface,L.; Ogin, S.; Smith,P.; "The Effect of Temperature on Matrix Crack Development in Cross Ply Polymer Composite Laminates" Proc. ECCM 5, pp-141, 1992

40. Murakami,R.; Masuda, M.; Nonomura, T.; " The Effect of Content of Carbon Fiber, Test Temperature and Notch Radius on Fatigue Strength of CFRTP" Trans of Japanese Society of Mechanical Engineering Vol. 58 No 545A 1992.

41. Soutis C. and Turkmen D. " Moisture and Temperature Effects of The Compressive Failure of CFRP Unidirectional Laminates" Journal of Composite materials, Vol 31, n 8, 1997, pp 832-849.

42. Masashi Nakamura, Suzuki, H., Haraguchi, T., Watanabe, Y.; "Influence of Environmental Temperature on Fatigue Reliability at Elevated Temperature For Carbon Fiber Reinforced PEEK (on the growth mechanism from mesocracks to macrocrack)" JSME International Journal, series A, Vol 41,n 1, 1998.

43. Buggy A. Carew M. "Effect of Thermal Ageing on Carbon Fiber Reinforced Polyetheretherketone (PEEK) Part I Static and Dynamic Flexural Properties" Journal of material science, Vol 29, n 7, Apr 1994, pp 1925-1929.

44. Andrew L. Gyekenyesi "Isothermal Fatigue Behavior and Damage Modeling Of High Temperature Woven PMC" Papers ASME 98-GT-106.

45. Peters P. W. M and Andersen S. I "The Influence Of Matrix Fracture Strain and Interface Strength on Cross-Ply Cracking In CFRP in The Temperature Range Of -100°C To +100°C" Journal of composite materials, Vol 23, Sept. 1989, pp 944-960.

46. Milan Mitrovic and Carmen Greg P. "Effect of Fatigue Damage in Woven Composites On Thermo-Mechanical Properties and Residual Compressive Strength" Journal of composite material, Vol 30, n 2, 1996, p 164-189.

47. Asp L. E. "The Effects of Moisture and Temperature on The Interlaminar Delamination Toughness of a Carbon/Epoxy Composite" Composite science and Technology, Vol. 58, n. 6, June 1998, pp 967-977.

48. Matsuhisa, Y.; King, J.E.; "Effects of Temperature on Monotonic and Fatigue Properties of Carbon Fiber Epoxy Cross Ply Laminates" Journal de Physique Vol 3, Nov. 1993.

49. Yoshihiko U.; Kitamura, T.; Ohtani,R.; "Delamination Behavior of a Farbon fiber-reinforced Thermoplastic Polymer at high Temperature" Composite science and Technology 53, 1995.

50. Curtis,P.T.; Moore,B.B.; "A Comparison of the Fatigue Performance of Woven and Non-woven CFRP Laminates in Reversed Axial Loading" International Journal of Fatigue, No 2 1987.

51. Reifsnider, K. L; Damage and Damage Mechanics; (Reifsnider, K. L. ed), "Fatigue of Composite Material" Composite Material Series Vol. 4, Elsevier, 1991, pp 11-77

52. American Society of Testing and Materials, Vol. 03.01; ASTM Designation # D-3039/D-3039M-93: Standard Test Method for Tensile Properties of Polymer Matrix Composite Materials, 1993

53. Poursartip, A., Ashby, M. F., Beaumont, P. W. R.,; The Fatigue Damage Mechanics of a Carbon Fiber Composite Laminate I – Development of the model; Composite Science and Technology; Vol 25, n 3, 1986, pp. 193-218

54. Wang, S. S., and Chim, E. S. M.,; Fatigue Damage and Degradation in random Short –fiber SMC Composite; Journal of Composite Materials, Vol 17, 1983, pp 114

55. Hwang, W., and Han, S.,; Fatigue of Composites-Fatigue Modulus Concept and Life prediction; Journal of Composite Materials, Vol 20, 1986, pp 154.

56. Hwang, W., and Han, S.,; "Cumulative damage models and Multi-Stress Fatigue Life Prediction"; Journal of Composite Materials, Vol 20, 1986, pp 125

Vitae

- **Rehan Ikram Khan**
- Born at Lahore, Pakistan in 1971
- Completed higher secondary school from Lahore in 1986
- Received Bachelor of Science (B.S) degree in Mechanical Engineering from University of Engineering and Technology, Lahore, Pakistan in 1995
- Served Packages Ltd. Lahore as Production Engineer
- Joined KFUPM as Research Assistant in September 1998
- Received Master of Science (MS) degree in Mechanical Engineering from KFUPM, Dhahran, Saudi Arabia in December 2000